Quantifying and understanding the aggregate risk of natural hazards

Submitted by

Alasdair Hunter

to the University of Exeter as a thesis for the degree of Doctor of Philosophy in Mathematics, May 2014.

I certify that all material in this thesis which is not my own work has been identified and that no material is included for which a degree has previously been conferred upon me.

. . . . . .

Alasdair Hunter

Abstract

Statistical models are necessary to quantify and understand the risk from natural hazards. A statistical framework is developed here to investigate the effect of dependence between the frequency and intensity of natural hazards on the aggregate risk. The aggregate risk of a natural hazard is defined as the sum of the intensities for all events within a season. This framework is applied to a database of extra tropical cyclone tracks from the NCEP-NCAR reanalysis for the October to March extended winters between 1950 and 2003.

Large positive correlation is found between cyclone counts and the local mean vorticity over the exit regions of the North Atlantic and North Pacific storm tracks. The aggregate risk is shown to be sensitive to this dependence, especially over Scandinavia. Falsely assuming independence between the frequency and intensity results in large biases in the variance of the aggregate risk. Possible causes for the dependence are investigated by regressing winter cyclone counts and local mean vorticity on teleconnection indices with Poisson and linear models. The indices for the Scandinavian pattern, North Atlantic Oscillation and East Atlantic Pattern are able to account for most of the observed positive correlation over the North Atlantic.

The sensitivity of extremes of the aggregate risk distribution to the inclusion of clustering, with and without frequency intensity dependence, is investigated using Cantelli bounds and a copula simulation approach. The inclusion of dependence is shown to be necessary to model the clustering of extreme events.

The implication of these findings for the insurance sector is investigated using the loss component of a catastrophe model. A mixture model approach provides a simple and effective way to incorporate frequency-intensity dependence into the loss model. Including levels of correlation and overdispersion comparable to that observed in the reanalysis data results in an average increase of over 30% in the

200 year return level for the aggregate loss.

Acknowledgements

This project was jointly funded by the National Environment Research Council and the Willis Research Network. I have been very fortunate in conducting this work under the expert guidance of Professor David Stephenson, without whose encouragement and direction, this thesis could not have been completed. I would also like to thank my co-supervisors Dr. Mark Holland (Exeter) and Ian Cook (Willis Re.) for highly useful suggestions and feedback throughout the project. I am also very grateful to my original supervisor, Dr. Renato Vitolo, for his enthusiasm and support in the first year of the project.

The database of cyclone tracks used in this thesis were kindly provided by Dr. Kevin Hodges of Reading University. The synthetic dataset used in Chapter 5 of this thesis was also developed after receiving invaluable feedback from Dick Whittaker.

Special thanks to Dr. Theo Economou and Dr. Ben Youngman for proof reading chapters of this thesis and providing much needed assistance at various stages of the project. An honourable mention goes out to the other inhabitants of the 319 office over the years for providing an enthusiastic and supportive working environment.

Finally I would like to thank my parents, Alastair and Rosemary Hunter, for their unwavering support throughout the project.

Contents

Contents **5**

List of Figures **9**

List of Tables **11**

1 Introduction **12**

1.1 Motivation 12

1.2 Research questions 16

1.3 Thesis plan 17

2 Background **19**

2.1 Aim 19

2.2 Quantifying the risk to society from natural hazards 19

2.2.1 Point process models 21

2.2.2 Generalised linear modelling of rates 22

2.2.3 Random effects and mixture models 23

2.2.4 Copulas 24

2.2.5 Extreme value analysis 25

2.2.6 Catastrophe modelling 26

2.3 Extra tropical cyclones 27

2.3.1 Storm track identification 28

2.4 European extra tropical cyclone risk 29

2.4.1 Clustering 32

2.4.2 Aggregate risk 35

2.5 Data 38
2.5.1 Cyclone track database 38
2.6 Summary 40

3 Understanding the aggregate risk of extra tropical cyclones 42
3.1 Aim 42
3.2 Collective risk models 42
3.2.1 Frequency and intensity 43
3.3 Climatology of aggregate risk 45
3.4 Quantifying the frequency-intensity dependency 48
3.4.1 Sample correlation 49
3.4.2 Covariance between the frequency and intensity 50
3.4.3 Sensitivity to choice of reanalysis data: NCEP-NCAR and ERA40 53
3.5 Can climate modes explain the frequency-intensity dependence? . . 55
3.5.1 Large scale flow patterns 55
3.5.2 Regression modelling of frequency and intensity 59
3.5.3 Modelled covariance 64
3.6 Regression models for all grid points 64
3.7 Discussion about possible physical mechanisms 69
3.7.1 Positive correlation 69
3.7.2 Negative correlation 72
3.8 Summary 73

4 Extremes 75
4.1 Aim 75
4.2 Managing aggregate extremes of natural hazards 75
4.2.1 Clustering of extremes 78
4.3 Methods for exploring extremes of the aggregate risk 80
4.3.1 Non-parametric methods 80
4.3.2 Parametric methods 81

4.3.3 Monte Carlo methods 83
4.3.4 Uncertainty assessment 87
4.4 Results 89
4.4.1 Non-parametric 89
4.4.2 Parametric 92
4.4.3 Monte Carlo methods 94
4.5 Summary 103

5 Incorporation of dependency into the loss component of Catastrophe Models 105

5.1 Aim 105
5.2 Catastrophe models 106
5.2.1 Mathematical formulation of a catastrophe model 106
5.3 Methods 109
5.3.1 Current Practice 110
5.3.2 Mixture model approach 111
5.3.3 Parameter estimation: constant dispersion 113
5.3.4 Intensity dependent dispersion 116
5.4 Model implementation 118
5.5 Results 120
5.5.1 Aggregate exceedance probability 121
5.5.2 Conditional exceedance probability 125
5.5.3 Occurence exceedance probability 128
5.5.4 Clustering and frequency-intensity dependence 130
5.6 Conclusions 133

6 Discussion and Conclusions 135

6.1 Summary of findings 135
6.2 Thesis questions revisited 138
6.3 Discussion 139
6.4 Possible directions for future work 140

A **142**

A.1 Collective risk models 142

A.2 Analysis of modelling assumptions 143

A.3 Sample estimators 144

B **146**

B.1 Axioms of coherence 146

C **148**

C.1 Parameter estimation: Linear link function 148

C.2 Parameter estimation: Log link function 149

List of Figures

1.1 Economic losses from natural hazards between 1980-2012. 13
1.2 Map of natural hazards occurring in 2011. 15

2.1 Dispersion statistic for Berlin cyclone counts 34
2.2 Storm tracks from the 1989/90 winter 39
2.3 Storms passing near Gothenburg 40

3.1 Example of a marked point process 44
3.2 Climatology of the aggregate risk 46
3.3 Models for the variance of the aggregate risk. 48
3.4 Correlation maps: of counts n and local mean vorticity y 49
3.5 Ratio of modelled variance to sample variance 52
3.6 Correlation maps: NCEP NCAR/ERA40 54
3.7 Schematic of the frequency-intensity relationship 55
3.8 Maps of the NAO,SCP and EAP 57
3.9 Correlation maps of the 700mb stream function Ψ_{700} and n,y. . . . 58
3.10 Deviance residuals from a Poisson GLM 60
3.11 Residuals from a linear model. 62
3.12 Parameter estimates for Poisson regression coefficients. 65
3.13 Parameter estimates for linear regression coefficients 66
3.14 Correlation maps for N and Y 67
3.15 Regression coefficient estimates for the North Pacific 68
3.16 Correlation maps of N and Y (North Pacific) 69
3.17 Regression coefficients for the SCP on the zonal wind. 72

4.1 Plots of y and n for cyclones near Gothenburg 76
4.2 Example of an AEP curve. 77
4.3 Empirical AEP curves for Gothenburg cyclones 90
4.4 Ratio of Cantelli bounds 91
4.5 Time series of s at Gothenburg and Barcelona. 92
4.6 Quantile-quantile plots of the fitted GPD model for s. 93
4.7 AEP curves for the GPD models 94
4.8 Quantile-quantile plots for models of N Y and W 95
4.9 Cyclone counts, local mean vorticity and the variance of the vorticity. 96
4.10 Plots of the DKW confidence bands for s 98
4.11 AEP curves for the Monte Carlo simulated s 100
4.12 Dispersion of the simulated n 102

5.1 Schematic of a CAT model 107
5.2 Relationship between the mixing variable and the response variables 112
5.3 ELT rate and expected loss parameters 118
5.4 AEP curves from the ELT 122
5.5 AEP curves conditional on the mixing variable Z 124
5.6 Plots of the CEP from the ELT 125
5.7 Plots of the simulated y and z 127
5.8 OEP curves from the ELT 128
5.9 OEP curves conditional on Z 129
5.10 Simulated n and y 131
5.11 Dispersion of n against u 132

List of Tables

2.1 European winter storm losses 1980-2012 37

3.1 Poisson regression coefficient estimates for counts 61
3.2 Linear regression coefficient estimates for local mean vorticity . . . 63

4.1 Summary statistics from the Monte Carlo simulation study on uncertainty estimates 99
4.2 Summary statistics from the Monte Carlo simulation study on modelling assumptions 101

5.1 Summary statistics for the Monte Carlo simulation study. 123
5.2 Sample correlations from the ELT simulation study 130

Chapter 1

Introduction

1.1 Motivation

In 2011, natural hazards resulted in a total of 27,000 fatalities and $380 billion in damages worldwide, of which $105 billion was insured (Source: Munich Re. NatCatService[1]). These losses were due to 820 distinct hazard events, including the Tohōku earthquake, the Thailand floods, Hurricane Irene and European extra tropical cyclone Joachim. Although 2011 saw the highest economic losses on record, it can be viewed as part of a global trend of increasing losses from natural hazards (see Fig.1.1). Socio-economic losses from natural hazards have been increasing since 1950, mainly due to increases in the global population and exposed values which are often concentrated in vulnerable regions (Smolka, 2006).

The United Nations International Strategy for Disaster Reduction[2] (UNISDR) define a natural hazard as a natural process or phenomenon that may cause loss of life, injury or other health impacts or property damage. The UNISDR state that there is no such thing as a "natural" disaster, only a natural hazard. By decreasing societies exposure to hazards and increasing their resilience the damage caused by a natural hazard can be reduced, and disaster averted. Scientific assessment of the risk posed by hazards plays a vital role in improving resilience by inform-

[1] https://www.munichre.com/touch/naturalhazards/en/natcatservice/natcatservice/index.html
[2] http://www.unisdr.org

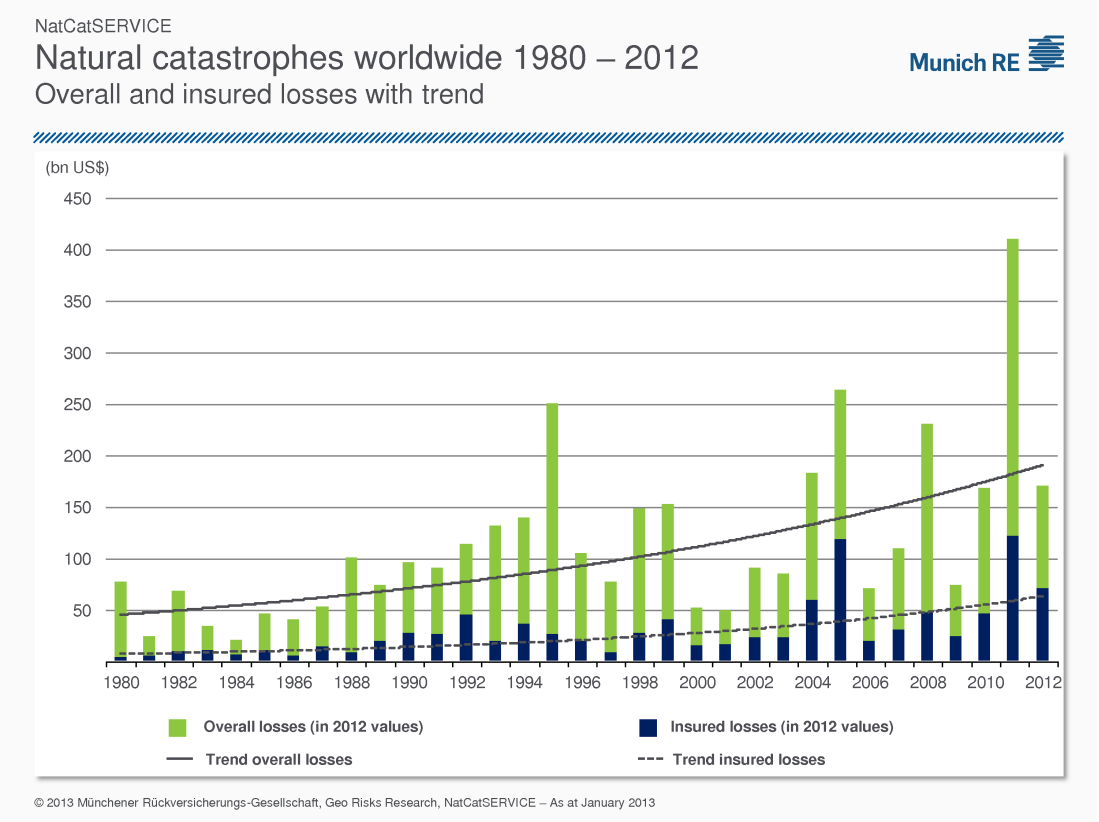

Figure 1.1: Economic losses from natural hazards between 1980-2012. Source: Munich Re. NatCatSERVICE

ing government policy, building regulations and emergency response preparations (Rougier et al., 2013). Insurers assist in mitigating the impact of natural hazards by providing protection to industry and civilians; around 40% of economic losses in industrialised countries are absorbed by the insurance industry (Kunreuther et al., 2013). The insurers therefore need to be able to reliably assess their exposure to risk; natural hazards can have a severe impact on an insurer if they have a high concentration of policies in a hazard prone area (Grossi and Kunreuther, 2005).

Being able to estimate the total claims which could arise from natural hazards within a year is thus crucial for insurers in determining premiums and capital reserves, as well as how much coverage they should provide in a specific location. The short records and trends in the loss data make historic loss experience an unreliable estimator for future claims (Kukush et al., 2004). Instead natural

catastrophe insurers use scientific models of natural hazards, known as catastrophe (CAT) models. These models are developed using a combination of observational data, knowledge of physical laws and expert judgement (Grossi and Kunreuther, 2005). Many insurers develop in-house catastrophe models, as well as using proprietary models from the three main catastrophe modelling firms; Risk Management Solutions (RMS), Applied Research Insurance(AIR) and EQECat (Banks, 2005). To ensure CAT models are as reliable as possible they are regularly updated to include the latest research developments in the fields of atmospheric science and engineering (Clark, 2002).

Catastrophe models often make simplifying assumptions about complex physical processes (Rougier et al., 2013). Insurers and catastrophe modelling firms use different approaches to model the same hazard, a consequence of which is that investigating the risk from the same hazard event using different models can result in significantly different modelled losses (Cole et al., 2010). This ambiguity is a cause of concern for model users; their perceived risk depends upon their choice of model, and assessing models is not straightforward. Open-source CAT models have been developed for hurricane (Vickery et al., 2006) and earthquake hazards (Kircher et al., 2006) with the stated aim of creating a standard methodology for estimating losses from natural hazards (Grossi and Kunreuther, 2005). However for most other regions and hazards the methodology used in constructing a CAT model is not publicly available thereby hindering scientific discussion (Clark, 2013).

This thesis develops a framework for the statistical modelling of the aggregate risk of natural hazards. Here the aggregate risk refers to the distribution of total loss from the sum of all hazard events in a season or year. Aggregate risk is the main focus as it has received relatively little attention in the literature, despite its importance to the insurance industry. Previous studies have considered hazard counts within a season, which is a special case of an aggregate loss where the intensity is unity for each event. Therefore, studying the distribution of aggregate loss is

a natural extension of previous research on the distribution of hazard counts. The framework is used to assess the impact of different modelling assumptions on the aggregate risk. Statistical methods are used to investigate the role of atmospheric forcing and other physical processes in determining the aggregate risk of natural hazards. An investigation is then conducted on how to implement relevant findings into the financial component of a catastrophe model.

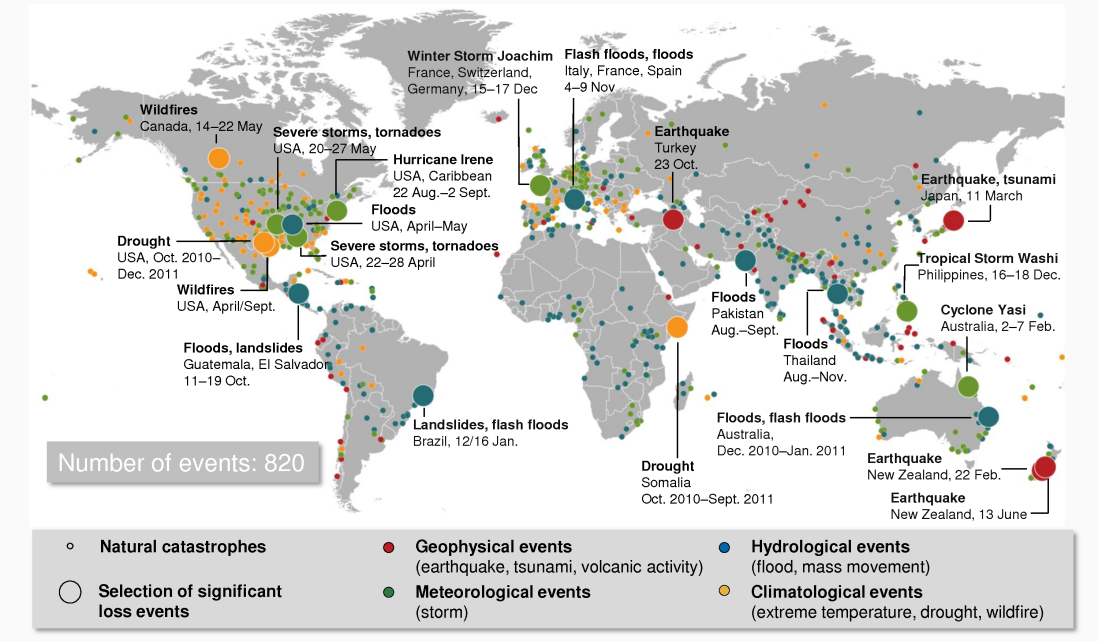

Figure 1.2: Map of natural hazards occurring in 2011 which resulted in enough socio-economic loss to be classified as a catastrophe. Source: Munich Re. NatCat-SERVICE

Almost every region of the globe is at risk from natural hazards in different forms (Fig. 1.2). These hazards can loosely be categorized into geological and hydro-meteorological events. Geological hazards are those caused by subterranean faults and magma chambers, such as earthquakes and volcanoes (Woo, 1999). Hydro-meteorological hazards are events caused by atmospheric, hydrological or oceanographic processes, such as floods, tropical and extra tropical cyclones (Rougier et al., 2013). Between 1950 and 2009 windstorm hazards (tropical and extra tropical cyclones) were responsible for 80% of all natural hazard related insured losses[3].

[3]https://www.munichre.com/touch/naturalhazards/en/naturalhazards/meteorological-

In Europe extra tropical cyclones have caused tens of billions of Euros in insured losses since 1990, and quantifying the risk of further losses has been identified as being of the highest priority for the global reinsurance industry[4]. For this reason extra tropical cyclones have been used as a case study throughout the thesis. Modelling the aggregate risk of extra tropical cyclones is of particular interest due to the temporal clustering of storms in the Northern Hemisphere (Mailier et al., 2006). Clusters of extra tropical cyclones can result in economic losses comparable to those of a U.S. hurricane, and due to the structure of reinsurance contracts a cluster of events can cost more than a single event with the same total loss (Vitolo et al., 2009). Climate models have been shown to underestimate clustering (Kvamstø et al., 2008) and the physical drivers of clustering remains an active area of ongoing research (e.g. Hanley and Caballero (2012); Pinto et al. (2013). Catastrophe modelling firms have recently attempted to include clustering into their windstorm models but as the models are not open to scrutiny it is difficult to assess how effectively this has been accomplished[5]. Here the impact of clustering will be considered within a broader aggregate risk framework that includes storm intensity as well as the frequency. This research is relevant to other natural hazards which have been shown to cluster, e.g. floods and hurricanes (Villarini et al., 2013; Mumby et al., 2011).

1.2 Research questions

The aim of this research is to develop a flexible framework which can be used to quantify and understand the aggregate risk of natural hazards. This framework will be used to investigate the sensitivity of the aggregate risk to different modelling assumptions. This thesis will address the following main questions:

hazards/storm/index.html

[4]http://www.willisresearchnetwork.com/research-and-impact/natural-hazard-and-risk/european-windstorm.html

[5]http://www.air-worldwide.com/Publications/AIR-Currents/2010/European-Windstorms-Implications-of-Storm-Clustering-on-Definitions-of-Occurrence-Losses/

- Is there dependence between the frequency and mean intensity of hazards within a season/year?
- How does frequency intensity dependence affect the distribution of aggregate losses (aggregate risk)?
- How can the dependency be diagnosed and incorporated into the loss component of catastrophe models?

1.3 Thesis plan

Chapter 2 provides a brief overview of relevant statistical techniques for modelling the risk from natural hazards. Extra tropical cyclones are introduced as a case study, and the database of storm tracks used later in the thesis is described.

Chapter 3 develops a framework for quantifying the aggregate risk of natural hazards. This framework is applied to the database of extra tropical cyclones. The variance of the aggregate risk of winter storms is found to be very sensitive to covariance between the frequency and intensity. Regression models using large-scale atmospheric indices as covariates are invoked to explain this covariance.

Chapter 4 considers extremes in aggregate loss. The impact of frequency-intensity dependence on extremes of the aggregate risk. The inclusion of this dependence is also shown to be necessary to model clustering of extreme events. The performance is compared of parametric, non-parametric and simulation methods in modelling the aggregate risk.

Chapter 5 presents a mathematical formulation of the loss component in catastrophe models. This component is then extended to allow the inclusion of frequency-intensity dependence. The impact of frequency-intensity dependency on a hypothetical insurer's loss distribution is investigated.

Chapter 6 summarised the main findings of this thesis and discusses potential areas for future research.

Chapter 2

Background

2.1 Aim

This chapter first discusses statistical methods that are used for modelling the risk of natural hazards which are relevant to this thesis. The second part of the chapter provides a brief overview of the scientific literature for extra tropical cyclones and the risk they pose to Europe. The dataset of extra tropical cyclone tracks used throughout the thesis is then introduced.

2.2 Quantifying the risk to society from natural hazards

Collin's Dictionary defines risk as "the chance of disaster or loss" (Sinclair-Knight, 2002). Natural hazards such as floods, earthquakes and windstorms present a major source of risk to society and the cost is measured in human lives and damage to infrastructure and ecosystems as well as in financial loss. Decision makers such as governments and insurers need to be able to quantify the risk from such events in order to manage it. For example, European insurers have legal requirements to maintain sufficient capital to ensure that claims will be paid promptly and the insurer can remain solvent (Banks, 2005). These capital requirements are part of

the Solvency II regulatory framework[1], and are defined using estimates of the Probable Maximum Loss (PML), which often corresponds to a high quantile (e.g. the 0.995 quantile - the 200 year return value) of an insurer's modelled loss distribution (Woo, 2002).

The rarity of extreme natural hazards coupled with trends in the observations make empirical estimates of the PML using historic data unreliable (Grossi and Kunreuther, 2005). For example, an earthquake may occur along a fault line once every twenty, fifty or one hundred years, in comparison to other types of insured risk such as car accidents or household fires which occur in most countries on a daily basis. Insurance claims have risen dramatically over the past decades for many different natural hazards such as U.S. hurricanes (Pielke Jr and Landsea, 1998), European windstorms (Barredo, 2010) and Japanese typhoons (Kukush et al., 2004). Trends in the loss data are largely due to socio-economic changes (population growth, migration) resulting in changes in the exposure to natural hazards (Pielke Jr et al., 2008). However, the hazards themselves are also non-stationary due to forcing by the atmosphere and ocean (Rougier et al., 2013), resulting in annual and decadal variability in the loss data.

Statistical analysis has been widely used in the literature to assess the risk posed by natural hazards. The methods used vary depending upon the data available and the modeller's objectives, but studies have typically focused on estimating return levels using extreme value techniques and quantifying trends and the role of atmospheric forcing with regression analysis (Rougier et al., 2013, Chapter 5). Some of the fundamental concepts used in the literature and in this thesis are now introduced.

[1] http://ec.europa.eu/internal$_m arket/insurance/docs/solvency/solvency2/faq_e n.pdf$

2.2.1 Point process models

The point process framework has been widely used for understanding and predicting the risk from natural hazards, such as earthquakes, floods and hurricanes (Vere-Jones, 1995; Rossi et al., 1984; Katz, 2002). Events occur at irregular times T_i with variable intensities X_i, where $i = 1, ..., N(t)$ (Stephenson, 2008). The homogeneous Poisson process is the canonical point process, where the number of points $N(t)$ follows a Poisson distribution,

$$Pr(N = k|\lambda t) = \frac{\lambda^k e^{-\lambda t}}{k!}. \tag{2.1}$$

Homogeneous refers to the rate parameter λ remaining constant in time, see (Rice, 2007, Section 2.1). The mean and variance of the homogeneous Poisson distribution are defined by the rate parameter such that $E[N] = Var(N) = \lambda$. Equality of the mean and variance for count data is known as equidispersion. However, count data frequently exhibit over dispersion $Var[N] > E[N]$ (Cameron and Trivedi, 2013). Following the approach of Mailier et al. (2006) a dispersion statistic ϕ, can be defined as

$$\phi(N) = \frac{Var[N]}{E[N]} - 1,$$

For a homogeneous Poisson process $\phi(N) = 0$, and for overdispersed data $\phi(N) > 0$. Overdispersion in count data is commonly modelled by using a distribution with more flexibility in the choice of the variance, such as the Negative Binomial distribution (Cameron and Trivedi, 2013). If $N \sim NB(p, r)$ is negative binomially distributed with parameters p, r, then the probability that $N = k$ is

$$Pr(N = k) = (1 + \frac{p}{r})^{-r} \frac{\Gamma(r + k}{k!\Gamma(r)} \left(\frac{p}{p + r}\right)^k,$$

and $E[N] = p$, $Var[N] = p + p^2/r$ (Rice, 2007). Therefore the negative binomial is always over dispersed.

2.2.2 Generalised linear modelling of rates

Regression analysis is widely used in studies on hydro-meteorological hazards to assess the influence of climatic factors on attributes of a natural hazard, such as the frequency or intensity. The motivation for using regression models is improving understanding of the physical mechanisms that govern hazards and developing models for prediction/forecasting purposes, (Rougier et al., 2013, Chapter 5). The use of regression analysis for prediction is particularly common in Atlantic hurricane studies, such as in Elsner and Jagger (2006) where the May-June averaged North Atlantic Oscillation (NAO) and Southern Oscillation indexes are used to predict July-November U.S. hurricane counts.

Let Y be the time series of some hazard attribute (e.g. the counts), $Y = \{Y_j, j = 1, ..., m\}$. The dependence of the mean of Y, on k time varying factors $Z_1, .., Z_k$ can be modelled using the Generalised Linear model (GLM) framework (Davison, 2003, Section 10.3). The probability distribution of the response variable Y is chosen from the exponential family of distributions. The mean of Y at time j, $E[Y_j]$, is related to the explanatory variables linearly, via some link function g;

$$g(E[Y_j]) = \beta_0 + \sum_{i=1}^{k} \beta_i z_{i,j}, \tag{2.2}$$

where $z_{i,j}$ is the realisation of the ith explanatory variable at time j. The intercept parameter (β_0) and slope coefficients (β_i) can be estimated by Maximum Likelihood methods (Cameron and Trivedi, 2013, Section 2.3). Considering the case of count data, the Poisson process provides the simplest model; the rate parameter λ for a Poisson distributed random variable N is related to explanatory variables Z, and g is the log-link function;

$$N|Z_1, ..., Z_k \sim Poisson(\lambda) \tag{2.3}$$

$$log(\lambda_j) = \beta_0 + \sum_{i=1}^{k} \beta_i z_{i,j}, \tag{2.4}$$

and therefore the mean and variance of N both vary with the explanatory variables. A Poisson regression approach was used in Mailier et al. (2006) to investi-

gate whether large-scale flow indices could explain overdispersion of extra tropical cyclone counts. That is, for a Poisson regression model the rate is no longer homogeneous and the dispersion is

$$\phi(N) = \frac{Var[e^{\beta_0+\beta_1 z_1+\ldots+\beta_k z_k}]}{E[e^{\beta_0+\beta_1 z_1+\ldots+\beta_k z_k}]},$$

and therefore for a log-link $\phi \geq 0$ (Mailier et al., 2006).

2.2.3 Random effects and mixture models

There are often further unobserved explanatory variables in addition to the observed ones (Aitkin et al., 2009, Chapter 8). Such unobserved variables can be included in regression models by extending Eqn. 2.2,

$$g(E[Y_j]) = \beta_0 + \sum_{i=1}^{k} \beta_i z_{i,j} + \gamma W, \tag{2.5}$$

where γ is the regression coefficient for the unobserved random variable W, which is assumed to have some known probability distribution. Models of this type are called random effects models (Cameron and Trivedi, 2013, Section 9.4). A special case of this is when Eqn. 2.5 consists only of the random effects term and a linear link function, $E[Y_i] = \gamma W$. This type of model can be used for modelling over dispersion in count data. A Poisson process with a stochastic rate $\Lambda = \gamma W$ is called a Poisson mixture distribution.

$$p_N(k) = P(N(t) = k) = \int_0^\infty \frac{e^{-\lambda t}(\lambda t)^k}{k!} dF_\Lambda(\lambda);$$

where $p_N(k)$ is the probability the random variable N takes the value k $Pr(N = k)$, (Rolski et al., 2009, Section 8.5). The resulting Poisson mixture is always overdispersed since

$$\begin{aligned} E[N] = \sum_{k=1}^{\infty} k p_N(k) &= \int_0^\infty k e^{-\lambda} \frac{\lambda}{k!} dF_\Lambda(\lambda) \\ &= \int_0^\infty \lambda dF_\Lambda(\lambda) = E[\lambda] \end{aligned}$$

and

$$E[N^2] = \sum_{k=0}^{\infty} k^2 p_N(k) = E[\Lambda] + E[\lambda^2].$$

The variance of N is then

$$Var[N] = E[N^2] - E[N]^2 = E[\Lambda] + Var[\Lambda]$$

and therefore $Var[N] > E[N]$ (McNeil et al., 2005). The Negative Binomial distribution can be shown to be a mixture of Poisson distributions where the rates are Gamma distributed, (McNeil et al., 2005, Section 10.2). The mixture model approach has been widely used for modelling over dispersion and dependence in Credit Risk (Frey and McNeil, 2003). Similar ideas are used in Chapter 5 of this thesis for modelling financial losses for natural hazards.

2.2.4 Copulas

The risk presented by a natural hazard cannot be characterized by a single attribute in most cases, for example river management depends upon both flood peak and flood volume (Salvadori, 2007). These attributes or variables may not be independent. Copulas provide a useful tool in risk modelling for describing the dependence between random variables. The joint distribution of the random variables is decomposed into the individual (marginal) distributions and a copula which models the dependence between them. A d dimensional copula C is a distribution function on $[0,1]^d$, with standard uniform margins (McNeil et al., 2005). The following theorem from Sklar (1973), states all multivariate density functions can be represented by copulas.

Theorem Let F be a joint distribution function, with marginal distributions $F_1, ..., F_d$. Then there exists a d copula C such that

$$F(x_1, .., x_d) = C(F_1(x_1), .., F_d(x_d)). \tag{2.6}$$

For the proof see e.g. (Sklar, 1973; McNeil et al., 2005). The marginal distributions and associated parameters of $F_1, \ldots, F_d$ can be estimated as usual, a suitable "family" for the copula (e.g. Gaussian, Gumbel, Clayton), can be obtained through analysis of the dependence between the marginals. For example, if observations of two random variables X and Y, with arbitrary marginals suggested upper but not

lower tail dependence then a Gumbel copula may be appropriate. The copula can then be calibrated by estimating the dependence between X and Y using copula based dependence measures such as the rank correlation and tail dependence coefficients (McNeil et al., 2005). Rank correlation measures are used for calibrating copulas to data as they depend only on the bivariate distribution of a copula and not on the marginal distributions.

The implementation of a Gaussian copula is presented in Chapter 4 of this thesis.

2.2.5 Extreme value analysis

It is often necessary to quantify properties of extremes beyond what can be estimated empirically from observational data. Extreme value theory provides useful models for the behaviour of extremes in the tail. Extreme value techniques are derived from a limit theorem, which states that the block maxima of stationary random observations tend asymptotically to one of the generalized extreme value (GEV) distributions (Coles, 2001). The use of only the maxima discards potentially useful information. An alternative approach is the peaks over threshold method (POT), where all values above a (high) threshold are included. The amount by which an event exceeds the threshold u can be modelled by the generalized Pareto distribution,

$$Pr(X > x|X > u) = \left[1 + \xi \left(\frac{x-u}{\sigma}\right)\right]^{-1/\xi}. \tag{2.7}$$

where the parameter σ determines the scale of the GPD distribution and ξ the shape of the tail (Embrechts et al., 1997). The POT approach has been used in hazard modelling for floods (Katz et al., 2002), Atlantic hurricanes (Jagger and Elsner, 2006) and European extra tropical cyclones (Kunz et al., 2010).

The risk posed by a particular type of hazard is often expressed in terms of the return period for an observed variable (Della-Marta et al., 2009). The return period T is the reciprocal of the exceedance probability, i.e. $T = 1/Pr(X > x)$. The return level x_T is the quantile having return period T, i.e. the $1 - 1/T$ quantile.

Equation 2.7 can be rewritten in terms of the return level x_T, that is if $\xi \neq 0$, and the number of events in a year follows a Poisson process with rate λ then the T-year return level is,

$$x_T = u + \frac{\sigma}{\xi}[1 - (\lambda T)^{-\xi}], \tag{2.8}$$

(Coles, 2001). When $\xi = 0$ the T-year return level is, $x_T = u + \sigma log(\lambda T)$.

In risk management, capital requirements are often based on the expected value of losses exceeding some T year return level (McNeil and Frey, 2000). This quantity can be derived from the GPD model by first calculating the 1 in 200 year threshold u, then the mean excess of X exceeding u is

$$E[X - u|X > u] = \frac{\sigma_u}{1 - \xi} \tag{2.9}$$

(Embrechts et al., 1997). An introduction to statistical modelling of extremes is covered in Coles (2001), and a more specialized treatment from a financial perspective can be found in Embrechts et al. (1997). A GPD is used in Chapter 4 of this thesis to model the 1-200 year return level losses.

2.2.6 Catastrophe modelling

Catastrophe models are designed to simulate large datasets of synthetic events (Banks, 2005). These synthetic hazards are designed to be physically plausible, and are intended to represent the diversity of events which can occur. These simulated hazards are then applied to the users exposure (e.g. a portfolio of insured properties) to estimate the resulting damages were the hazards to occur. Catastrophe modelling is described in more detail in Chapter 5 of this thesis, and for an introduction to the development and use of a catastrophe model see Grossi and Kunreuther (2005).

All approaches to modelling natural hazards have limitations. While extreme value analysis provides a useful tool for modelling the PML from an individual event, it does not inform the user about the total PML due to all events. Similarly regression analysis has been widely used to improve understanding of the frequency

and intensity of natural hazards, but the subsequent implications for the aggregate loss are rarely considered. One exception to this has been U.S. hurricanes, where model fitting for total annual losses is appealing due to a public available set of normalized 21st century losses (Pielke Jr and Landsea, 1998; Pielke Jr et al., 2008). These total loss models typically consist of two independent components, one for the occurrence of events and one for the losses associated with individual events (Katz, 2002). However many of the studies make questionable assumptions. For example, even though the frequency and magnitude of claims are often regressed on the same set of climate covariates, past studies have not explicitly considered dependency between the frequency and intensity (Jagger et al., 2008; Katz, 2002). A framework for investigating the aggregate loss and the underlying modelling assumptions is introduced in the next chapter.

2.3 Extra tropical cyclones

In Europe, extra tropical cyclones are a major source of insured loss. For example, in Germany alone these extreme 'windstorm' events have been estimated to account for over 50% of all natural hazard related insured losses (Klawa et al., 2003). Examples of such events include windstorm Lothar, which made landfall in December 1999, resulting in 110 fatalities and $5.9 billion in insured losses and windstorm Daria which caused 94 fatalities and $5.1 billion in insured losses in January 1990 (see Table 2.1).

Extra tropical cyclones play a crucial role in determining the climate of the mid-latitudes. They are important for the transport of heat and moisture polewards (Wallace and Hobbs, 2006). One of the earliest publications providing an overview of the life cycle of an extra-tropical cyclone was Bjerknes and Solberg (1922) and is referred to as the Norwegian model. In the Norwegian model, cyclones are assumed to occur due to instabilities in a pre existing front. A front or frontal zones are sharp horizontal gradients or discontinuities in wind and temperature (Wallace and Hobbs, 2006). In Bjerknes and Solberg (1922) it was proposed that cyclones form

(cyclogenesis) along the polar front which separates cold air over higher latitudes from the warmer southern latitudes. The Norwegian model is a largely qualitative model, developed without access to upper air measurements (Mailier et al., 2006). The Norwegian model has remained influential to subsequent research, but it is now accepted that cyclones occur as a consequence of large scale forcing associated with horizontal temperature gradients and that the existence of a polar front is not a necessary condition for cyclogenesis (Carlson, 1991).

2.3.1 Storm track identification

Many extra-tropical cyclones start to grow in the cyclogenesis regions over the east coasts of North America and Asia. The warm waters of the Gulf stream and Kuroshio and the cold air from the continents result in the low level temperature gradients required for cyclone formation (Hoskins and Valdes, 1990). The subsequent cyclones are then steered by the westerly winds across the North Atlantic and North Pacific before decaying (cyclolysis) near western Europe and the west coast of North America (Hoskins and Hodges, 2002). The Atlantic and Pacific of enhanced cyclone activity are often referred to as storm tracks. It should be noted that the term storm tracks is used to refer to the path taken by an individual cyclone during its life cycle, as well as to describe a region of enhanced cyclone activity. In this thesis the latter definition of a storm track is used.

Most studies on extra tropical cyclones have used one (or both) of two methodologies for exploring storm tracks (Hoskins and Hodges, 2002). The first approach involves measuring statistics, such as the variance, at grid points for atmospheric variables (e.g. sea level pressure) which are relevant to extra tropical cyclones for synoptic timescales (one day to one week). This is sometimes called an *Eulerian* approach, and has been used in studies such as Hoskins and Valdes (1990) to investigate the behaviour of storm tracks. An Eulerian approach has the advantage of being straightforward to implement and provides a general storm track activity measure. The second approach involves observing individual storms throughout

their life cycles which can be done manually using synoptic charts or by using automated feature tracking methods, e.g. Hodges (1994). This is referred to as a *Lagrangian* approach and has become more widely used in recent years due to the increased accessibility of automated tracking algorithms.

Hoskins and Hodges (2002) compared the Eulerian and Lagrangian approaches for diagnosing storm track statistics for the ECMWF reanalysis (ERA-15) using a range of atmospheric variables, such as mean sea level pressure (MSLP) and vorticity. The Eulerian method was to consider the band passed filtered variance of these variables, while the Lagrangian approach used Hodges tracking algorithm (Hodges, 1994) to identify and track individual cyclonic and anti-cyclonic features as defined by these variables. Both approaches identified the North Atlantic and North Pacific storm tracks and provided measures of the activity. The Lagrangian approach had the advantage of being able to differentiate between cyclonic and anti-cyclonic systems as well as provided information about individual systems.

2.4 European extra tropical cyclone risk

Accurate assessments of the frequency and intensity of extra tropical cyclones is crucial for those working in fields such as engineering and reinsurance (Della-Marta et al., 2009). Few studies have modelled the risk of extra tropical cyclones in financial terms due to a lack of available loss data for researchers (Pinto et al., 2007). Studies relying on loss data for extra tropical cyclones are also hampered by the non-stationarity of economic losses due to changes in economic and societal vulnerability (Barredo, 2010). Instead a large number of studies have been conducted on extra tropical cyclone data using both reanalyses and Global Circulation Models (GCM) (Ulbrich et al., 2009). The conclusions of these studies are sensitive to the choice of dataset, which cyclone attribute is considered and how it is tracked (Raible et al., 2008). A comparison of tracking methods found that agreement was generally higher between methods for stronger cyclones than weaker cyclones and that for cyclone count statistics there was a strong qualitative agreement with the

exception of certain regions, particularly the Mediterranean (Neu et al., 2012). A study comparing cyclone statistics between the NCEP-NCAR and ERA40 datasets found reasonably good agreement over northern Europe and eastern North America, but not over the extra tropical oceans (Wang et al., 2006).

Trends

Past and future changes in extra tropical cyclone activity due to anthropogenic climate change is an area of interest for researchers. Investigations into such changes is complicated by changes in observational data, such as the spatial and temporal density and the observing systems, which can result in spurious trends in the data (Bengtsson et al., 2004). For the Northern Hemisphere however, there has been found to be general agreement in the reanalysis datasets, with few sudden shifts or inhomogeneities (Ulbrich et al., 2009).

Although historical trends are sensitive to the data and methodology used there are some broad conclusions that can be drawn from the literature for the Euro-Atlantic region. A study using the ERA-40 and NCEP-NCAR reanalyzes found a decreasing trend in counts over central Europe but an increasing trend over northern Europe for both datasets (Trigo, 2006)). These findings agree with (Wang et al., 2006) where a decrease in cyclone frequency was found over the mid-latitude North Atlantic and an increase over Northern Europe, due to a northward shift of the storm track.

Climate change experiments

GCM output has been used in the literature to quantify projected changes in extra tropical cyclone activity under different greenhouse gas emission scenarios. Simulations of future climate using models from the Coupled Model Inter comparison Project (CMIP5) were used in Zappa et al. (2013), where there was found to be a small but significant increase in the number of all cyclones over the British Isles, and an increase in the mean wind speed of the most intense cyclones over the same

region and central Europe between December and February when considering the multi-model means. These conclusions agreed qualitatively with earlier studies using single climate models (Leckebusch and Ulbrich, 2004) . In Sansom et al. (2013) an investigation of the robustness of cyclone frequency changes to the choice of CMIP5 models was conducted, and it was concluded that climate change signals were statistically significant and not dependent upon the choice of model.

As well as the changes in the physical attributes of extra tropical cyclones, climate models have been used to investigate the change in loss potentials for Europe under future climate conditions (Pinto et al., 2007; Leckebusch et al., 2007). Both of these studies estimate losses using a loss index developed in Klawa et al. (2003), using the upper 2% quantile of windspeeds and population data. The conclusions were similar with both studies showing increased loss potential for parts of Europe under a no adaptation hypothesis. A similar approach using a proprietary loss model instead of the loss index was considered in Schwierz et al. (2010). Here the change in return levels for the annual mean loss, and the 10,30 and 100 year return periods were shown to increase for a European market portfolio under climate change projections. All three studies considered the exposure (population, insured property values) constant, therefore changes in future loss distributions were due solely to projected changes in extra tropical cyclone activity.

Modulation by climate modes

The level of activity along the storm tracks and their position exhibits variability on timescales ranging from days to decades. This variability can partly be explained by changes in the large scale atmospheric circulation patterns which also vary over these timescales (Stephenson et al., 2006; Seierstad et al., 2007; Raible, 2007). For example, positive phases of the North Atlantic Oscillation pattern have been shown to be associated with increased cyclone occurrence and a polewards shift of the position of the North Atlantic storm track (Rogers, 1997). Conversely negative phases of the NAO are associated with a southward shift of the storm

track and decreased cyclone occurrence. This relationship arises as the NAO modulates environmental factors such as the position of the jet stream which in turn influences cyclone steering (Pinto et al., 2009). As well as cyclone steering the positive phase of the NAO is linked to larger areas with suitable growth conditions for extreme cyclones (Pinto et al., 2009). Here extreme cyclones were shown to occur more frequently during strongly positive phases of the NAO, as well as having longer lifetimes and higher intensities. An extreme value approach used in Sienz et al. (2010), where the NAO index was used as a covariate for the parameters of a GPD fitted to cyclone intensity measures, broadly supported these conclusions.

Much less attention has been paid in the literature to the relation between the Scandinavian pattern (SCP) and the East Atlantic Pattern (EAP) and extra tropical cyclone activity. Although the NAO is the dominant driver of cyclone activity over much of the North Atlantic ocean, over mainland Europe regression studies have consistently found the SCP coefficient to be significant (see e.g. Mailier et al. (2006) Fig. 8c, Vitolo et al. (2009) Fig. 11 e,f and Seierstad et al. (2007) Fig. 4 c). Therefore inclusion of these patterns is also important in extra tropical cyclone risk studies for Europe.

2.4.1 Clustering

An area of ongoing research, which is of substantial interest to the insurance community, is the clustering of windstorms over Europe. The first rigorous statistical analysis of the clustering of extra tropical cyclones was presented in Mailier et al. (2006). The NCEP-NCAR reanalysis was used to investigate the clustering of monthly cyclone counts over the Northern Hemisphere. Overdispersion in cyclone counts was found to be greater than expected by chance over the exit region of the North Atlantic storm track and the central North Pacific. The cyclone counts over the western Atlantic and North Pacific regions of the storm track were more regular than to be expected by chance (under-dispersed counts). Mailier et al. (2006) used a Poisson regression approach, as described in Section 2.2, is used to investigate

possible atmospheric drivers of clustering. Two possible physical mechanisms proposed in the study to explain the clustering of extra tropical cyclones are described below.

Secondary cyclogenesis was first proposed along with the Norwegian model in Bjerknes and Solberg (1922). Here the primary or parent cyclone creates a front in its wake along which new secondary cyclones can form. The existence of secondary cyclogenesis has been validated in later studies, for example Dacre and Gray (2009), which showed that not all North Atlantic extra tropical cyclones that form over the Gulf Stream make it to western Europe. Instead some cyclones dissipate over the middle of the Atlantic after giving rise to secondary cyclones which track further eastwards towards Europe.

However, the clustering process of secondary cyclogenesis does not occur for most observed storm clustering. For example, an analysis of the Christmas storms of 1999 shows that the spatial separation between Lothar and Martin at the time of genesis for Martin was 3500km, making secondary cyclogenesis unlikely (Mailier et al., 2006) . The second mechanism suggested in Mailier et al. (2006) for clustering is the rate varying affect of background atmospheric conditions. Large-scale flow patterns such as the NAO associated with the position and strength of the jet stream, can result in increased numbers of cyclones following similar trajectories,and thereby clustering. In Mailier et al. (2006) it was concluded that clustering was largely due to this rate variation as shown in the residuals of the Poisson regression.

The dependence of clustering on the length of winter and the individual cyclone intensity was further investigated in Vitolo et al. (2009). Clustering was found to increase with winters up to 6 months in length, as well as with intensity threshold (see Fig. 2.1). As in Mailier et al. (2006), the relationship between cyclone counts and large scale flow patterns was analyzed. As well as the NAO, the EAP and the

SCP were found to be key drivers of the observed cyclone clustering over parts of Europe. The increased clustering for more intense storms was discussed in Hanley and Caballero (2012), where it was shown that the same atmospheric conditions were responsible for cyclone steering and intensification.

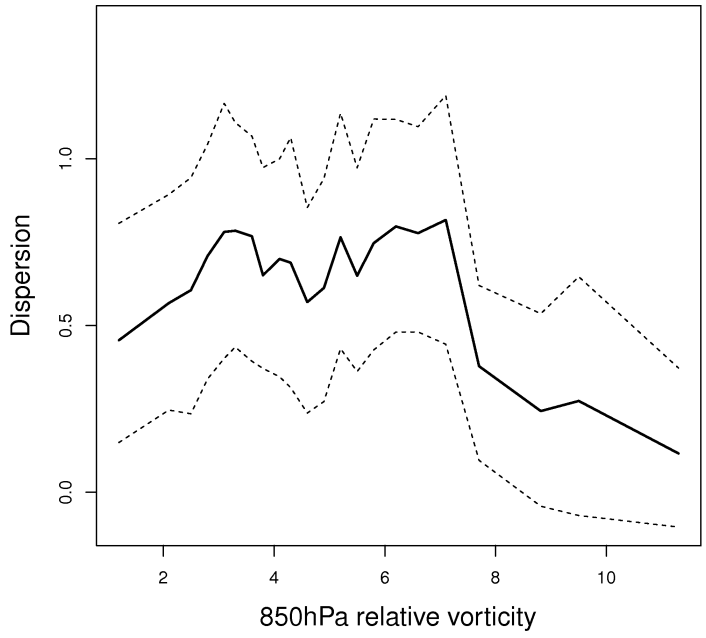

Figure 2.1: Dispersion statistic (solid line) and 90% bootstrap confidence interval (dashed) of the 3-monthly cyclone counts at the approximate location of Berlin (12.5E,52N) as a function of the 850 hPa relative vorticity threshold used to select the most intense cyclones

Clustering of extra tropical cyclones has also been investigated in climate model output (Kvamstø et al., 2008). The ARPEGE general circulation model was able to reproduce the spatial patterns of extra tropical cyclone clustering although with diminished magnitude. The relationship between the large scale flow patterns and cyclone counts was not well reproduced by the ARPEGE model. Clustering under future climate conditions were investigated in Pinto et al. (2013). A large ensemble of ECHAM5/MPI-OM1 (European Centre Hamburg Version 5 /Max Planck Institute Version - Ocean Model Version 1) global climate model (GCM) simulations was used to investigate the ability of climate models to reproduce clustering and changes in clustering over the North Atlantic under future climate conditions. Clus-

tering of cyclone counts in the ensemble over western Europe was found to decrease under present greenhouse gas emission scenarios between 2060-2100, particularly for intense cyclones.

2.4.2 Aggregate risk

Several studies have estimated return periods for extra tropical cyclones, based on physical variables (Della-Marta et al., 2009; Kunz et al., 2010; Sienz et al., 2010) and financial loss (Rootzén and Tajvidi, 1997; Schwierz et al., 2010). As discussed at the end of Section 2.2.6, these methods are unsuitable for calculating insurer's PML, which depends on the aggregation of all losses in a year, not just individual events. Insured losses from extreme European windstorms, taken from the Extreme Windstorm Catalogue[2] (XWS), are reported in Table 2.1. The cluster of cyclones which struck Europe in December 1999 resulted in over $ 14 billion in insured losses, of which the most expensive event, Lothar, accounts for only around half (Table 2.1). Similarly for the January/February 1990 cluster (including Wiebke and Herta), which resulted in a total of $16.7 billion in insured losses, the most expensive event Daria was again responsible for only around half. Therefore modelling the behaviour of extreme events individually is not sufficient in quantfying the aggregate loss distribution.

Wang et al. (2006) introduced a measure of seasonal aggregate extra tropical cyclone activity, defined as the sum of the mean intensities (determined using mean sea level pressure (MSLP)) of all cyclones in a season. This aggregate measure was used to compare cyclone activity between the NCEP-NCAR and ERA40 reanalysis, which found the datasets to be in good agreement over northern Europe and eastern North America. However the study did not consider return periods for this metric, or the relation with large scale flow patterns or any other modelling assumptions. Similarly a measure of the aggregate daily storm severity was introduced in (Leckebusch et al., 2008), to investigate storm severity under anthro-

[2]http://www.europeanwindstorms.org

progenic climate change, but not the relation between aggregate cyclone activity and clustering or large scale flow patterns.

Insurers need to be able to reliably assess the risk from the aggregation of extreme events. However, no published studies have formally assessed the aggregate risk of extra tropical cyclones, particularly with regards to clustering or climate change. In Pinto et al. (2013) and Vitolo et al. (2009) the potential for clustering to result in large cumulative losses is discussed anecdotally but not formally investigated. A framework for aggregate loss that can investigate the effect of clustering, climate change and environmental factors that influence cyclone steering and intensification would allow more accurate assessment of the risk for decision makers.

Name	Date	Insured losses (USD)	Maximum Vorticity	Affected countries
Daria	25/1/1990	8.2bn	11.9	BEL, FRA, DEU, NLD, GBR
Lothar	26/12/1999	8.0bn	6.43	FRA, DEU, SWI
Kyrill	18/1/2007	6.7bn	8.6	AUT, BEL, FRA, DEU, IRL, NLD, GBR
87J	16/10/1987	6.3bn	10.2	FRA, GBR
Vivian	26/2/1990	5.6bn	9.5	BEL,FRA, DEU, NLD, GBR
Klaus	24/1/2009	3.5bn	9.3	AND, FRA, DEU, ITA,ESP, SWI
Martin	27/12/1999	3.3bn	9.2	FRA, ITA, SWI
Xynthia	27/2/2010	2.9bn	9.6	BEL, FRA, DEU, POL, PRT, ESP, SWE, GBR
Anatol	3/12/1999	2.6bn	11.0	DNK, DEU, SWE
Erwin	8/1/2005	2.2bn	9.8	DNK, IRL, NOR, SWE, GBR
Herta	3/2/1990	1.5bn	13.4	BEL, FRA, DEU, NLD, GBR
Wiebke	28/2/1990	1.4bn	7.8	BEL, FRA, DEU, NLD, SWI, GBR
Emma	29/2/2008	1.4bn	9.6	AUT, BEL, CZE, DEU, NLD, POL, SWI
Gero	11/1/2005	0.6bn	8.6	IRL, GBR
Ulli	3/1/2012	0.2bn	10.2	GBR
Dagmar	26/12/2011	0.04bn	8.6	FIN, NOR

Table 2.1: European windstorms that have resulted in high insured losses (Source: Extreme Wind Storms (XWS) Catalogue). The insured losses have been adjusted to 2012 values. Country codes are, Austria (AUT), Andorra (AND), Belgium (BEL), Czech Republic (CZE), Denmark (DEN), Finland (FIN), France (FRA), Germany (DEU), Great Britain (GBR), Ireland (IRL), Italy (ITA), Netherlands (NLD), Norway (NOR), Poland (POL), Portugal (PRT), Spain (ESP), Sweden (SWE), Switzerland (SWI).

2.5 Data

This thesis has used historical storm tracks from two reanalysis datasets. Reanalysis datasets are derived from numerical weather prediction models (NWP) which have assimilated historic observations.

2.5.1 Cyclone track database

The cyclone tracks considered here were obtained from the 6-hourly reanalyzes of the extended October-March winters between 1950/1 - 2002/3, which was produced jointly by the National Centers for Environmental Prediction and the National Center for Atmospheric Research (NCEP-NCAR reanalysis) (Kalnay et al., 1996; Kistler et al., 2001), as well as the ERA40 reanalysis of the October-March winters between 1958-2002/3 produced by the European Centre for Medium-Range Weather Forecasts (ECMWF) in collaboration with many institutions (Uppala et al., 2005). The mean sea level pressure (MSLP) and the zonal and meridional $850mb$ wind components were extracted. This dataset has been widely used in previous extra tropical cyclone studies e.g. Mailier et al. (2006); Vitolo et al. (2009); Zhang et al. (2004).

An objective tracking algorithm was used on the data extracted from the NCEP-NCAR reanalysis to provide storm tracks defined at 6-hourly intervals, from October 1950 to March 2003 (Hodges, 1994; Hodges et al., 1995; Hodges, 1999). The tracking algorithm calculates the following intensity variables: vorticity, sea level pressure and max wind speed (Fig. 2.2). In this thesis relative vorticity ξ_{850} is used as an intensity measure, which is less influenced by the background state of the atmosphere than MSLP as it focuses on smaller spatial scales. The vorticity has also been used effectively as the cyclone intensity measure in previous studies on extratropical cyclone risk (Mailier et al., 2006; Vitolo et al., 2009).

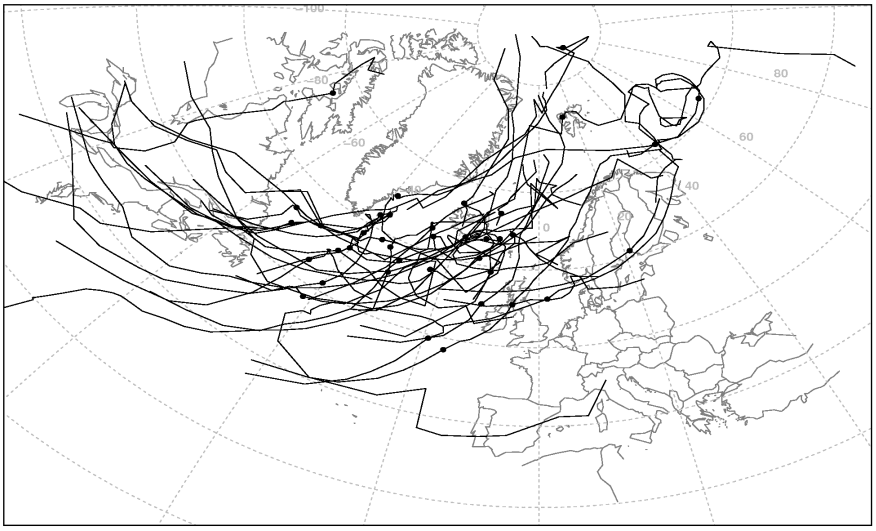

Figure 2.2: Cyclone tracks for the October 1989 to March 1990 extended winter. Only a subset of tracks is plotted: ones where any 6-hourly MSLP value reached below 960hPa. Nadir positions are denoted with solid circles (Source Economou et al. (2014)).

As in Mailier et al. (2006) a spatial grid covering the Northern Hemisphere between $[180W, 180E]$ in longitude and $[20N, 80N]$ in latitude was used to provide a set of reference points. Here the spatial resolution was 2.5° in both longitude and latitude. At each grid point the vorticity of cyclones as they passed within ±10° was recorded (Fig 2.3). Time series of the total winter counts and winter local mean vorticity could then be constructed for all grid points for each winter. Previous studies have typically used aggregation periods of one or three months (e.g. Vitolo et al. (2009)). Here the extended winter (six month) aggregation period is used instead as it reflects the aggregation period of losses which would be used by an insurer.

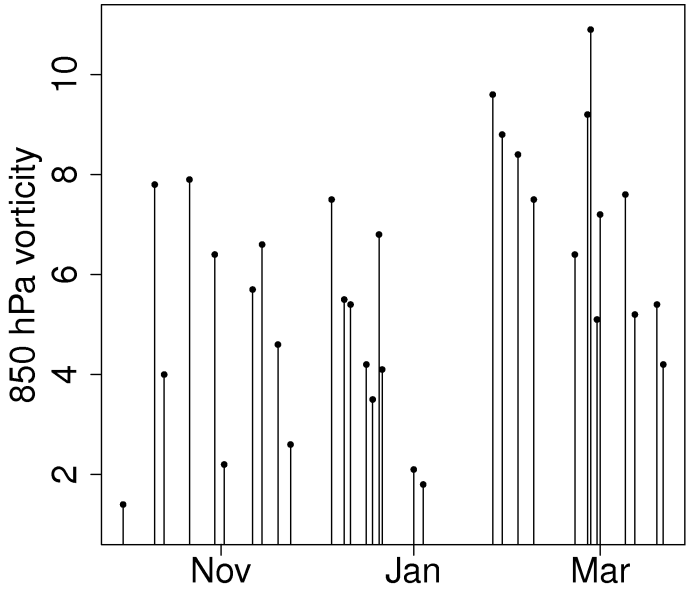

Figure 2.3: Time series of cyclone transits passing near Gothenburg [12.5°E, 57.5°N] between October 1989 and March 1990.

The results of any analysis of cyclone tracks will be sensitive to the database, tracking algorithm and cyclone intensity measure used (Ulbrich et al., 2009). To assess the robustness of any analysis to the choice of database parts of the analysis conducted in this thesis was also repeated for the ERA 40 reanalysis (European Centre for Medium-Range Weather Forecasts 40 Year Re-analysis) and shown in Chapter 3. Alternative tracking methods and intensity measures were not considered here, however an investigation into extra tropical cyclones using an alternative tracking method and intensity measure was found to produce qualitatively similar results to alternate studies which used Hodges algorithm and vorticity as an intensity measure (Pinto et al., 2013).

2.6 Summary

Previous studies have focused on individual attributes of hazards such as their frequency or intensity, or the risk from individual extreme events. An exception to this is U.S. hurricanes, where a few studies have considered total losses under re-

strictive conditions, e.g. Katz (2002); Jagger et al. (2008). In this thesis, a general framework for aggregate losses is introduced and modelling assumptions are investigated in detail. Particular attention will be paid to modelling the extremes of the aggregate loss due to the relevance of this quantity for society and the insurance sector.

This chapter has described methods used in the literature. Extra tropical cyclones have been introduced as a relevant case study for developing a framework for modelling aggregate risk. The same database of extra tropical cyclone tracks as used in Mailier et al. (2006) and Vitolo et al. (2009) is used here.

Chapter 3

Understanding the aggregate risk of extra tropical cyclones

3.1 Aim

In this chapter the aggregate risk of Northern Hemisphere extra tropical cyclones is investigated. Models for the aggregate risk using teleconnection indices as explanatory variables are then analyzed. The robustness of these results is considered by testing sensitivty to choice of reanalysis data.

3.2 Collective risk models

The risk posed to society by natural hazards is often accumulative involving both the frequency of occurrence and the intensity of events. To fully quantify the aggregate risk from extra tropical cyclones one requires a measure of cyclone activity which includes both the frequency and intensity. Such a metric exists in the risk management community called the annual aggregate loss (AAL) and is defined as the sum of the intensities (losses) for all events in a year. The distribution of the AAL can be investigated using a collective risk model (Prabhu, 1961). In this section the basic formulation of a collective risk model is described and applied to extra tropical cyclones.

Collective risk theory has its roots in the actuarial literature, dating back to the start of the 20th century (Houston, 1960). In the collective risk model formulation both the number of claims and size of individual claims are assumed random. The AAL is therefore modelled as the sum of a random number of random variables and so is sometimes also called the random sum model (McNeil et al., 2005). Collective risk theory was developed by Filip Lundberg between 1909-1939, however it was not widely adopted by the actuarial community as the relatively large amount of computational power required to apply the theory made it of little practical use (Borch, 1967). Increases in computer power allowing the implementation of techniques such as Monte Carlo simulation have resulted in collective risk theory becoming widely adopted by the insurance industry over the latter half of the 20th century, and collective risk models are now considered the bread and butter of insurance mathematics (Embrechts et al., 1997). Collective risk theory also has the potential to be used in climate science, for example to model annual U.S. hurricane losses (Katz, 2002) or total monthly precipitation (Katz and Parlange, 1998).

3.2.1 Frequency and intensity

Extremes in a single meteorological variable at a specific location can be modelled as a marked point process (see Section 2.2). Events occur at irregular times T_i with variable intensities X_i (see Fig. 3.1). For natural hazards the occurrence of events is typically modelled as a Poisson process, where $N(t)$ denotes the number of occurrences in a time interval $[0, t]$ (McNeil et al., 2005). Each individual occurrence has a mark or intensity[1] $X_1, ..X_N$ (see Fig. 3.1). The number of occurrences N is a non negative integer valued random variable, while the intensities X_i are real valued random variables. The aggregate risk, also referred to here as the aggregate loss, S is the aggregate total intensity of the N events that occur in a given time

[1]Intensity is often used to refer to the rate parameter of the Poisson distribution. In this thesis intensity refers to the mark size X.

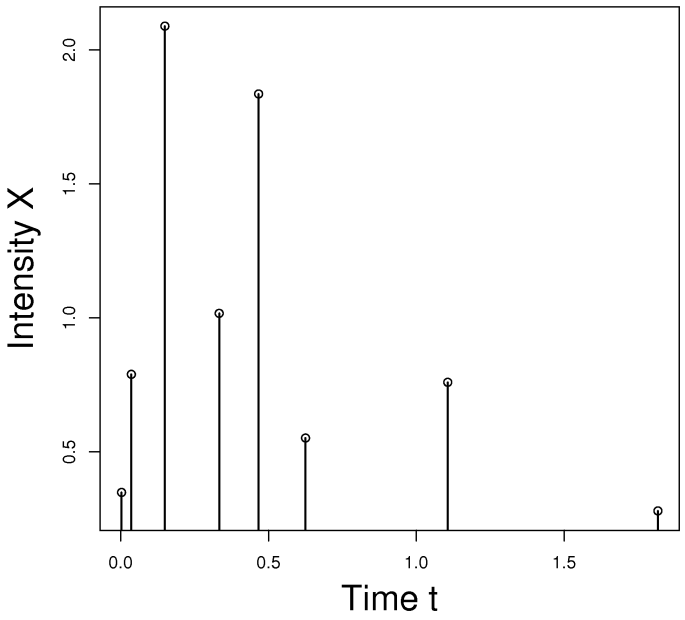

Figure 3.1: Example of a marked point process

period (e.g. over a season or year);

$$S = X_1 + ... + X_N = \sum_{i=1}^{N} X_i.$$

The mean expected aggregate loss can be expressed using the law of total expectation by conditioning on the number of events N

$$E[S] = E_N[\sum_{i=1}^{N} E[X_i|N]] = E[N]E[Y] + Cov(N, Y),$$

where Y is the mean intensity; ($Y = \sum_{i=1}^{N} X_i/N$). The variance of the aggregate risk from the law of total variance is

$$\begin{aligned} Var(S) &= E_N[(\sum_{i=1}^{N} X_i|N)] + Var_N(E[\sum_{i=1}^{N} X_i|N]) \\ &= Cov(N^2, Y^2) - [Cov(N, Y)]^2 - 2Cov(N, Y)E[N]E[Y] \\ &+ Var(N)E[Y]^2 + Var(Y)E[N^2] \end{aligned} \tag{3.1}$$

see Appendix A for details.

3.3 Climatology of aggregate risk

Here the aggregate risk of extra tropical cyclones for the Northern Hemisphere is investigated using the storm tracks obtained from the NCEP NCAR reanalysis as described in Chapter 2. The aggregate risk of extra tropical cyclones is estimated at each grid point as the sum of the vorticities of all cyclones passing within $\pm 10^o$ of latitude over the extended winter (Oct-Mar).

The mean cyclone counts $\bar{n}$ (see Fig. 3.2 a) show the location of North Atlantic and North Pacific storm tracks, agreeing with that shown in Hoskins and Hodges (2002). Areas of high cyclone activity can be seen in the lee of the Rockies in North America and east of the Urals as in Hoskins and Hodges (2002). The sample variance in cyclone counts s_n^2 (Fig. 3.2b) is greatest over the storm tracks with the maximum towards the exit region of the storm tracks. These findings agree qualitatively with those of the mean and variance of monthly counts in Mailier et al. (2006) and the 3 monthly counts in Vitolo et al. (2009), where both studies considered winter storm tracks from the NCEP-NCAR reanalysis.

Maxima of the sample local mean vorticity $\bar{y}$ can be noted over the North Atlantic and North Pacific storm tracks (Fig. 3.2 c). The variance in winter local mean vorticity is greatest along the north/south edges of the storm track, as well as a maxima over the North Western Pacific (Fig. 3.2 d).

The sample mean aggregate risk for the 6 month winter, $\bar{s}$, and variance s_s^2, shows a broadly similar pattern to the sample mean and variance of the cyclone counts (Fig. 3.2 e,f). This suggests that regional variation in the mean and variance of the aggregate loss might possibly be largely accounted for by regional variation in cyclone counts.

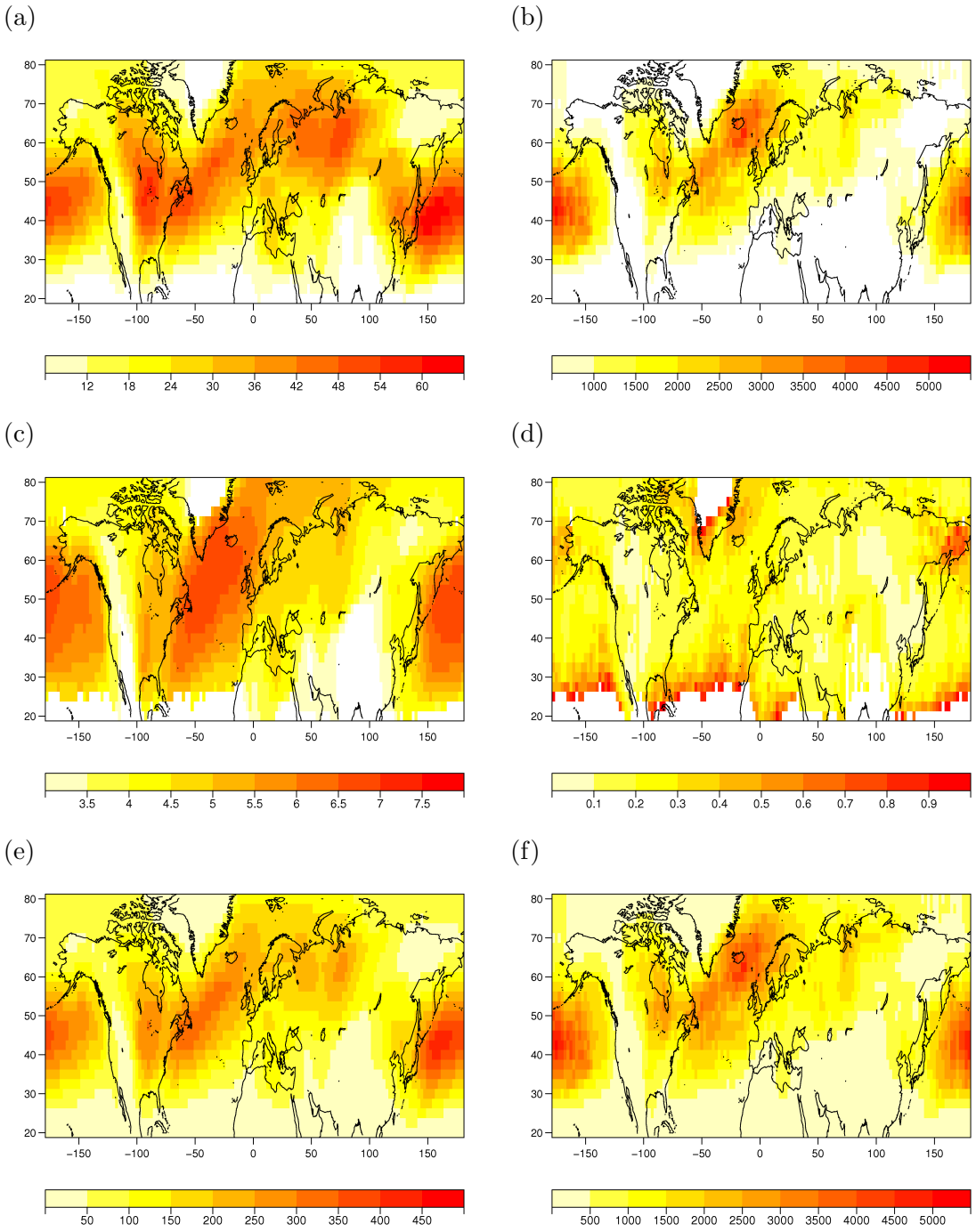

Figure 3.2: (a) Sample mean $\bar{n}$ cyclone counts per 6 month winter and (b) sample variance s_n^2 of winter cyclone counts, (c) sample winter local mean vorticity $\bar{y}$ (d) sample variance s_y^2 , (e) sample winter mean $\bar{s}$ of the aggregate loss and (f) sample variance s_s^2

To quantify sources of variation in the aggregate risk, the sample variance of s is expressed in terms of y, as in Eqn. 3.1, as $s_s^2 = V_n + V_y + V_c$, where

$$\begin{aligned} V_n &= s_n^2 \bar{y}^2 \\ V_y &= s_y^2 \bar{n^2} \\ V_c &= cov(n^2, y^2) - cov(n, y)^2 - 2cov(n, y)\bar{y}\bar{n} \end{aligned} \tag{3.2}$$

and $cov(.)$ is the sample covariance between n and y (see Appendix A for details). The terms V_n, V_y are non-negative as the sample mean and variance of the counts and vorticity is non-negative. The V_c can be negative if there is negative covariance between n and y. From Eqns. 3.1 and 3.2, positive covariance will increase the variance of the aggregate loss (both sample and population variance), conversely negative covariance results in lower s_s^2 and $Var[S]$. The component due to variance in counts, V_n, accounts for a large proportion $(50 - 80\%)$ of the variance in the aggregate loss of extra tropical cyclones over the North Atlantic and North Pacific storm tracks (see Fig. 3.3 a). Over the Kuroshio and the Gulf Stream, which are the primary regions of cyclogenesis for the storm tracks, $V_n > s_s^2$ (therefore $V_c < 0$) and over North Western Europe and the edges of the North Pacific storm track V_n accounts for less than half of s_s^2. The variance component due to variance in intensity, V_y, (Fig. 3.3b) account for less of the variance in s than V_n however still makes a significant contribution over the Gulf Stream and the Kuroshio. The variance component due to covariance between counts and intensity, V_c, (Fig. 3.3 c) accounts for the least of the variance in s along much of the storm tracks but is non-negligible and positive (negative) over the cyclesis(cyclogenesis) regions for the storm tracks. Including covariance between frequency and intensity is thus necessary for accurately modelling the variance in the aggregate risk of extra tropical cyclones.

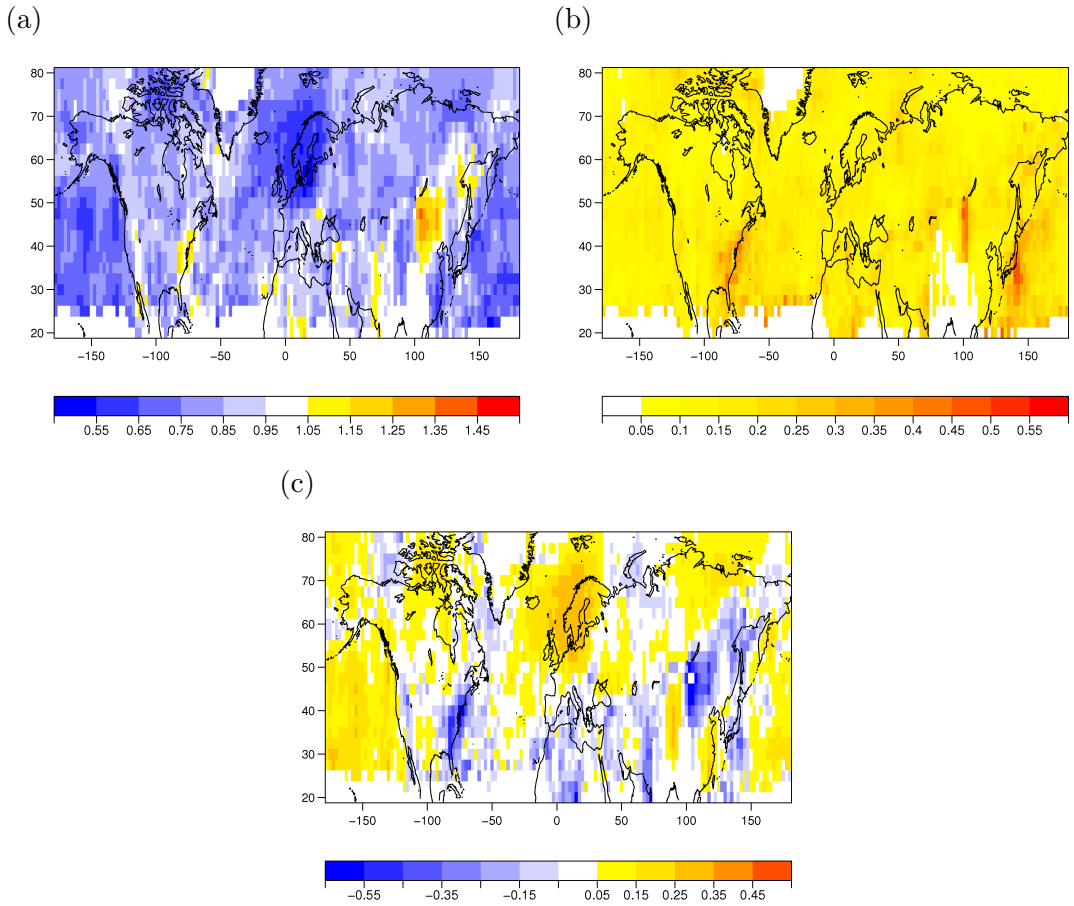

Figure 3.3: Proportion of variance in s accounted for by a) counts V_n/s_s^2 b) cyclone intensities V_y/s_s^2 c) covariance between the frequency and intensity V_c/s_s^2

3.4 Quantifying the frequency-intensity dependency and its impact on aggregate risk

It is of interest to further diagnose the magnitude and extent of correlation between the frequency and intensity. In this section correlation between frequency and intensity is quantified both for original and detrended time series of counts and local mean vorticity. Three parametrizations of a collective risk model are then proposed to investigate the impact of various modelling assumptions.

3.4.1 Sample correlation

Figure 3.4 shows a map of the (Pearson's) sample correlation r between n and y. Positive correlation between the frequency and mean intensity of extra tropical cyclones along the North Atlantic storms track can be seen over Scandinavia, Northern Germany and the Benelux countries ($r = 0.2 - 0.6$), as well as negative correlation over the Gulf Stream ($r = -0.3$). The North Pacific storm track shows similar patterns, with positive correlation towards the exit region of the storm track and negative correlation over the Kuroshio.

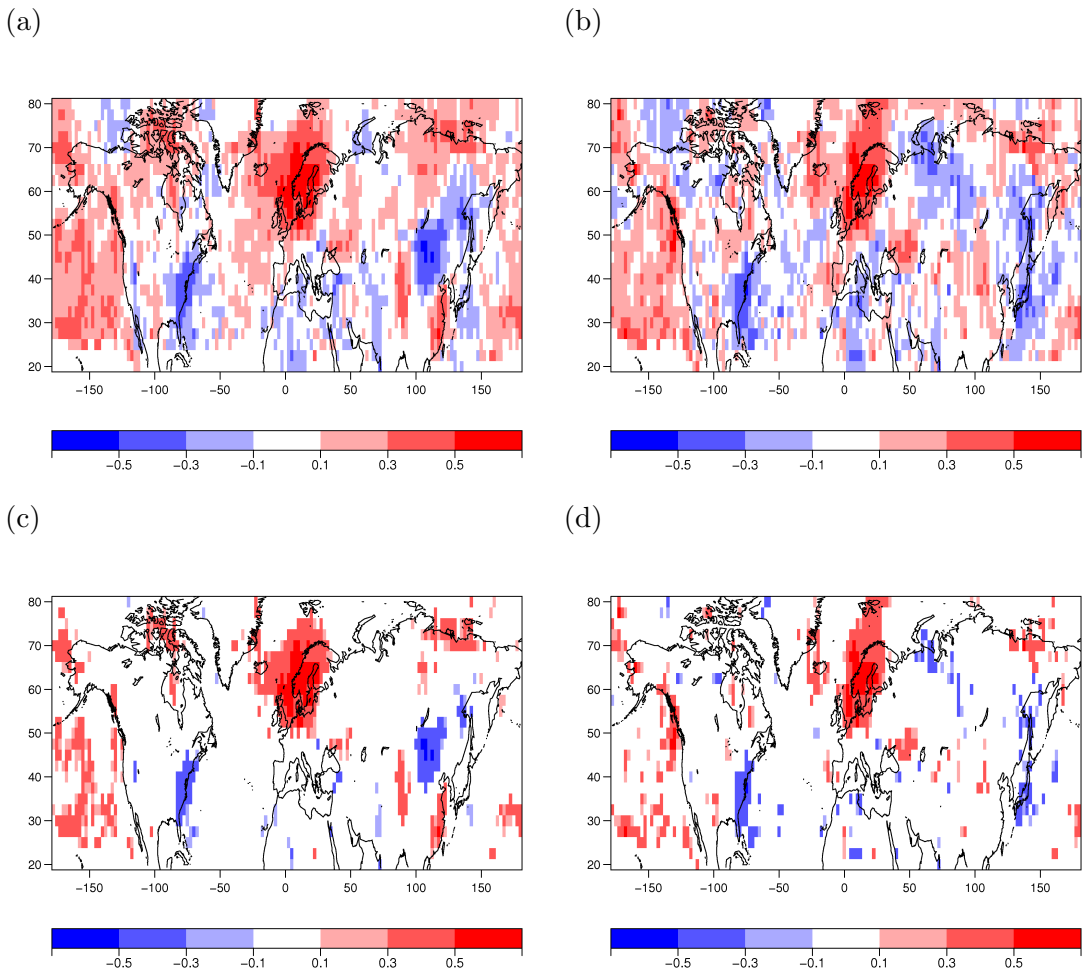

Figure 3.4: (a) Map of the correlation between n, y. b) Map of the correlation between $\Delta n, \Delta y$. Correlation between c) n and y and d)$\Delta n, \Delta y$ which is significant at the 5% level determined using the *cor.test* function in *R*.

Previous studies have shown that there are increasing trends in intense cyclone counts for the NCEP NCAR reanalysis between 1950-2003 (e.g. Mailier et al. (2006); Vitolo et al. (2009)). The time series of n and y at each grid point was detrended using a first order differencing method to assess if the observed correlation was due to trends in both the counts and local mean vorticity. Here we define Δn and Δy as

$$\begin{aligned} \Delta y_t &= y_t - y_{t-1}, \\ \Delta n_t &= n_t - n_{t-1}, \end{aligned}$$

where t is the extended winter. Figure 3.4 b shows the map of the correlation between Δn and Δy. For the North Atlantic storm track the magnitude and sign of the correlation between Δn and Δy is roughly equal to the correlation between n, y (Fig. 3.4 b) . The statistical significance of the correlation was assessed using the *cor.test* function in R, and values of $cor(n, y)$ and $cor(\Delta n, \Delta y)$ which were significant at the 5% level are shown in Fig. 3.4 c,d. The positive correlation over northern Europe and negative correlation over the Gulf stream can both be seen to be statistically significant at the 5% level, while much of the positive correlation over the North Pacific is insignificant after detrending. From this we can infer that the correlation between frequency and intensity of Northern European extra tropical cyclones is not primarily due to trends in the data. Increasing trends in Pacific cyclone frequency and intensity were investigated in Graham and Diaz (2001), where it was shown that these trends were unlikely to be an artifact of the observations or of reanalysis procedures, but are instead attributed to slow changes in background conditions such as increasing sea surface temperatures in the western tropical Pacific.

3.4.2 Covariance between the frequency and intensity

Three parametrizations of a collective risk model are proposed here for the mean and variance of S (see Appendix A.2 for detailed derivations). The purpose of these models is to test assumptions such as N and X are independent, and X_i and

X_j independent for $i \neq j$. The first parameterization, M_1, assumes there is linear dependence between N and X, and only allows for covariance between consecutive cyclones. Covariance is considered between consecutive cyclones as there may be some dependence due to secondary cyclogenesis, however there is no reason to assume non-neighboring cyclones will be related. The first model assumes that:

$$\begin{aligned} \mu_X|N &= \beta_0 + \beta_1 N \\ \sigma_{XX}|N &= \begin{cases} \sigma_X^2 & \text{for} \quad i = j \\ \rho\sigma_X^2 & \text{for} \quad i = j \pm 1 \\ 0 & \text{otherwise,} \end{cases} \end{aligned} \tag{3.3}$$

where ρ,σ_{XX} is the correlation and covariance between consecutive cyclone intensities respectively. The mean and variance of S can then be shown to be given by

$$\begin{aligned} \mu_S &= \beta_0\mu_N + \beta_1(\sigma_N^2 + \mu_N^2) \\ \sigma_S^2 &= \sigma_X^2\mu_N + 2(\mu_N - 1)\rho\sigma_X^2 + \beta_0^2\sigma_N^2 + \beta_1^2\sigma_N^2 + 2\beta_0\beta_1(\mu_{N^3} - \mu_N\mu_{N^2}) \end{aligned} \tag{3.4}$$

(see Appendix A.2). Sample estimates for σ_X^2 (s_x^2), ρ ($cor(x_i, x_j)$) were calculated from the dataset at each grid point, along with maximum likelihood estimates and standard errors for $\hat{\beta}_0, \hat{\beta}_1$ which were calculated using the lm function in R (not shown). Figure 3.5 shows the modelled variance σ_S^2 of the aggregate risk as well as the ratio of the modelled variance to the sample variance (σ_S^2/s_s^2). From Figure 3.5a,b σ_S^2 can be seen to provide a reasonable approximation to the sample variance s_s^2, as it is within $\pm 5\%$ for most grid points

For the second model parameterization, M_2, X and N are assumed independent and Eqn. 3.3 becomes $E[X_i] = \hat{\beta}_0 = \bar{x}$. Figure 3.5 c,d shows σ_S^2 underestimates s_s^2 by between $10 - 50\%$ over the storm tracks, with the greatest discrepancy over northern Europe and the eastern Pacific. For regions of cyclogensis over the Gulf Stream and eastern China, σ_S^2 is greater than the sample variance s_s^2 by up to 50%.

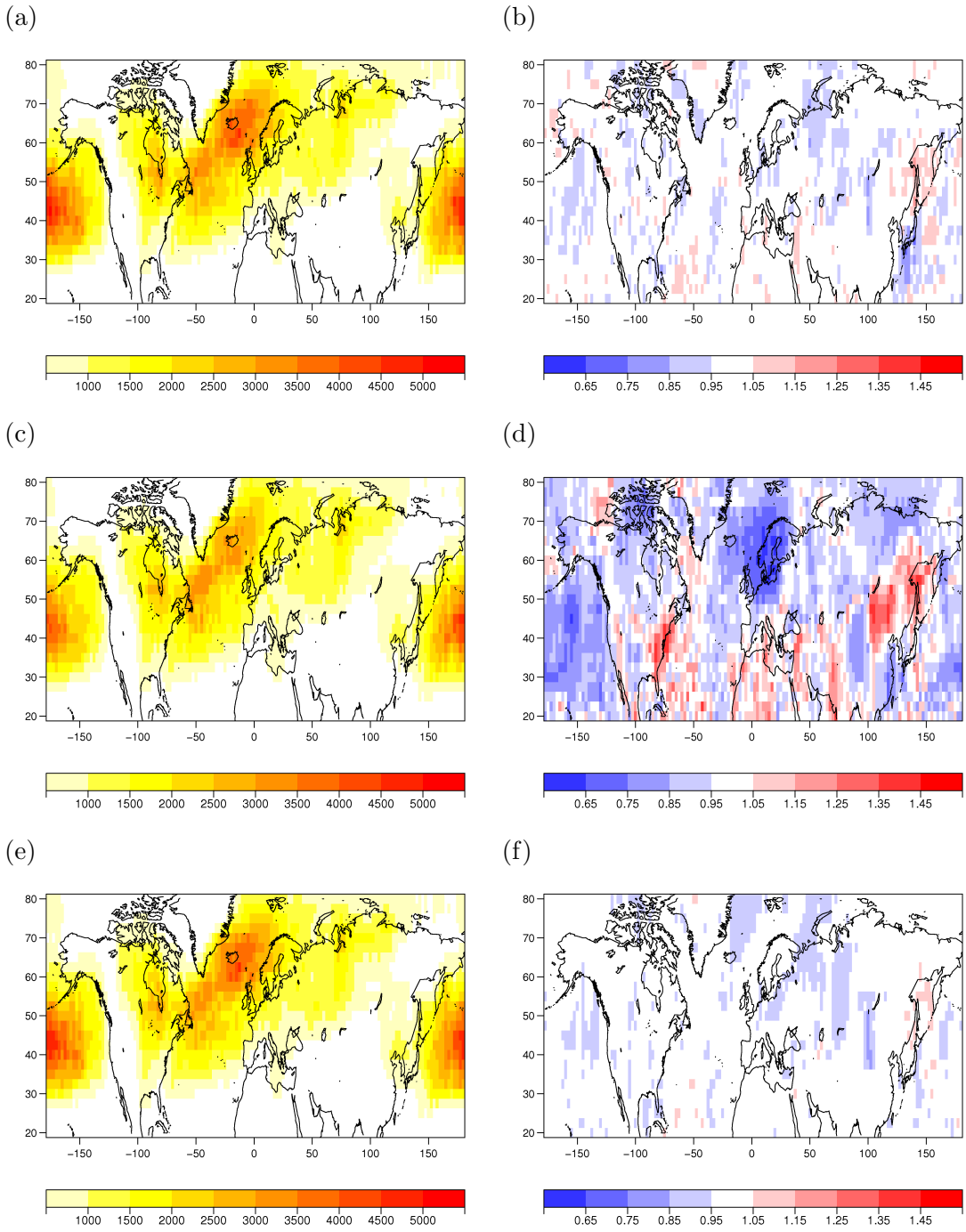

Figure 3.5: Left column; modelled variances σ_S^2 , right column; ratio of the modelled variance to the sample variance σ_S^2/s_s^2 . a,b) M_1 c,d) M_2 e,f) M_3

For the third model parametrization, M_3, X and N are again assumed linearly related but X_i, X_j are now assumed independent ($\rho = 0$). The modelled variance σ_S^2 (Fig. 3.5 e,f)) provides a reasonable approximation for s_s^2 although there is some

under estimation to the east of the Scandinavia.

The collective risk model is able to account for variance in the aggregate risk S, under suitable modelling assumptions. When X and N are assumed independent the model underestimates the variance of S over the exits of the storm track, and overestimates variance over the Gulf stream and the Kuroshio. Assuming independence between the intensities of consecutive cyclones does not significantly effect the modelled variance.

3.4.3 Sensitivity to choice of reanalysis data: NCEP-NCAR and ERA40

The sensitiviy of the existence of correlation to the choice of dataset was assessed using the ECMWF reanalysis (ERA-40). Cyclone tracks were obtained from the ERA-40 reanalysis using the same methodology as for the NCEP-NCAR reanalysis. Figure 3.6 shows the map of the correlation between n and y for both reanalysis datasets. Positive correlation is seen in both datasets over the same region of northern Europe as well as over the Pacific, and negative correlation can be seen over the east coast of the United States and eastern China. The main difference is that the positive correlation in ERA-40 over North Europe (North Pacific) is of smaller magnitude and extent than for the NCEP-NCAR reanalysis. Differences in storm tracks in the NCEP-NCAR and ERA-40 reanalysis has been noted in the literature (Trigo, 2006), but the findings here regarding the location and sign of the correlation between the datasets are in broad agreement.

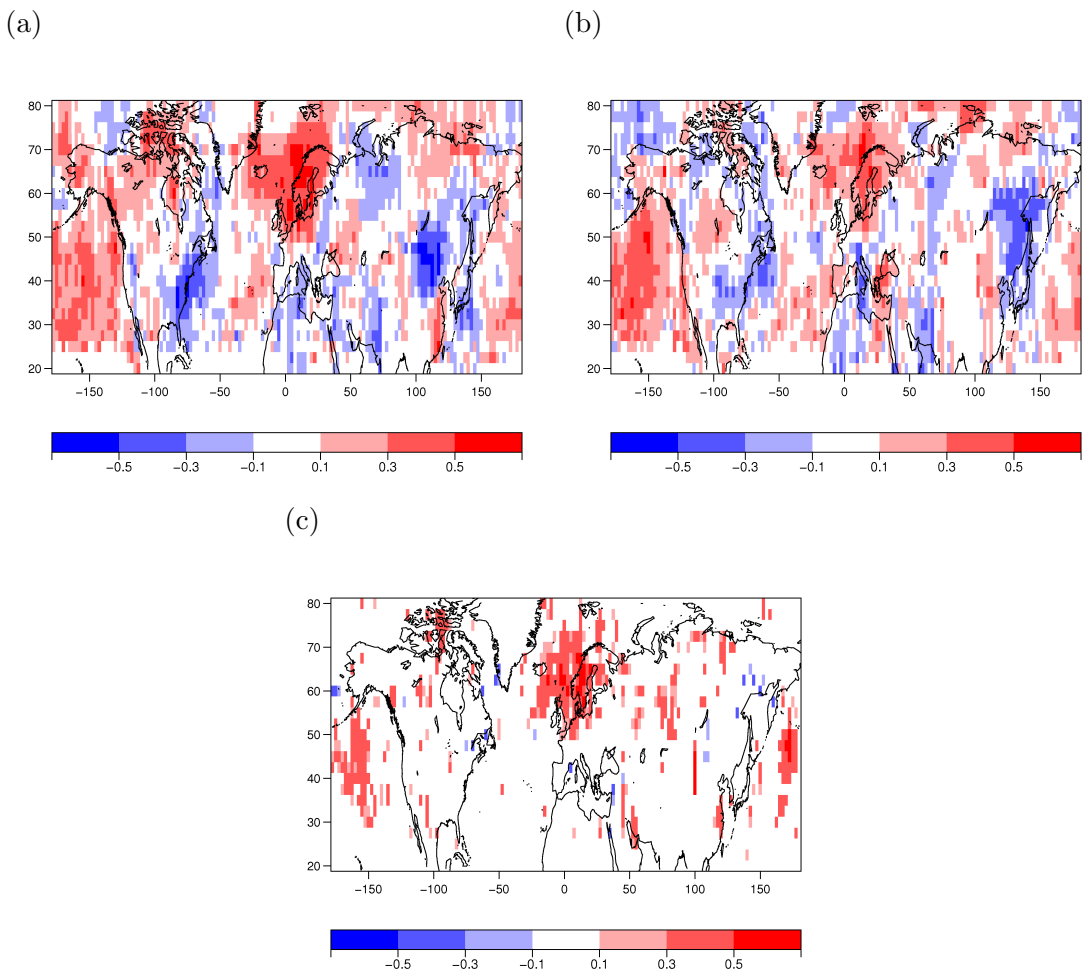

Figure 3.6: a) Map of the correlation between n, y for the NCEP-NCAR Reanalysis between 1958:2000. b)Map of the correlation between n, y for the ERA-40 Reanalysis between 1958:2000 c) Map of the correlation between n and y for the subset of the 50% most intense cyclones at each grid point for NCEP-NCAR 1958:2003

The correlation was also considered between the subset of the 50% most intense cyclones at each grid point for the NCEP-NCAR dataset (Fig. 3.6 c). The positive correlation over Scandinavia remain the most robust feature. The regions of negative correlation over the Gulf stream and Kuroshio have both dissapeared though, meaning the negative correlation is a feature of the weaker systems.

3.5 Can climate modes explain the frequency-intensity dependence?

This section investigated whether correlation between frequency and intensity could be due to joint forcing by underlying large-scale flow patterns (see Fig. 3.7). To test this hypothesis, winter cyclone counts and local mean vorticity are both regressed on the same set of climate indices as explanatory variables. Similar approaches have been successful in previous studies for explaining the clustering of extra tropical cyclones (Mailier et al., 2006; Vitolo et al., 2009).

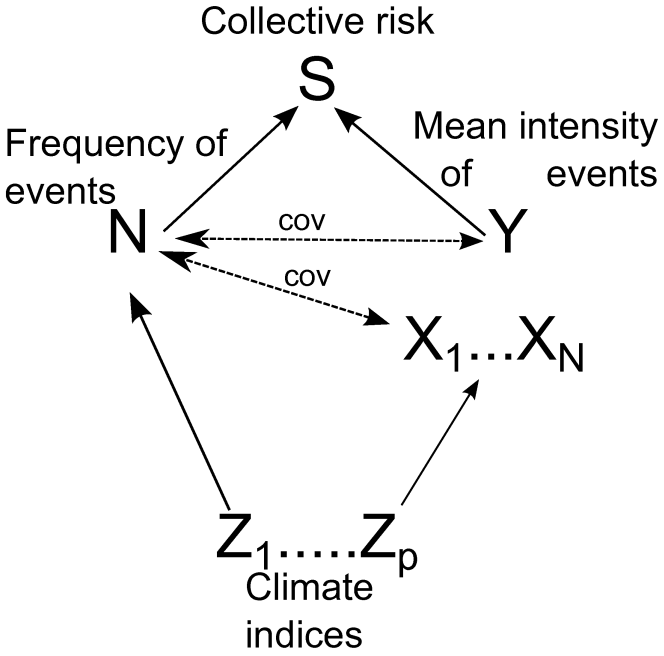

Figure 3.7: Schematic showing the suggested relationship between large scale flow patterns, frequency and intensity and the aggregate risk.

3.5.1 Large scale flow patterns

Barnston and Livezey (1987) identified 10 teleconnection patterns which describe the state of the large scale flow for the Northern Hemisphere. Monthly indices for these teleconnection patterns between 1950-2003 were obtained from the Climate

Prediction Center[2]. The indices were calculated using Rotated Principal Component analysis applied to monthly mean 700-mb geopotential height anomalies between January 1964 - July 1994, then for every month, 10 leading orthogonal functions (EOFs) are selected and the amplitudes are standardized to zero mean and unit variance. The teleconnection indices are mutually uncorrelated by definition, making them useful as a basis of explanatory variables in regression models.

The North Atlantic Oscillation (NAO), the leading mode of climate variability in the Northern Hemisphere, is characterized by a meridional dipole of pressure anomalies of opposite sign located over Iceland (low) and the Azores (high). The positive phase, which corresponds to below normal pressure over Iceland, has already been linked to increased cyclone activity over the North Atlantic in previous studies (Pinto et al., 2009; Rogers, 1997). The East Atlantic pattern (EAP) and Scandinavian pattern (SCP) are also important modes of variability in the winter months, and describe changes in pressure and in the position and speed of the North Atlantic jet stream which can influence cyclone activity (Woollings et al., 2010; Bueh and Nakamura, 2007). Plots of the $700mb$ stream function (Ψ_{700}) regressed on 6 month winter mean values of the NAO, EAP and SCP are shown in Fig. 3.8. The Azores-Iceland dipole pattern can be seen for the NAO (Fig. 3.8 a). For the SCP, the primary center of action can be seen over Scandinavia, with weaker centers of opposite sign to the west of Europe and over Mongolia (Fig. 3.8b). The EAP shows a similar pattern to the NAO but shifted south-east (Fig 3.8c).

[2]http://www.cpc.ncep.noaa.gov/data/teledoc/telecontents.shtml

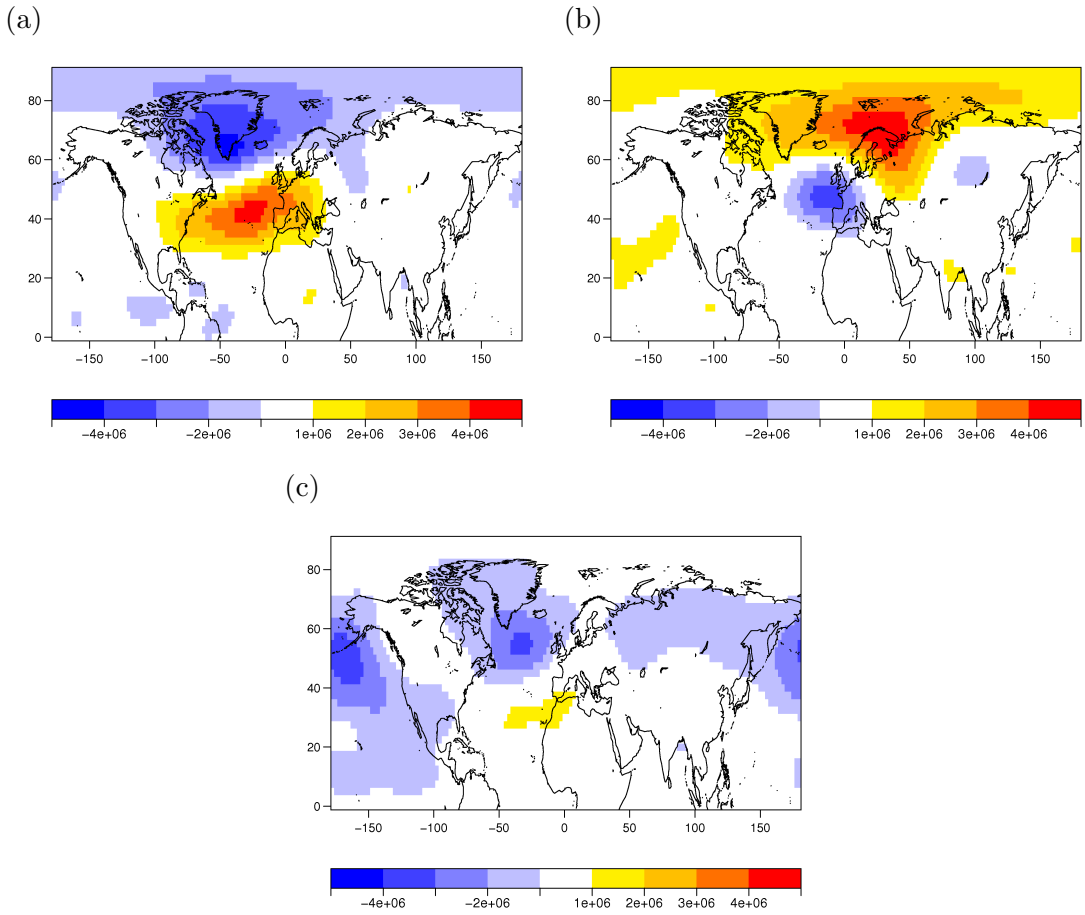

Figure 3.8: Maps of the linear regression coefficient of the a) NAO b) SCP c) EAP index winter mean regressed on the 700mb stream function Ψ_{700}

Extra tropical cyclones passing within ±10° north or south of the grid point nearest Gothenburg (Sweden) [12.5°E,57.5° N] were analyzed in detail as this location exhibits the strongest positive correlation between the frequency and intensity ($r = 0.47$). Cyclones passing the grid point closest to Barcelona (Spain) [2.5°E, 40° N] were also investigated as this is a location which has low negative correlation between n and y ($r = -0.10$). Correlation maps of n, y and the $700mb$ stream function were used to identify possible teleconnection patterns driving both frequency and mean intensity of extra tropical cyclones. The $700mb$ stream function was chosen as it had been used in a previous study investigating the relation between large-scale flow and extra tropical cyclone activity in the same region (Bueh and

Nakamura (2007)).

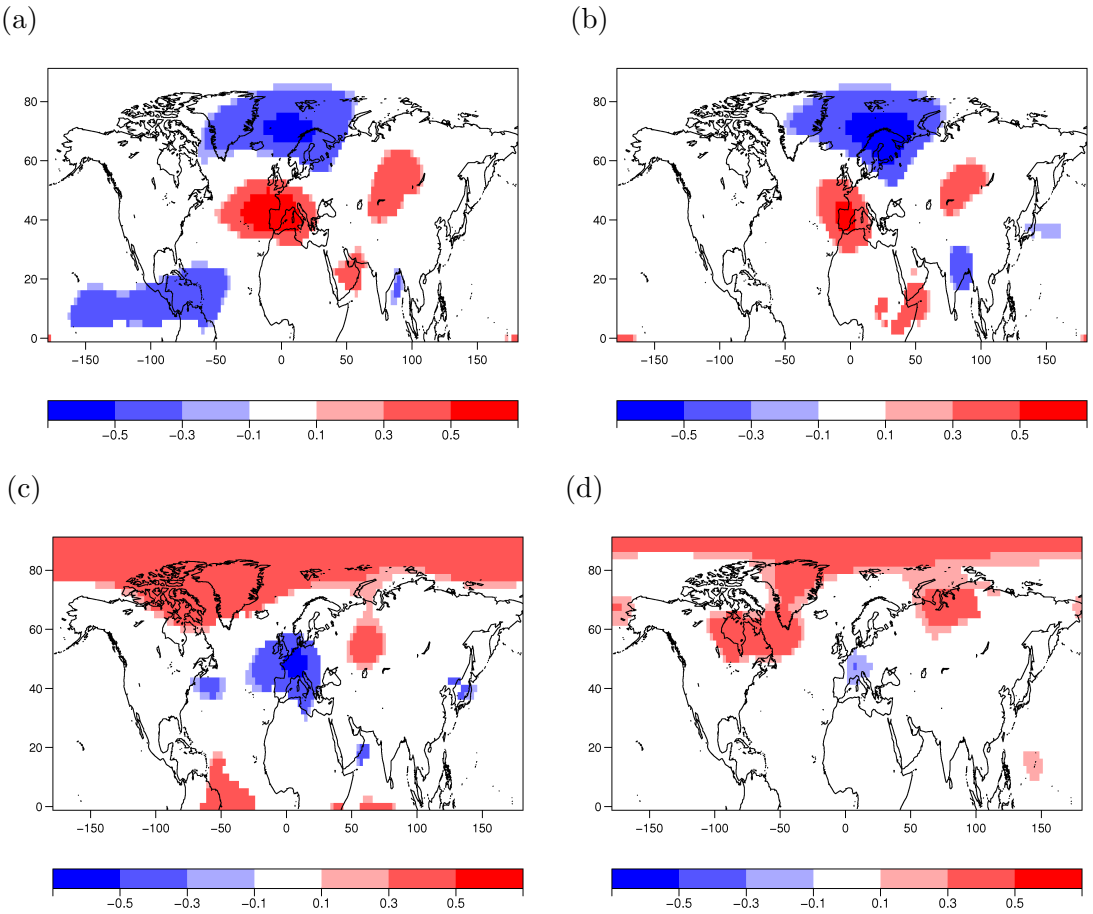

Figure 3.9: Plots of the correlation between the stream function Ψ_{700} and (a) Gothenburg cyclone counts n (b) Gothenburg mean vorticity y (c) Barcelona cyclone counts n (d) Barcelona mean vorticity y.

Correlation maps for n and y with Ψ_{700} at Gothenburg (Fig. 3.9a,b) show a broadly similar pattern, which shows a strong resemblance to the SCP shown in Fig. 3.8b, with a centre of action over Scandinavia and another of opposite sign over western Europe. The correlation of $\bar{\Psi}_{700}$ and n for Barcelona shows a centre of action centred over central Europe, with two other centres; one of opposite sign over west Russia/Kazakhstan, and another of the same sign located over the Gulf Stream (see Fig. 3.9(c)). The map of the correlation between the mean intensity y and Ψ_{700} also shows a tripole pattern, except the centre of action over Central

Europe is now the weakest of the three, and the location of the other two centres has been shifted northwards. A possible cause for the lower correlation between Barcelona frequency and intensity is due to the different atmospheric mechanisms which appear to be driving the steering and intensification.

3.5.2 Regression modelling of frequency and intensity

Regression models were developed for the frequency N and mean intensity Y to formally assess the association with large-scale flow patterns. Two models for counts and two for local mean vorticity were considered in this analysis. The first model for N and Y used teleconnection patterns considered particularly relevant for the North Atlantic region as explanatory variables. As well as the three North Atlantic teleconnection patterns discussed above, there is the East Atlantic/West Russian (EWP) pattern and the Polar/Eurasian (POL) pattern active in the region for some winter months. The second set of explanatory variables which was considered briefly were the teleconnection patterns relevant for the Pacific region.

As mentioned in Chapter 2, the occurrence of natural hazards can be modelled using a Poisson distribution. The winter cyclone counts N for Gothenburg and Barcelona were modelled as Poisson distributed with rate parameter λ_n (see e.g. Aitkin et al. (2009) for more on Poisson regression in R). The mean number of cyclone counts was related to the winter means of the teleconnection patterns using the following generalised linear model:

$$N \sim Poisson(\lambda_n)$$
$$log(\lambda_{n,t}) = \beta_0 + \sum_{k=1}^{6} \beta_k z_{k,t},$$

see Chapter 2. Here $k = 1, \ldots, 6$ and $t = 1, \ldots, 53$ is the year and $z_{2,t}, , ..., z_{6,t}$ are the values of the extended winter means of the teleconnection indices for the North Atlantic in year t. The Polar/Eurasian pattern $z_{6,t}$ is inactive during October, November and March and is set to zero for these months. The coefficient β_1 accounts for any linear time trend, and $\beta_2, ..\beta_6$ are the dependence of the cyclone

counts on the teleconnection patterns.

The goodness of fit for a generalized linear model can be assessed using the deviance residuals. When the model is well specified then the deviance residuals should be normally distributed with mean zero. A plot of the quantiles of the deviance residuals against a theoretical normal distribution is shown in Fig. 3.10a. Apart from a slight deviation in the lower tail (suggesting the model is not as appropriate for years with low counts), the deviance residuals are well-behaved. The plot of the log fitted values against the deviance residuals (Fig. 3.10 b) also suggests a good fit for the model; the residuals are evenly spread around zero and with approximately constant variance.

(a) (b)

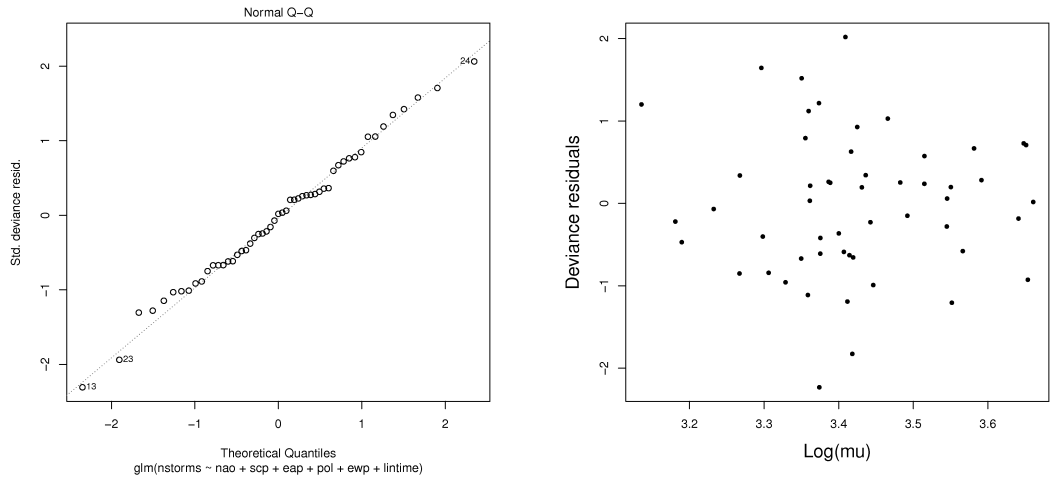

Figure 3.10: a) QQ- plot of standardized deviance residuals. b)Deviance residuals plotted against log fitted values

Following Vitolo et al. (2009), a Lagrange multiplier test is used to formally assess if there is overdispersion/underdispersion not accounted for by the Poisson regression. This is done by testing for overdispersion against the Katz system where the test statistic is

$$TLM = 0.5 \sum_{i=1}^{m} [(n_i - \mu_i)^2 - n_i] / \sqrt{0.5 \sum_{i=1}^{m} \mu_i^2},$$

see Cameron and Trivedi (2013) Sec. 5.4.1. At Gothenburg, there was found to be some (residual) underdispersion of counts, but it is not significant at the 5% level. From this and the residual analysis the Poisson GLM is concluded to be an appropriate model for the winter cyclone counts.

Maximum likelihood estimates for the coefficients ($\hat{\beta}_k$)for the winter count models for Gothenburg and Barcelona are given in Table 3.1. For the grid point closest to Gothenburg, only the SCP showed a significant (according to a t-test at the 5% level) relationship with the winter cyclone counts. The SCP is negatively associated with the number of cyclones passing near Gothenburg. For extra tropical cyclones passing near Barcelona only the NAO shows a significant (negative) relationship with counts. These findings are consistent with those of Vitolo et al. (2009); Mailier et al. (2006), where the SCP slope estimate was significant over most of Scandinavia, including the Gothenburg grid cell.

Indices	z_k	Gothenburg $\hat{\beta}_k$	Barcelona $\hat{\beta}_k$
Time	z_1	0.17 (0.14)	-0.23(0.19)
NAO	z_2	0.09 (0.06)	**-0.20** (0.09)
EAP	z_3	0.02 (0.05)	0.11 (0.07)
SCP	z_4	**-0.19** (0.06)	-0.04 (0.09)
EWP	z_5	0.03 (0.08)	-0.09 (0.11)
POL	z_6	-0.03 (0.08)	-0.21 (0.11)

Table 3.1: The regression coefficient estimates in the Poisson regression of cyclone counts over Gothenburg and Barcelona. Standard errors are in brackets, estimators with $p \leq 0.05$ are in bold.

Normal linear regression was found to be suitable for modelling winter local mean vorticity Y, with the modelled intensity regressed against the same teleconnection indices as the modelled counts. The extended winter local mean vorticity

is then

$$Y \sim N(\mu_y, \sigma)$$
$$\mu_{y,t} = \alpha_0 + \sum_{k=1}^{6} \alpha_k z_{k,t}.$$

The $z_{k,t}$ is the same as for the Poisson model, and the regression coefficient estimates α_k have the same interpretations as above except they are (linearly) related to winter local mean vorticity instead of cyclone counts.

The linear model fit is assessed using plots of the residuals. As with the deviance residuals for the Poisson models, the residuals should be Normally distributed, with mean zero and constant variance. The plot of the residuals against fitted values (Fig. 3.11 a) shows no evidence of heteroscedasticity (funelling) and so gives no reason to question the model fit. The quantile-quantile plot (Fig. 3.11 b) of the sample residuals against theoretical also support the model fit, although there is some deviance from the 45^o line in the tails.

(a) (b)

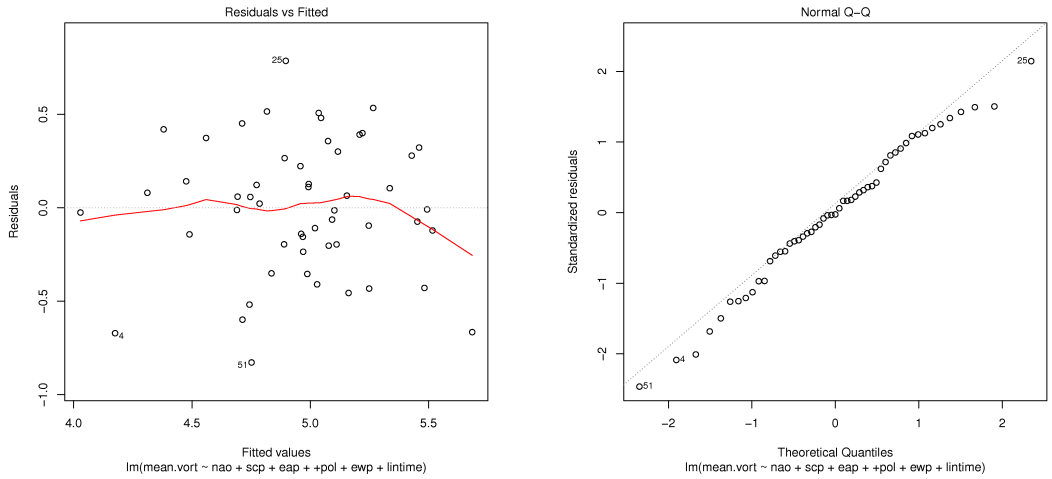

Figure 3.11: a) Left: Density estimate of the residuals. Right: Normal QQ- plot of the residuals. b)Residuals vs fitted

Maximum likelihood estimates for the regression coefficients for Gothenburg and Barcelona mean vorticity ($\hat{\alpha}_k$) are given in Table 3.2. The estimate for the

Indices	z_k	Gothenburg $\hat{\alpha_k}$	Barcelona $\hat{\alpha_k}$
Time	z_1	**0.91** (0.29)	0.04 (0.38)
NAO	z_2	-0.12 (0.29)	0.08 (0.17)
EAP	z_3	-0.04 (0.10)	-0.23 (0.14)
SCP	z_4	**-0.58** (0.14)	0.18 (0.18)
EWP	z_5	0.09 (0.17)	0.22 (0.22)
POL	z_6	-0.10 (0.17)	-0.39 (0.22)

Table 3.2: The regression coefficient estimates in the linear regression of cyclone local mean vorticity over Gothenburg and Barcelona. Standard errors are in brackets, estimators with $p \leq 0.05$ are in bold.

time trend coefficient $\hat{\alpha_1}$ is highly significant over Gothenburg suggesting non-stationarity in the winter mean intensity. This is consistent with Vitolo et al. (2009) where non-stationarity was found for the counts of intense cyclones over the same region, but not for all cyclones. In Vitolo et al. (2009) it was suggested the increase in the rate of intense cyclones could be due to either climatic change or inhomogeneities in the reanalysis dataset. The SCP coefficient ($\hat{\alpha_4}$)is also highly significant for Gothenburg winter mean vorticity, suggesting this may be a driver of cyclone intensity. The model of Gothenburg mean vorticity has an R^2 value of 0.49 meaning just under half the variance in local mean vorticity is explained by the model. For Barcelona there none of the teleconnection indices are significant at the 5% level, although the EAP and POL are significant at the 10% level. The Barcelona model has a lower R^2 value of 0.22, suggesting large scale flow patterns are of less use in explaining winter mean intensity over this region.

3.5.3 Modelled covariance

The modelled covariance between $\hat{N}$ and $\hat{Y}$ for Gothenburg can be expressed as

$$\begin{aligned} Cov(\hat{N},\hat{Y}) &= cov(e^{\alpha_0+\alpha_1 z_1+....\alpha_6 z_6}, \beta_0+\beta_1 z_1+...\beta_6 k z_6) \\ &= cov(e^{\alpha_1 z_1}, \beta_1 z_1) + cov(e^{\alpha_2 z_2}, \beta_2 z_2) + cov(e^{\alpha_3 z_3}, \beta_3 z_3) + cov(e^{\alpha_4 z_4}, \beta_4 z_4) \\ &+ cov(e^{\alpha_5 z_5}, \beta_5 z_5) + cov(e^{\alpha_6 z_6}, \beta_6 z_6). \end{aligned} \tag{3.5}$$

since the teleconnection indices are uncorrelated by definition and so $cov(z_i, z_j) = 0$ when $i \neq j$. From Eqn 3.5 the modelled correlation can be estimated for Gothenburg, $cor(\hat{n}, \hat{y}) = 0.32$ (compared to the observed correlation $Cor(n, y) = 0.48$). The regression models using teleconnection indices as explanatory variables account for two thirds of the correlation over Gothenburg. Using the same methodology for Barcelona the modelled correlation is $Cor(\hat{N}, \hat{Y}) = -0.02$. Regression models using teleconnection indices as explanatory variables are thus suitable for reproducing the positive correlation between N and Y.

3.6 Regression models for all grid points

The analysis conducted at Gothenburg and Barcelona was repeated for all Northern Hemisphere grid points. The regression coefficients for the linear trend term, the NAO,SCP and EAP were significant for the models for N and Y over much of the North Atlantic and Europe. Reduced models with only these 4 explanatory covariates are now assessed.

The maximum likelihood estimates of the North Atlantic regression parameters for local mean vorticity and cyclone counts, $\hat{\alpha_k}$ and $\hat{\beta_k}$, $k = 1, .., 4$ are shown in Fig. 3.12 and 3.13 respectively. Statistical significance was determined with a t test at the 5% level. There is a clear relationship between large scale flow patterns and both winter cyclone counts and winter local mean vorticity (Figs. 3.12, 3.13). The NAO parameter for counts is statistically significant over much of the North Atlantic (Fig. 3.13b). The positive phase of the NAO is associated with an increase in extra tropical cyclones across Canada, Greenland and Iceland as well as north

Great Britain, as well as with a decrease in cyclones over the North West coast of Africa. Although the NAO appears to be the single greatest driver in cyclone counts of the 3 teleconnection indices considered here, it is not significant for the modelled winter cyclone counts over the region of Europe (Scandinavia, North Germany, Great Britain, Benelux) where the positive correlation was observed. The NAO parameter for local mean vorticity is significant over Iceland and most of the Norwegian sea. There appears to be very few grid points where the NAO parameter is significant for *both* the frequency and intensity.

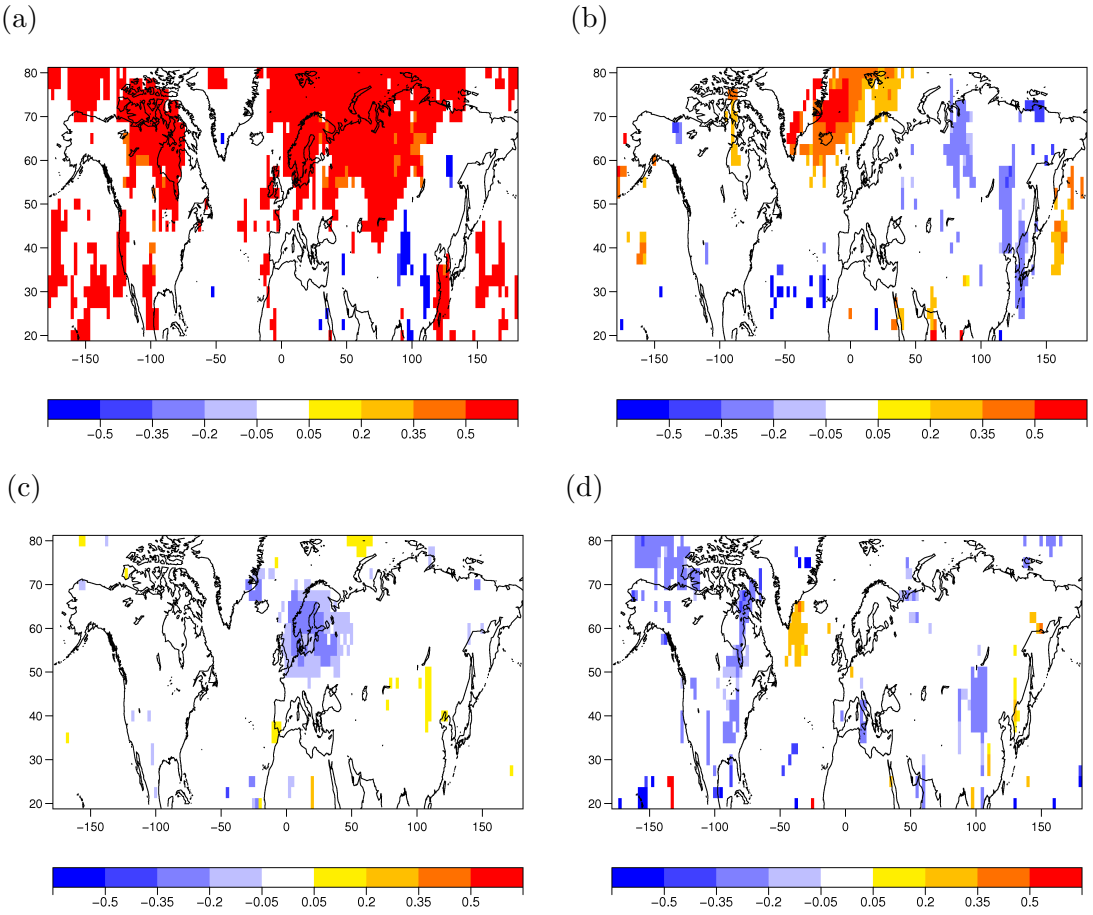

Figure 3.12: Estimates of α_k which were significantly different from zero (according to a t-test at the 5 % confidence level) for (a) linear time trend (b) North Atlantic Oscillation (c) Scandinavian pattern (d) East Atlantic Pattern.

From Fig. 3.13 c, the SCP coefficient for counts is significant over a region

extending from the east coast of Greenland, over Scandinavia and into eastern Europe. The SCP coefficient estimate for local mean vorticity is significant over Scandinavia, north Germany and the Benelux countries. From these plots it would seem likely that, as with Gothenburg, the SCP coefficients account for much of the correlation because of its importance for explaining both counts and mean intensity in many locations.

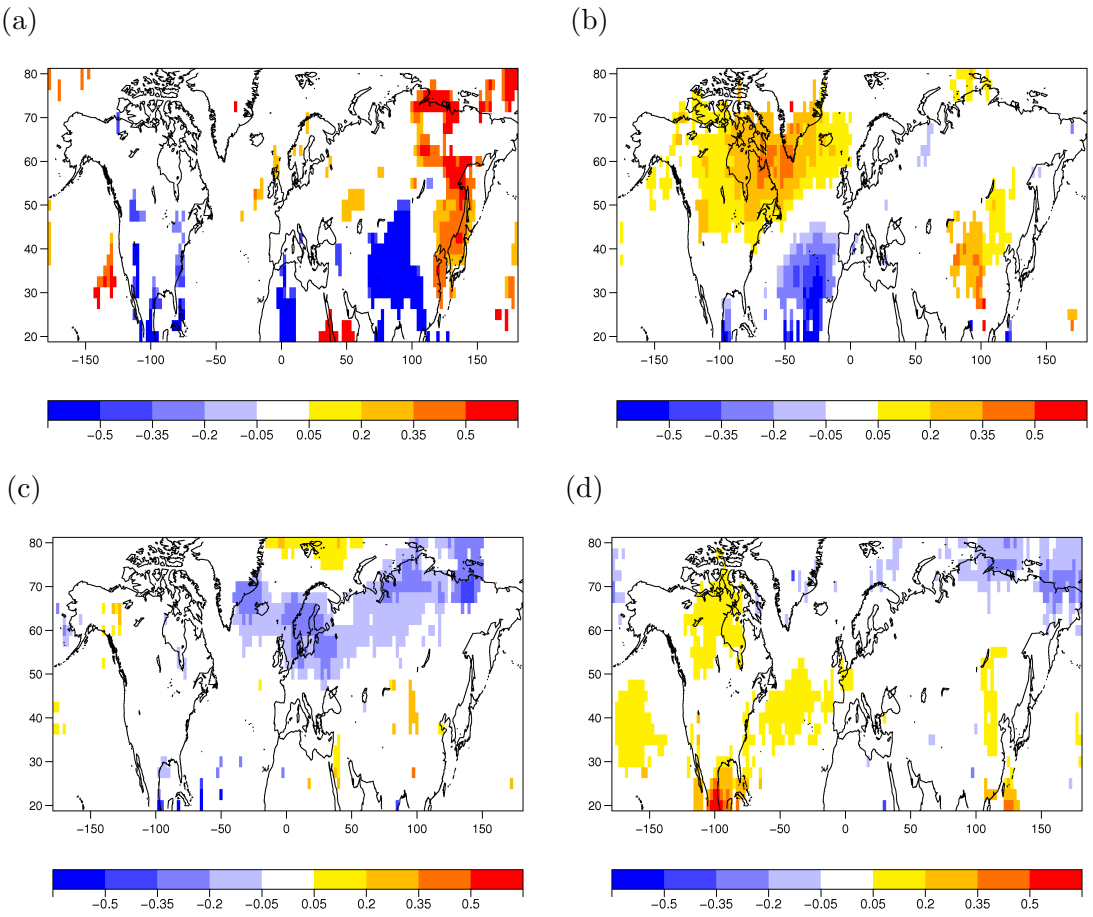

Figure 3.13: Estimates of β_k which were significantly different from zero (according to a t-test at the 5 % confidence level) for (a) linear time trend (b) North Atlantic Oscillation (c) Scandinavian pattern (d) East Atlantic Pattern.

The EAP coefficient is significant for cyclone counts over the Atlantic to the south and east of the United States (Fig. 3.13 d) . The EAP coefficient is also significant for local mean vorticity over some grid points in the eastern United

States and to the south east of Greenland (Fig. 3.12 d). There are few grid point where the EAP coefficient is significant for both counts and intensity. The time trend coefficient for counts is significant for part of the United States eastern seaboard and for a few grid point over and around the north of Great Britain. For local mean vorticity the time trend coefficient is significant for a large region of North Europe and over Canada. This agrees with the findings in Vitolo et al. (2009) where a linear time trend was not found to be significant for Poisson regression of 3 monthly counts over most grid points, but was found to be significant over Canada and north western Europe.

(a) (b)

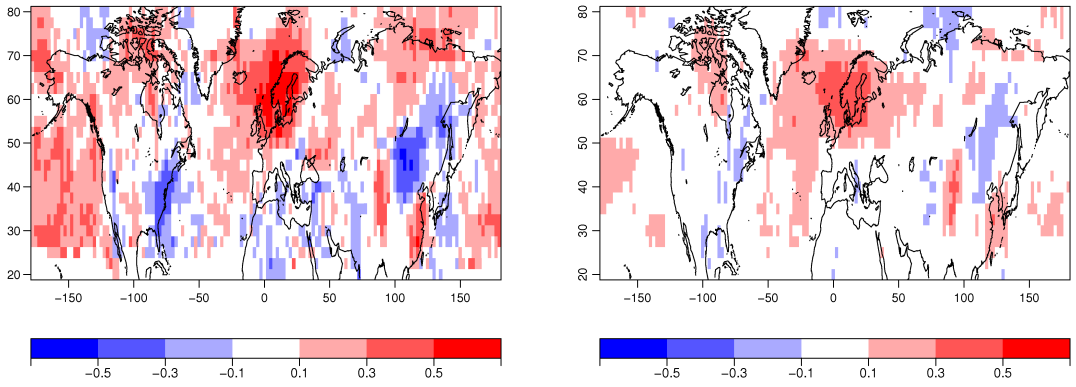

Figure 3.14: Plots of the correlation between the winter counts and local mean vorticity a) Sample b) Modelled correlation with North Atlantic teleconnection patterns as explanatory variables.

The coefficient estimates for the SCP are significant for both counts and mean intensity over much of the Scandinavian peninsula, as well as parts of Northern Germany and the Benelux countries. The plot of the modelled correlation (Fig. 3.14) shows that the large scale flow patterns account for much of the observed positive correlation for the Atlantic region.

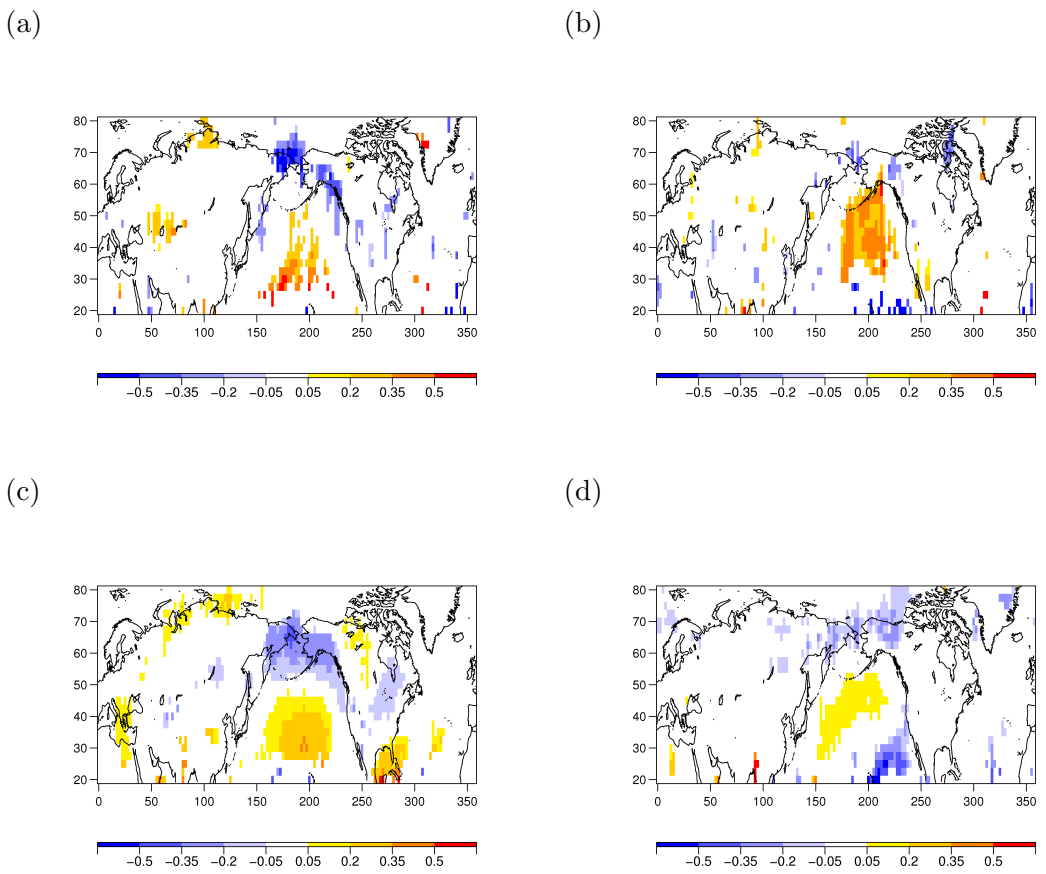

Figure 3.15: Estimates of α_k which were significantly different from zero (according to a t-test at the 5 % confidence level) for a) PNA b) EPA. Estimates of β_k for c) PNA d)EPA.

The analysis was repeated for the North Pacific region using a linear time trend and 4 teleconnection indices relevant for the region; the West Pacific pattern (WP), East Pacific/North Pacific pattern (EP), Pacific/North American pattern (PNA) and the Tropical Northern Hemisphere pattern (TNH). As well as the linear time trend, the PNA pattern and EPA were both found to be associated with changes in the frequency and intensity (see Fig. 3.15). The regression models with indices for the NPA and EP and a linear time trend as explanatory variables were able to reproduce most of the positive correlation over the North Pacific (Fig. 3.16).

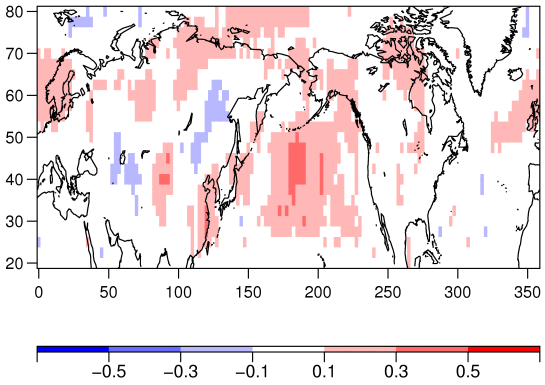

Figure 3.16: Plot of the modelled correlation from the regression models with North Pacific teleconnection indices as explanatory variables.

3.7 Discussion about possible physical mechanisms

The Scandinavian pattern modulates both cyclone frequency and mean intensity, and thereby induces positive correlation between the frequency and the intensity. Possible physical mechanisms are discussed here for how the Scandinavian pattern interacts with extra tropical cyclones. The negative correlation observed over the Gulf stream is also briefly considered.

3.7.1 Positive correlation

In the previous section it was shown that negative phases of the Scandinavian pattern are associated with increased cyclone activity; more occurrences with higher mean intensity. It is important to distinguish between cause and effect, as increased cyclone activity may also result in persistent negative SCP index values. The potential for synoptic scale activity, such as cyclones to influence the state of the background flow has been discussed in the literature, such as in Pinto et al. (2009) where it explains that cyclones themselves may play a major role in steering the phase of the NAO. However, in Whitaker and Sardeshmukh (1998) it was shown

that while transient eddies/cyclones can affect the background upper tropospheric circulation, the latter is more important in initiating eddy formation and controlling intensification.

Four key environmental factors which control cyclone intensification were considered in Pinto et al. (2009): latent energy (equivalent potential energy 850 hPa), upper air baroclinicity, horizontal divergence and jet stream strength. The growth of extreme cyclones was shown to be related to these four explanatory variables, with the jet stream location and velocity in particular showing a clear connection to extreme cyclone intensification. The major (i.e. NAO, EAP, SCP) extra tropical teleconnections esssentialy describe jet stream variability over the ocean basins (Woollings et al., 2010).

In Raible (2007) the occurrence of extreme intensified cyclones in Northern Europe are linked to a rotated NAO like pattern, which corresponds to the SCP as identified here and discussed in Section 3.5.1. In Hanley and Caballero (2012) it was also shown that intense European extra tropical cyclones occurred during an eastward shifted NAO-like pattern, which is again qualitively similar to a negative phase of the Scandinavian pattern. The large scale low-pressure system located over the Scandinavian peninsula, associated with negative values of the SCP index, helps steer extra tropical cyclones into Northern Europe, as well as generating an intense baroclinic jet streak which acts to intensify cyclones. In particular, a case study of extreme storm Daria was conducted which showed that the background atmospheric conditions *preceded* Daria's birth (Hanley and Caballero, 2012) .

Most of the studies cited above have investigated the link between environmental factors and cyclone clustering over synoptic time scales. Synoptic variability over the North Atlantic and Europe is related to the NAO and other teleconnection patterns, which in turn has been related to the occurence and development of cyclones over synoptic time scales (Pinto et al., 2009). However this thesis has

considered aggregate cyclone activity over a longer 6 month extended winter period due to its relevance for the insurance industry. The same arguments put forward for linking teleconnection patterns and extra tropical cyclone activity for shorter time periods remain valid for the 6 month aggregated period. In particular the winter mean NAO has been linked to inter annual variability in the mid Tropospheric baroclinicity (Baldwin et al., 1994). The baroclinicity in the mid Troposphere is related to surface temperature gradients which in turn influence cyclone activity (Raible, 2007).

The relation between the Scandinavian pattern and its climatic impact, as well as possible forcing mechanisms is discussed in Bueh and Nakamura (2007). For negative phases of the SCP the 200mb zonal wind anomalies are observed over Northern Europe over the same region positive correlation is observed (see Fig. 3.17), as well as increased baroclinicity over the same area. It was shown in Bueh and Nakamura (2007) that there is positive feedback over the exit region of the North Atlantic storm track between the Scandinavian pattern and passing cyclones. This positive feedback between extra tropical cyclones and the background atmospheric flow is a possible mechanism for the frequency-intensity dependence found here, as well as the observed clustering of intense cyclones shown in Vitolo et al. (2009); favourable environmental conditions result in increased cyclone activity through enhanced steering and intensification, which in turn help maintain these conditions.

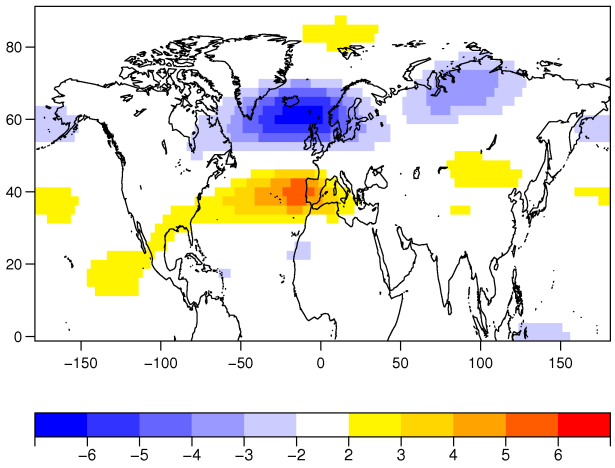

Figure 3.17: Maps of the linear regression coefficient for the 200mb zonal wind U_{200} on the 6 month SCP index.

3.7.2 Negative correlation

The negative correlation discovered over the Gulf stream is also possibly due to some interaction between the background atmospheric flow and extra tropical cyclones. However none of the regression coefficients from either the North Atlantic or North Pacific local mean vorticity models are significant over the Gulf stream. One possible mechanism is the velocity and position of the North Atlantic subtropical and/or eddy driven jet stream. In Pinto et al. (2009) factors contributing to the development of extreme North Atlantic cyclones was considered. It was shown that during strongly positive phases of the NAO the jet stream over North America is enhanced, resulting in increased cyclogenesis and more extreme storms over the North Atlantic. However extra tropical cyclones originating from the West Atlantic/North American east coast typically develop slowly, not reaching maximum intensification until further East into the Atlantic (Dacre and Gray, 2009). In Pinto et al. (2009) it can be seen that during strongly negative NAO phases, although there are fewer extreme cyclones, they reach their point of maximum intensification closer to the eastern U.S.

3.8 Summary

A framework for quantifying aggregate risk is introduced in Section 3.2. This framework is then applied to extra tropical cyclones using a database of tracks for the Northern Hemisphere (covering October-March winters from 1950-2003). Statistical models were used to investigate the sensitivity of the variance of the aggregate risk to dependence between the frequency and intensity of cyclones as well as dependence between successive events.

Statistically significant correlation was found between the frequency and intensity of extra tropical cyclones over parts of northern Europe including Scandinavia, Germany and Great Britain as well as the eastern end of the North Atlantic storm track. The findings for extended winter cyclones counts agreed with those of Vitolo et al. (2009), concerning linear trends in intense cyclones over Scandinavia, and the effect of large scale flow patterns on cyclone counts.

Joint modulation by large-scale flow patterns is shown to be responsible for generating the covariance between cyclone frequency and mean intensity. The Scandinavian pattern in particular is strongly negatively correlated with both counts and local mean vorticity over much of northern Europe. Regressing the counts and local mean vorticity on the Scandinavian pattern index is able to reproduce most of the observed correlation. Other important teleconnection indices for both frequency and intensity are the North Atlantic Oscillation and the East Atlantic pattern.

The correlation between the frequency and local mean vorticity was also considered for the subset of the 50% most intense cyclones at each grid point. The positive correlation for the North Atlantic was largely unchanged when considering the subset of more intense cyclones. The negative correlation was found to be mainly a feature of the weaker systems. As more intense events are responsible for the majority of insured losses the negative correlation is not considered further in the

thesis. The sensitivity of the results to the choice of dataset was also assessed. The sign and location of the correlation was shown to be the same for storm tracks in the ERA-40 reanalysis.

Chapter 4

Modelling the influence of frequency-intensity dependence on the risk of extreme aggregate loss

4.1 Aim

The aim of this chapter is to quantify the effect of frequency-intensity dependency on the extremes of the aggregate loss distribution. Section 4.2 discusses the need for insurers to be able to quantify and understand extremes of the aggregate loss, and the influence of clustering and frequency-intensity dependence on these extremes. Methods for exploring the extremes are then introduced in Section 4.3 and applied to extratropical cyclones over Europe in Section 4.4.

4.2 Managing aggregate extremes of natural hazards

Although extremes of most types of natural hazards are usually rare they can account for a disproportionately large share of damage (Stephenson, 2008). Extremes

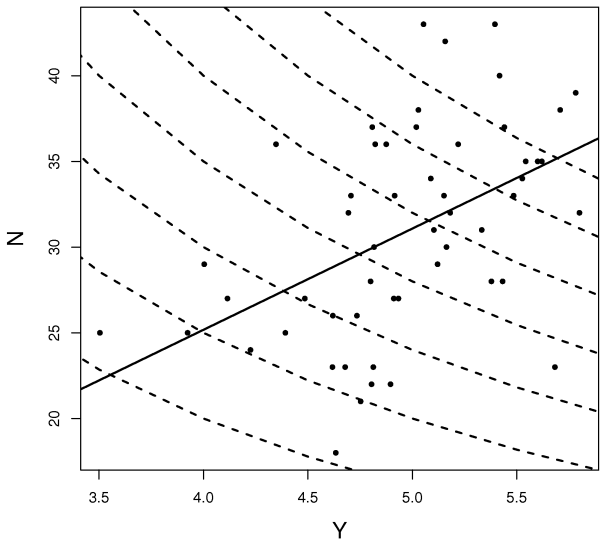

Figure 4.1: Plot of sample local mean vorticity y against counts n for cyclones passing near Gothenburg. Contours of the aggregate risk, $S = NY$, have been added for S = 80, 100, 120, 140, 160, 180, 200. The solid line is the linear regression line of n on y.

of aggregate losses are due to either an above average number of occurrences, the occurrence of one or more high intensity events, or a combination of both (see Fig 4.1). These extremes are of particular interest to insurers as they have legal capital requirements based upon the probable maximum loss (PML) they can expect to occur (see Chapter 2).

Exceedance probability curves are widely used in the insurance industry to assist in visualizing the distribution of losses and determining a suitable PML metric (Grossi and Kunreuther, 2005). For the aggregate loss $S = X_1 + ... + X_N$ the aggregate exceedance probability (AEP) is

$$AEP(s) = 1 - Pr(S \leq s) = 1 - F_S(s), \tag{4.1}$$

where F_S is the cumulative distribution function (cdf) of S (see Fig. 4.2). A natural choice for the PML index could be a suitably high quantile of of S (Woo (2002)). In risk management this is called the value-at-risk VaR_p, which is defined as the

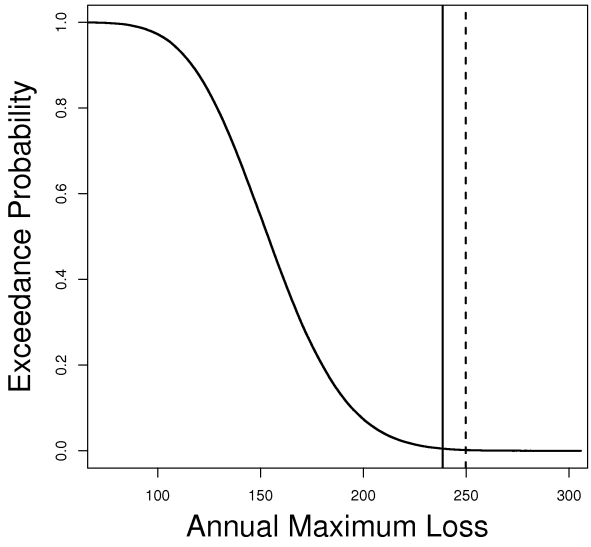

Figure 4.2: Example of an annual aggregate loss exceedance probability curve. The vertical solid black line is the $VaR_{0.995}(s)$ and the dashed black line is the $ES_{0.995}(s)$

smallest value such that the probability VaR_p is exceeded is $1-p$ [1]

$$VaR_p = F_S^{-1}(p),$$

where F_S^{-1} is the quantile function of S (McNeil et al. (2005) Section 2.2). The VaR is subject to a number of limitations, in particular it does not provide any information on losses above the quantile defined threshold and is not a coherent risk measure, as defined by the axioms of coherence (see Appendix B). Coherence of a risk measure is desirable for a number of reasons, in particular because it is necessary for a risk measure to be used in portfolio diversification (Dowd and Blake, 2006). An alternative risk measure to the VaR_p is the expected shortfall, ES_p,

$$ES_p(s) = \frac{1}{1-p}\int_p^1 VaR_p(s)du = E(S|S > VaR_p),$$

which is the average loss given VaR_p has been exceeded; the ES_P is never less than the VaR_p . The expected shortfall thus gives information on extreme losses

[1]Usually denoted by α, here p is used instead as α is used later in this chapter for confidence intervals.

exceeding VaR_p as well as being a coherent risk measure (see McNeil et al. (2005) Section 6.1). Both of these risk measures will be used in this chapter to investigate the extremes of the aggregate loss.

The impact of temporal clustering of extremes on the PML for European windstorms has been of concern for the insurance community in recent years (see Chapter 2). The frequency-intensity dependence investigated in the previous chapter could have implications for modelling the clustering of extremes, which in turn could influence the VaR_p and ES_p. This chapter will seek to quantify the effect of clustering and frequency-intensity dependence on the extremes of the aggregate loss distribution. Before considering specific methods for investigating extremes of the aggregate loss distribution, it is possible to show, using the Poisson process limit for extremes, that the clustering of extreme events will be ineffective without frequency-intensity dependence.

4.2.1 Clustering of extremes

Theorem (Coles, 2001) Section 7.3 Consider a sequence $\{N, X_i\}$, where N is the number of occurences and X_i $(i = 1, ..., N)$ is the individual occurence magnitude. Let S be the length of the sequence exceeding a threshold u,

$$S = \sum_{i=1}^{N} I(X_i > u),$$

where I is the indicator function. If X and N are independent, and X_i, X_j are independent for all $1 < i, j < N, i \neq j$, then the dispersion of S,

$$\phi(S) = \frac{Var[S]}{E[S]} - 1 \to 0,$$

as $u \to \infty$, irrespective of the distribution of N.

Proof. If the random variable X_i has cumulative distribution function F_X such that $F_X(u) = 1 - q$, then X has probability q of lying within the region $[u, \infty)$. Let Q be a Bernoulli random variable; $Q \sim Ber(q)$. If N and X_i are independent then

the total number of events in a year which exceed a threshold u, S, is a Binomial distribution

$$S \sim Bin(N, q).$$

The expectation of S is then

$$E[S] = \sum_{i=1}^{N} Q_i = E[N]q,$$

and from the law of total variance,

$$\begin{aligned} Var[S] &= E[N]Var(Q) + Var(N)(E[Q])^2 \\ &= E[N]q(1-q) + q^2 Var(N). \end{aligned}$$

The dispersion of S given u is

$$\begin{aligned} \phi(S) &= \frac{E[N]q(1-q) + q^2 Var(N)}{qE[N]} - 1 \\ = \frac{q^2 Var(N) - q^2 E[N]}{qE[N]} &= q\left[\frac{Var[N]}{E[N]} - 1\right]. \end{aligned} \tag{4.2}$$

As the intensity threshold increases the probability that a loss $Pr(X_i \geq u) = q \to 0$, hence as $u \to \infty$, $\phi(S) \to 0$.

□

Considering the case when N is Poisson distributed with $E[N] = Var[N] = \lambda$ then Eqn. 4.2 becomes

$$\phi(S) = \frac{q^2\lambda - q^2\lambda}{q\lambda} = 0.$$

as expected. This shows that if the frequency N and intensity X are independent then the distribution of counts for events exceeding an intensity threshold u will converge to a Poisson process with increasing u. This contradicts what has been observed in for European extra tropical cyclones, where the overdispersion parameter has been shown to increase for more extreme events (Vitolo et al., 2009).

4.3 Methods for exploring extremes of the aggregate risk

This section introduces methods for investigating the sensitivity of the extremes of the aggregate loss distribution to clustering and frequency-intensity dependence.

4.3.1 Non-parametric methods

Non-parametric methods can be used to estimate risk measures from the data without making distributional assumptions. This relies on a large amount of loss data being available, and empirical estimation of risk measures for the 1 in 200 year return level is impossible using a dataset of shorter length (McNeil and Frey, 2000). The empirical AEP can be calculated from a sample of aggregate losses $s_1, ...s_m$ as

$$AEP(u) = 1 - F_s(u) = 1 - \frac{1}{m}\sum_{i=1}^{m} I(s_i \leq u)$$

where I is the indicator function and F_s is the empirical distribution function for s_i (Harmantzis et al. (2006)). The empirical VaR_p is

$$VaR_p(s) = F_s^{-1}(p) = s_{(i)},\ p\epsilon\left(\frac{i-1}{m}, \frac{i}{m}\right)$$

where $F_s^{-1}(p)$ is the pth empirical quantile and $s_{(1)} \leq .... \leq s_{(m)}$ are the order statistics. Finally, the empirical ES_p is

$$ES_p(s) = \frac{\sum_{i=mp}^{m} s_{(i)}}{m - mp}.$$

As only 53 years of data was available from the NCEP-NCAR reanalysis the exceedance probability for the aggregate risk of extratropical cyclones considered in the previous chapter can only be calculated up to $(1 - p) \approx 0.019$. Another limitation of this empirical method is that by estimating the risk measures directly from the sample aggregate loss s, nothing is learned about the effect of frequency-intensity dependency.

Bootstrap confidence intervals can be constructed for the empirical AEPs to investigate if frequency-intensity dependence effects the return levels of the aggregate loss. By assuming independence between the frequency and intensity a block boostrapping method can be used to construct confidence intervals for the return level at T years (and thus the exceedance probabilities $p = 1 - 1/T$) as follows.

For r in $1, ..., R$;

1. Construct a resampled (with replacement) time series of cyclone counts $n^*_{1,r}, ..., n^*_{m,r}$.
2. Construct a resampled (with replacement) time series of cyclone local mean vorticity $y^*_{1,r}, ..., y^*_{m,r}$.
3. Calculate the corresponding time series of aggregate losses $s^*_{1,r}, ..., s^*_{m,r}$ for each r, from the resampled counts and local mean vorticity.
4. Calculate the new resampled return levels; $q^*_{p,r}(s)$. Here $q^*_{p,r}(s)$ is the empirical quantile estimate for the rth resampled time series of aggregate losses s.

Then the 90% confidence intervals for the pth quantile are the $5th$ and $95th$ percentiles of the resampled $q^*_{p,r}(s)$. As n and y are assumed independent in this bootstrapping algorithm, if the empirical AEP curve for s diverges outside of the confidence intervals this would provide an indicator that inclusion of frequency-intensity dependence is necessary to model extremes of the aggregate loss.

4.3.2 Parametric methods

In the parametric approach extremes are modelled using a suitable distribution (or distributions) which are chosen through past experience, diagnostic plots and statistical analysis. Having selected a distribution the parameters can be estimated from the available data through method of moments, maximum likelihood or otherwise. Analytic results for compound distributions such as F_S are not typically available beyond the mean and variance (McNeil et al. (2005), Section 10.2). However this issue can be circumvented by fitting a distribution directly to the sample aggregate

loss s without considering the underlying frequency and intensity distributions or their covariance. Extreme value distributions are used here to investigate the behaviour of the tail of the aggregate loss distribution beyond levels which can be estimated empirically.

The peaks over thresholds approach introduced in Chapter 2 is used here to model the extremes of the aggregate losses. As well as modelling individual extreme events (Della-Marta et al., 2009; Kunz et al., 2010) the generalised Pareto distribution has been applied to aggregate claims data (McNeil et al. (2005), Chapter 10). The aggregate loss S is modelled as a GPD distribution,

$$S \sim GPD(\xi, \sigma),$$

where ξ, σ are the shape and scale parameters (Chapter 2). The AEP and VaR_p can be calculated from Eqn. 2.8,

$$VaR_p = u + \frac{\sigma}{\xi}[1 - (\frac{\lambda}{1-p})^{-\xi}].$$

The ES_p can be calculated from the mean excess function (Eqn. 2.9);

$$ES_p = \frac{VaR_p}{1-\xi} + \frac{\sigma_u}{1-\xi}.$$

This approach does not explicitly consider the effect of frequency-intensity dependence and clustering on the risk estimates. Instead the estimated VaR and ES will be compared with those obtained using the simulation methods in the following section to determine if it is possible to avoid consideration of the frequency and intensity distributions and model the aggregate losses directly.

Parameter estimation

For the GPD model the sample mean excess $e_m(u)$ is defined as

$$e_m(u) = \frac{\sum_{i=1}^{m}(s_i - u)I(s_i > u)}{\sum_{i=1}^{m} I(s_i > u)}$$

(Coles (2001) Section 4.3). If the data over a threshold u supports a GPD model then the mean excess function will become approximately linear, which means a

plot of the mean excess against threshold can be used to assist in determining a suitable u (McNeil et al., 2010). A mean excess plot with an increasing linear trend indicates a positive shape parameter ξ, a linear downward trend indicates a negative shape parameter and a horizontal line indicates $\xi = 0$. Having chosen a suitable threshold u, the shape ξ and scale parameters σ can be estimated by using numerical techniques to maximise the log-likelihood;

$$l(\sigma, \xi) = -klog\sigma - (1 + 1/\xi) \sum_{i=1}^{m} log(1 + \xi s_i/\sigma)$$

(Coles, 2001) Chapter 4. Here the maximization was done using the $gpd.fit$ function from the R package $ismev$. This function provides confidence intervals for the return levels using the delta method (Coles (2001), Chapter 4).

4.3.3 Monte Carlo methods

The third approach considered here for evaluating the aggregate loss risk measures is Monte Carlo simulation. The processes generating losses are modelled, then a large number of simulations can be produced to approximate the loss distribution. This method is more flexible than the previous two approaches and allows for a high level of complexity in the model. The calculation of the AEP, VaR and ES from the simulated losses are the same as in the empirical approach. For estimating risk measures from the upper tail of the aggregate loss distribution this simulation approach will take a long time to converge (McNeil et al., 2005, Section 8.5). This means many thousands of simulations are required, and the Monte Carlo method is a brute force approach.

Four models are proposed to investigate the sensitivity of the aggregate loss to different modelling assumptions regarding dependence and clustering. One approach to modelling the dependence between the frequency and intensity would be to introduce a mixing variable Z which is related to both N and X to mimic the effect of the large scale forcing shown in Chapter 3. However the use of a mixture model will result in overdispersion in N, (see Section 2.2). An approach which

introduces dependence without inducing overdispersion is required here to be able to investigate the impact of frequency-intensity covariance with and without clustering. A copula based approach presents such a method and is used here to model dependence between the frequency and mean intensity, without necessarily introducing overdispersion. The models for generating the frequency N and intensity X and thus the aggregate loss S are now described.

Model $\mathbf{M_1}$ - no clustering, X, N i.i.d. - the frequency of losses is Poisson distributed with constant rate λ, and the individual losses are gamma distributed with constant shape and rate parameters α, β,

$$\begin{aligned} N &\sim Pois(\lambda) \\ X &\sim Ga(\alpha, \beta). \end{aligned}$$

Model $\mathbf{M_2}$ - clustering, X, N i.i.d. - the losses are gamma distributed as in M_1. To allow for overdispersion the frequency of occurrence is Negative Binomially distributed with parameters p, r as in Section 2.2.1,

$$\begin{aligned} N &\sim NB(p, r). \\ X &\sim Ga(\alpha, \beta). \end{aligned}$$

Model $\mathbf{M_3}$ - no clustering, X, N dependent - both the mean and the variance of the individual losses are modelled as random variables $E[X] = Y$,$Var[X] = W$ and are related to the number of losses N, and each other, by a copula C. The multivariate distribution F_{NYW}, is the joint distribution of the number of losses N, the mean intensity Y and the variance of the intensity W. The joint distribution can be written in terms of the marginal distributions of N, Y, W and the copula C_{NYW};

$$F_{NYW}(n, y, w) = C_{NYW}(F_N(n), F_Y(y), F_W(w)).$$

The marginal distribution of the frequency is Poisson with parameter λ. The mean intensity Y is normally distributed with mean parameter μ_Y and variance σ_Y^2. The variance of the individual intensities W is also modelled as normally distributed

with mean μ_W and variance σ_W^2. Here C is a Gaussian copula with covariance matrix Σ. The frequency and intensity of losses for M_3 is then,

$$N \sim Pois(\lambda)$$
$$Y \sim N(\mu_Y, \sigma_Y^2)$$
$$W \sim N(\mu_W, \sigma_W^2)$$
$$X \sim Ga(Y^2/W, Y/W).$$

Model $\mathbf{M_4}$ - clustering, X, N dependent - the same model formulation as M_3 except the marginal distribution of N is Negative Binomial as in M_2.

$$F_{NYW}(n, y, w) = C_{NYW}(F_N(n), F_Y(y), F_W(w)),$$
$$N \sim NB(p, r),$$
$$Y \sim N(\mu_Y, \sigma_Y^2),$$
$$W \sim N(\mu_W, \sigma_W^2),$$
$$X \sim Ga(Y^2/W, Y/W).$$

Parameter estimation

For M_1, M_3 the parameter λ is estimated from the sample counts n as

$$\hat{\lambda} = \bar{n}$$

For M_2, M_4 the Negative Binomial parameters are estimated from n by the method of moments as,

$$\hat{p} = \bar{n},\ \hat{r} = \frac{\bar{n}^2}{s_n^2 - \bar{n}},$$

(Rice (2007) Section 8.7). The estimator for r requires $s_n^2 > \bar{n}$; the data must be overdispersed to permit a negative binomial distribution.

The estimates for $\hat{\alpha}$ and $\hat{\beta}$ for models M_1, M_2 are estimated from the sample losses x by optimizing the log likelihood for α using the R function $fitdistr$;

$$mlog\hat{\alpha} - mlog\bar{x} + \sum_{i=1}^{m} logx_i - m\frac{\Gamma'(\hat{\alpha})}{\Gamma(\hat{\alpha})} = 0,$$

and then substituting $\hat{\alpha}$ into

$$\hat{\beta} = \frac{\hat{\alpha}}{\bar{x}},$$

(Rice (2007), Section 8.5). For the models M_3, M_4 the parameters of the marginal distributions of Y are calculated from the sample mean intensity $\bar{y}$ (see Section 3.2.1)

$$\mu_Y = \bar{y},\ \sigma_Y^2 = s_y^2$$

and for the W;

$$\mu_W = \bar{w},\ \sigma_W^2 = s_w^2$$

The parameters of the Gamma distribution for X in models M_3, M_4 are then stochastic,

$$\hat{\beta} = \frac{Y}{W},\ \hat{\alpha} = \frac{Y^2}{W}.$$

The estimated covariance matrix $\hat{\Sigma}$ for the Copula will have diagonal elements $(1, 1, 1)$ and off diagonals $(\rho_\tau(N, Y), \rho_\tau(N, W), \rho_\tau(Y, W))$ where ρ_τ is Kendall's correlation coefficient (see e.g. Joe (1997) Section 2.1). To simulate the variables N, Y and W from a Gaussian copula, first generate a vector $D = (D_1, D_2, D_3)$ from a multivariate standard normal distribution with dimension 3 and correlation matrix Σ. Then D is transformed using the standard normal density function Φ to obtain uniform variables $U = (U_1, U_2, U_3)$. Using a quantile transformation U can then be converted into the marginal distributions of N,Y and W. The result is a multivariate distribution with density function $F_{NYW} = C(F_N, F_Y, F_W)$. The algorithm for generating from a Gaussian copula is thus,

- Generate $D \sim N_3(0, \Sigma)$
- Calculate $U = (\Phi(D_1), \Phi(D_2), \Phi(D_3))$
- Calculate $N = F_N^{-1}(U_1)$,$Y = F_Y^{-1}(U_2)$,$N = F_W^{-1}(U_3)$

see McNeil et al. (2005) Section 5.1 for a more detailed explanation.

4.3.4 Uncertainty assessment

The accuracy of estimates of the empirical AEP curve and the GPD parameters are constrained by the quantity and quality of observations available. For the Monte Carlo method the number of simulations which can be generated will be constrained by the resources (time and computing power) available to the modeller. Measures of variability are required to assess the closeness of the estimated AEP curves and associated risk measures to the true values.

Cantelli bounds

Upper bounds for the AEP curve can be calculated from Cantelli's inequality (Royden, 1953). This states that for a positive real random variable S with mean μ_s and variance σ_S^2

$$Pr(S \geq \mu_S + k\sigma_S) \leq \frac{1}{1+k^2} = \frac{1}{T} \tag{4.3}$$

where $k \geq 0$, and T is the return time. As well as calculating upper bounds for the empirical AEP estimates, Cantelli bounds can be used to consider the effect of covariance between the frequency and intensity on the aggregate loss S for exceedance probabilities beyond that which have been observed. To do this two cases are considered, in the first the frequency and intensity are considered independent, and μ_S, s_S^2 are estimated as,

$$\begin{aligned} \bar{s} &= \bar{n}\bar{y} \\ s_s^2 &= V_n + V_y, \end{aligned}$$

as in Section 3.3. In the second case, the the sample mean and variance of s are

$$\begin{aligned} \bar{s} &= \bar{n}\bar{y} + cov(n,y) \\ s_s^2 &= V_n + V_y + V_c, \end{aligned}$$

which will result in increased Cantelli bounds in Eqn. 4.3, when $cov(n,y) > 0$, and reduced Cantelli bounds when $cov(n,y) < 0$.

DKW bounds

Bounds for the AEP curve which depend upon the sample size could be used to help assess the number of simulations required in the Monte Carlo approach for the estimates of the tail to converge. Such an approach is suggested in Rougier et al. (2013); the uncertainty regarding the difference between the empirical distribution and the actual distribution can be quantified with the Dvoretzky-Kiefer-Wolfowitz (DKW) inequality (Massart, 1990). The DKW inequality states that for a natural number m, and random variables $S_1, ..., S_m$ with distribution function F_S and empirical distribution function $\hat{F}_{s,m}$, then the probability that $\hat{F}_{s,m}$ differs from F_S by more than ϵ is

$$P(sup|F_{s,m}(l) - F_S(l)| > \epsilon) \leq 2e^{2m\epsilon^2} \tag{4.4}$$

for every $\epsilon > 0$. Then rearranging 4.4 to obtain ϵ in terms of the confidence bands of width $1 - \alpha$ gives

$$\epsilon = \left(\frac{ln(2/\alpha)}{2m}\right)^{\frac{1}{2}}.$$

Here the DKW inequality is used to assess the number of simulations that should be conducted to be able to estimate the upper tail of the aggregate loss distribution.

Bootstrapping for high quantiles

A bootstrapping method which resamples n and y has already been suggested for investigating the assumption of independence on the estimation of exceedance levels. However when investigating confidence limits for high quantiles of a distribution, such as the $VaR_{0.995}$, uncertainty may be very large, and for sample sizes of $m < 1000$ confidence intervals will tend to be unreliable Rougier et al. (2013) Section 2.5. More reliable confidence intervals for $VaR_{0.995}$ can be constructed using a bootstrapping approach with variance stabilisation as follows. First the sample estimate for $VaR_{0.995}$ is obtained from the data as in Section 4.3.1, denoted here as $\hat{q} = VaR_{0.995}(s)$. The basic bootstrap $(1 - 2\alpha)$ confidence intervals, $\hat{\theta}$ are

$$\hat{\theta}_\alpha = 2\hat{q} - \hat{q}^*_{(R+1)(1-\alpha)}, \hat{\theta}_{1-\alpha} = 2\hat{q} - \hat{q}^*_{(R+1)(\alpha)}$$

where $\hat{q}^*$ is the sample statistic calculated from a simulated dataset (through bootstrap resampling), R denotes the number of repetitions of the resampling, $\hat{q}^*_{((R+1)(\alpha))}$ is the αth quantile of the resampled quantiles , and the confidence level is $1-2\alpha$ Davison (1997), Section 2.7 and 5.2. The accuracy of the bootstrap confidence intervals will depend upon the original sample size m as well as the number of replications R. A suitable transformation of $\hat{q}$ can stabilize the variance of the resampled quantile estimator and considerably improve the accuracy of the bootstrap confidence limits (Davison (1997), Section 5.2). Here, as in Rougier et al. (2013) Section 2.5.4, using a loose analogy with the exponential distribution the bootstrap is applied to the log of $\hat{q}$. The transformed bootstrap confidence intervals become

$$\hat{\theta}_\alpha = g^{-1}\left(2g(\hat{q}) - g(\hat{q}^*_{((R+1)(1-\alpha))})\right), \hat{\theta}_{1-\alpha} = g^{-1}\left(2g(\hat{q}) - g(\hat{q}^*_{((R+1)(\alpha))})\right),$$

where $g(\hat{q}) = log(\hat{q})$. Throughout this thesis the number of replications is $R = 999$.

4.4 Results

The methods introduced in the previous section are used to investigate the extremes of the aggregate loss distribution of extratropical cyclones. The results are partitioned into three sections; non-parametric, parametric and Monte Carlo methods. As in the previous chapter, cyclones passing the grid point nearest Gothenburg were analysed to investigate the effect of positive dependence on extremes of the aggregate risk, where vorticity is used as a proxy for financial loss. Cyclones passing the grid point closest to Barcelona are also analysed to consider the case when there is no significant correlation between the frequency and intensity. Throughout this section the $VaR_{0.995}$ and $ES_{0.995}$ are considered for (the 200 year return level) due to the importance of these values to insurers.

4.4.1 Non-parametric

The empirical AEP curves for s at Gothenburg and Barcelona are shown in Fig. 4.3. As only 53 years of data are available the $VaR_{0.995}$ and $ES_{0.995}$ cannot be estimated empirically. The bootstrapped confidence intervals can be seen to provide

a tighter measure of variability than the DKW bounds (Fig. 4.3). However the bootstrap intervals assume the sample counts n and local mean vorticity y are independent. For Gothenburg (Fig. 4.3 a) this assumption is not valid, and the empirical AEP curve is outside of the bootstrapped intervals for the upper and lower tails, suggesting extremes of the aggregate loss (both high and low) are sensitive to frequency-intensity dependence. The Barcelona sample aggregate loss is contained within the intervals, suggesting that the small amount of negative dependence at this location does not significantly effect the extremes. The sample aggregate risk will always be contained within the DKW bounds, with or without dependence, though for a small sample size ($m = 53$) the 95% confidence band is large ($\epsilon = \pm 0.187$).

(a) (b)

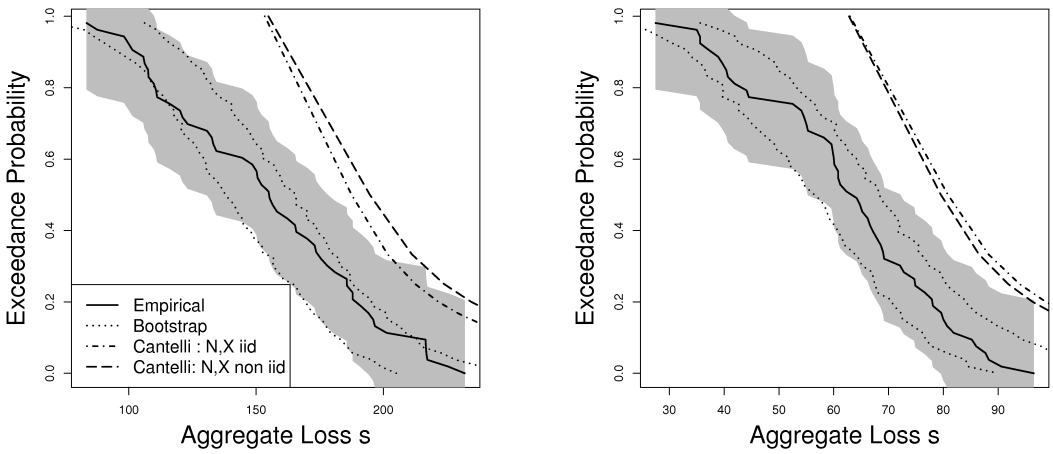

Figure 4.3: Empirical AEP curves, Cantelli bounds and bootstrapped confidence intervals for a) Gothenburg and b) Barcelona. Grey shading indicates the DKW 95% confidence bands.

The Cantelli bounds provide a (high) upper bound for the AEP curves and do not present a practical method for estimation of quantiles. However they can be used to investigate the behaviour of the tail of the aggregate loss. At Gothenburg the Cantelli bounds with and without dependence diverge with decreasing exceedance probabilities, where the upper bound for s is greater when dependence

is included (Fig. 4.3 a). At Barcelona the relation is reversed; the Cantelli bound with dependence has lower exceedance levels than the bound without dependence, although the difference between bounds is less than at Gothenburg (Fig. 4.3 b). As with the bootstrapped confidence intervals this suggests that positive dependence between the frequency and intensity results in an increase in the extremes of the aggregate loss. Conversely negative dependence may result in a decrease.

The percentage change in the Cantelli bounds for $VaR_{0.995}$ ($T = 200$ in Eqn 4.3) with the inclusion of dependence was $+13.0\%$ at Gothenburg and -5.0% at Barcelona. The ratio for the $VaR_{0.9}$ (1 in 10 year return level) with dependence/without dependence and $VaR_{0.995}$ with dependence/without dependence were calculated for all Northern Hemisphere grid points (Fig. 4.4). Similar conclusions can be drawn as from Gothenburg and Barcelona; locations with positive (negative) dependence show an increase (decrease) in the upper bound for the VaR when dependence is allowed and the difference between the bounds increases with greater return periods.

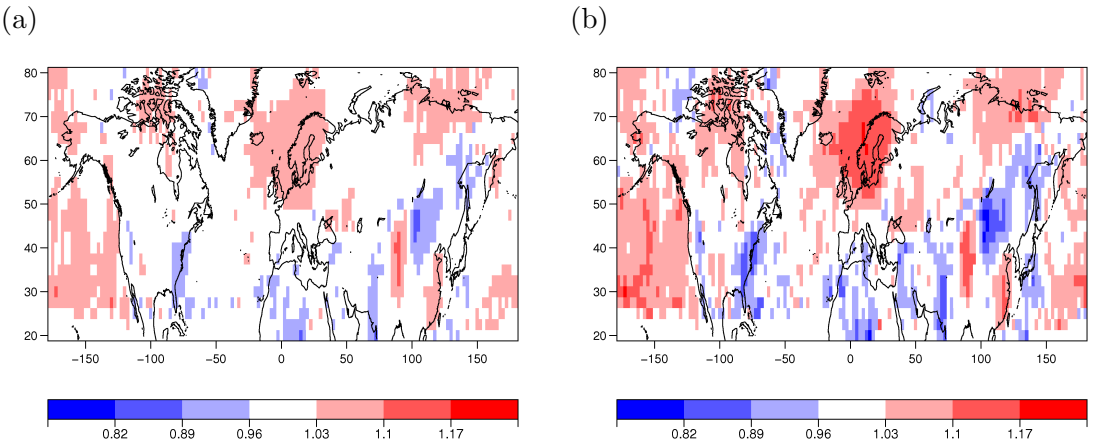

Figure 4.4: Plots of the ratio of the Cantelli bounds at each grid point with dependence/without dependence for (a)$VaR_{0.9}(s)$ (b) $VaR_{0.995}(s)$

The empirical models for the aggregate loss are inadequate for estimating the risk measures for the 1 in 200 year return level. The Cantelli bounds and boot-

strapped confidence intervals suggest that not accounting for positive (negative) dependence will result in underestimation (overestimation) of the extremes of the aggregate loss.

4.4.2 Parametric

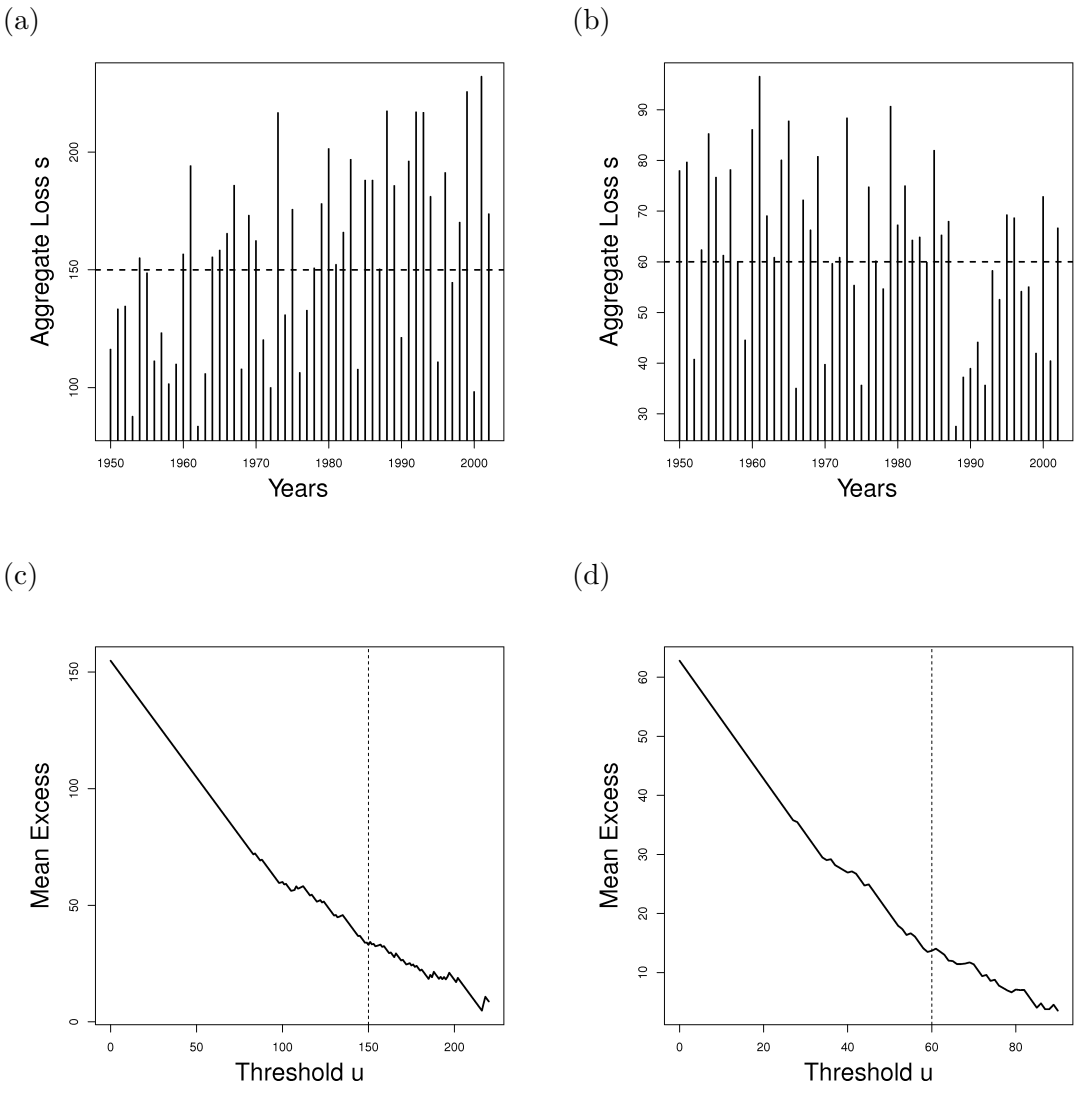

Figure 4.5: Time series of sample s for a) Gothenburg and b) Barcelona. The horizontal dashed line indicates the choice of threshold u for the GPD model. Mean excess plots for s at c) Gothenburg d) Barcelona. Vertical dashed lines indicate the choice of threshold parameter u for the GPD model.

Parameters for the GPD distribution were estimated for s at Gothenburg and Barcelona. Time series of s at each grid point are shown in Fig. 4.5 a, b. The mean excess plots were used to assist in determining suitable thresholds u for the GPD model, along with quantile-quantile plots of the fitted models (Fig 4.5 c, d). For Gothenburg a threshold of $u = 150$ was selected, and at Barcelona $u = 60$. The corresponding mle and standard errors of the parameters for Gothenburg were $\sigma = 57.7(13.1)$, $\xi = -0.68(0.19)$. For Barcelona the estimates were $\sigma = 21.5(4.64)$ and $-0.55(0.16)$. The negative shape parameter indicates a physical upper limit to the process at both locations.

The fit of the theoretical GPD cdf can be partially assessed by the quantile-quantile plots (Fig 4.6); the less scatter around the 45° line the better the skill of the model to reproduce the sample cdf. For both locations the GPD models provide a reasonable fit; the points are tightly scattered around the 45° line.

(a) (b)

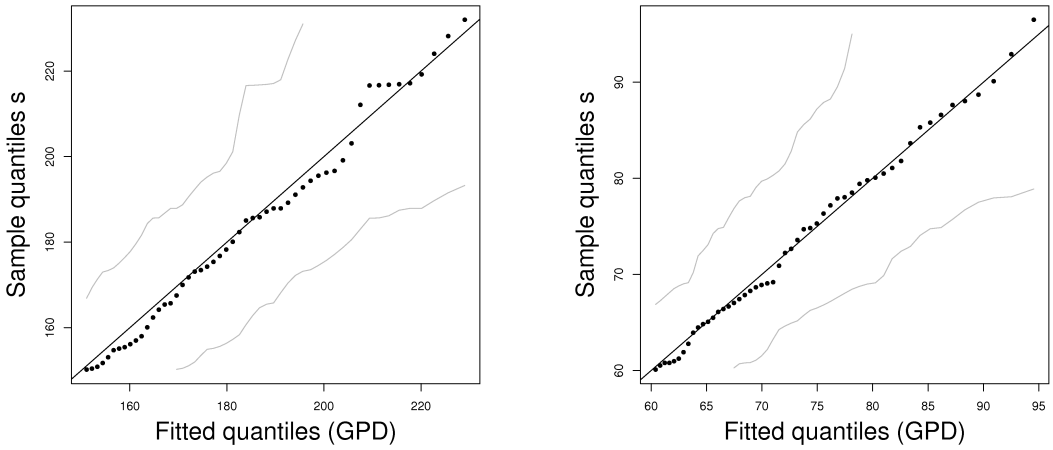

Figure 4.6: Quantile-quantile plots showing the fit of the theoretical GPD distributions for the a) Gothenburg grid point b) Barcelona grid point. Grey lines indicate the 95% confidence intervals. The solid black line is the 45° line

The AEP curves for the models are shown in Fig. 4.7. The empirical AEP curves are contained within the 95% (delta method) confidence intervals for all re-

turn levels. The risk measures obtained from the fitted GPD models are, at Gothenburg, $VaR_{0.995} = 231(224, 239)$ and $ES_{0.995} = 233$,and at Barcelona, $VaR_{0.995} = 96(91, 101)$ and the $ES_{0.995} = 97$. Despite the more sophisticated approach used here compared to the empirical estimates, at Gothenburg there is little difference between the maximum observed aggregate loss and the modelled $VaR_{0.995}$ (Fig. 4.7 a). The upper limits imposed by the model may be too low, resulting in the underestimation of the actual risk. This suggests that modelling the aggregate loss directly, without consideration of the underlying frequency and intensity distributions may not be effective.

(a) (b)

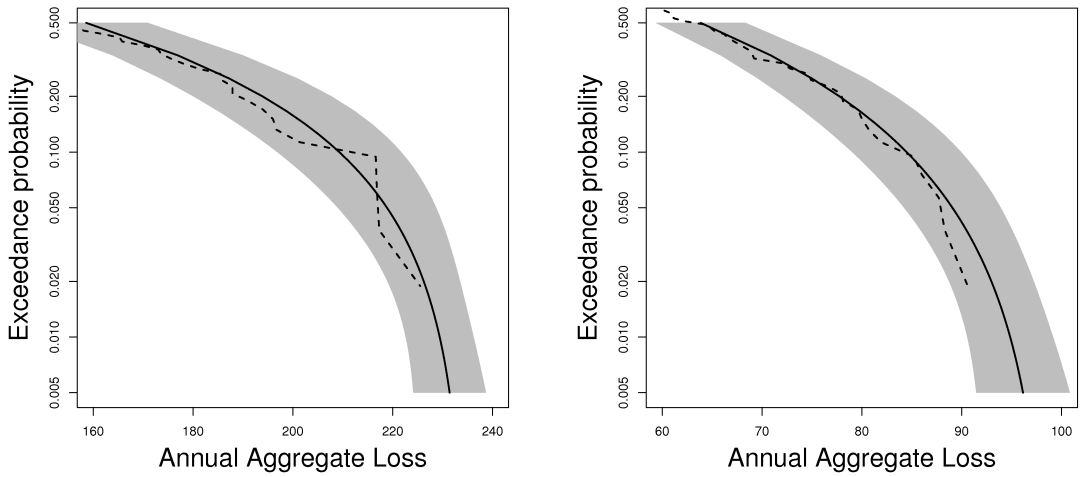

Figure 4.7: AEP curves for the theoretical GPD models at a) Gothenburg b) Barcelona. Grey shading indicates the 95% delta method confidence intervals. The dashed black line is the empirical exceedance probabilities.

4.4.3 Monte Carlo methods

The parameters for the four models described in Section 4.3.3 were fitted to cyclones passing the Gothenburg grid cell. The estimated rate parameter for the Poisson distribution was $\hat{\lambda} = 30.9$, and for the Negative Binomial distribution $\hat{p} = 30.9, \hat{r} = 148.9$. The gamma distribution for models M_1, M_2 had parameters $\hat{\alpha} = 5.47, \hat{\beta} = 1.01$ The quantile-quantile plot of the fitted Gamma distribution

against the sample vorticities indicates a reasonable fit (Fig. 4.8 a). The normal distribution parameters for the mean intensity and variance of the intensity were $\hat{\mu_Y} = 4.97, \hat{\sigma_Y} = 0.50$ and $\hat{\mu_W} = 4.40, \hat{\sigma_W} = 1.35$ respectively. There is some evidence that the tails of the fitted normal model is heavier than those of the sample local mean vorticity y, although the model again shows a reasonable fit, along with that of the vorticity variance w (Fig. 4.8 b, c).

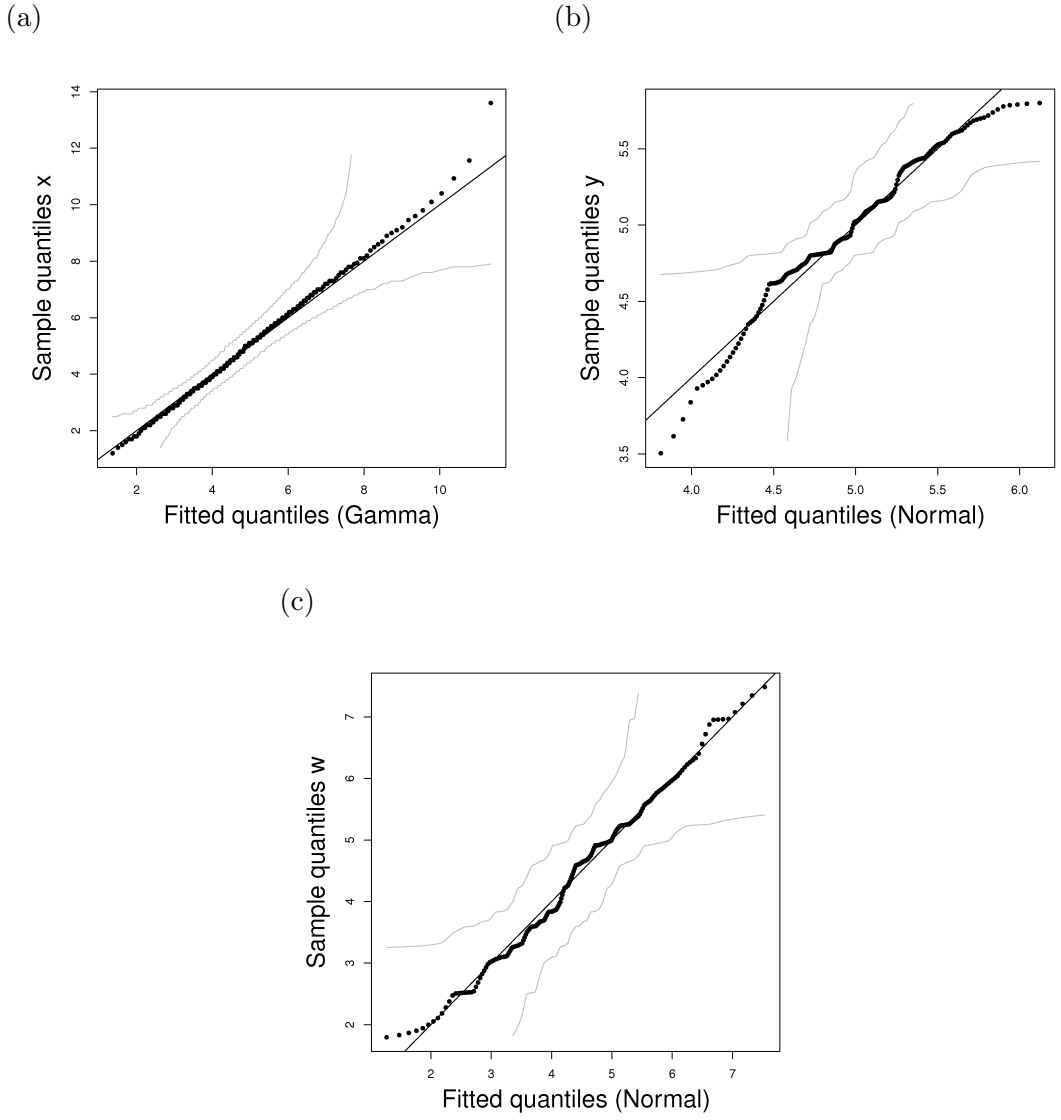

Figure 4.8: Quantile-quantile plots of a) the fitted Gamma model b) Normal model for y and c) Normal model for w. Lines as in Fig. 4.6

(a)

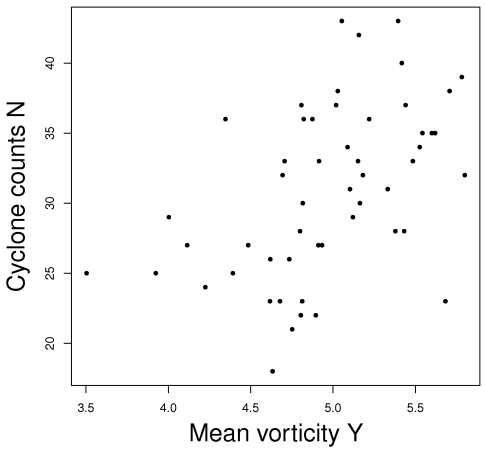

(b)

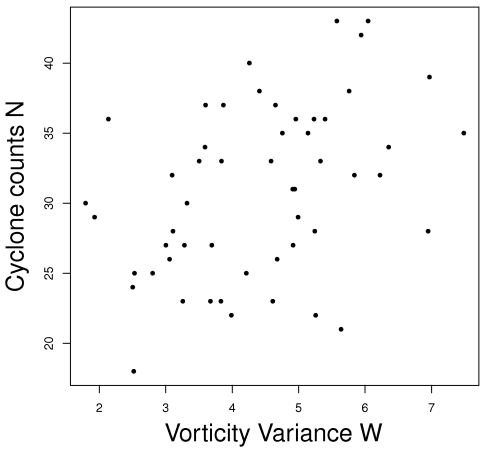

(c)

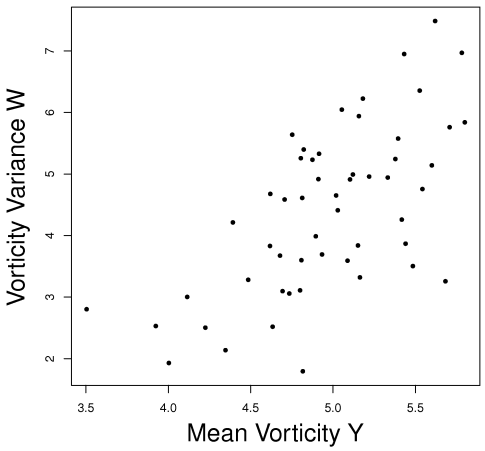

Figure 4.9: Plots of Gothenburg cyclone time series; a) Winter cyclone counts n and local mean vorticity y b) n and winter vorticity variance w c) n and y

To help assess whether a Gaussian copula was appropriate for modelling the dependence between N, Y and W, plots of the three variables are considered (Fig 4.9). If upper or lower tail dependence is present between N, Y and W this would suggest that another copula that allows for such extremal dependence, e.g. a Gumbel or Clayton copula, may be more suitable (McNeil et al. (2005) Section 5.1). Considering Fig. 4.9 there is no suggestion of extremal dependence between

any of the three variables, and thus a Gaussian copula is deemed suitable for use in the Monte Carlo simulations. The parameters for the correlation matrix Σ for the random vector $[N, Y, W]^T$ were;

$$\Sigma = \begin{bmatrix} 1.00 & 0.37 & 0.28 \\ 0.37 & 1.00 & 0.45 \\ 0.28 & 0.45 & 1.00 \end{bmatrix}.$$

The aggregate losses were simulated from models M_1, M_2 as follows.

For i in $1, \ldots, m$,

1. Simulate the number of losses n_i
2. Simulate the individual losses $x_{i,1} \ldots, x_{i,n_i}$ from $Ga(\hat{\alpha}, \hat{\beta})$
3. Calculate the aggregate loss $s_i = x_{i,1} + ...x_{i,n_i}$.

For the models M_3, M_4 the losses were simulated as follows.

For i in $1, \ldots, m$

1. Simulate $d_i \sim N_d(0, \Sigma)$
2. Calculate $u_i = (\Phi(d_{1,i}), \Phi(d_{2,i}), \Phi(d_{3,i}))$
3. Calculate n_i, w_i, y_i from $F_N^{-1}(u_{i,1}), F_Y^{-1}(u_{i,2}), F_W^{-1}(u_{i,3})$.
4. Simulate the individual losses $x_{i,1} \ldots, x_{i,n_i}$ from $Ga(y_i^2/w_i, y_i/w_i)$
5. Calculate the aggregate loss $s_i = x_{i,1} + ...x_{i,n_i}$,

To determine the number of simulations m required for the tail of the simulated loss distribution to converge, the model M_1 was approximated for different values of m (Fig. 4.10). For each m the Cantelli bounds, DKW bounds and bootstrapped confidence intervals for $VaR_{0.995}$ are shown. The simulated mean loss and bootstrapped confidence intervals are reported in Table 4.1. For all simulation run lengths m the Cantelli bounds are greater than the DKW confidence bands. The

Cantelli bounds are therefore not used further in the simulation study, as they offer no additional insight for the aggregate loss distribution.

(a) (b)

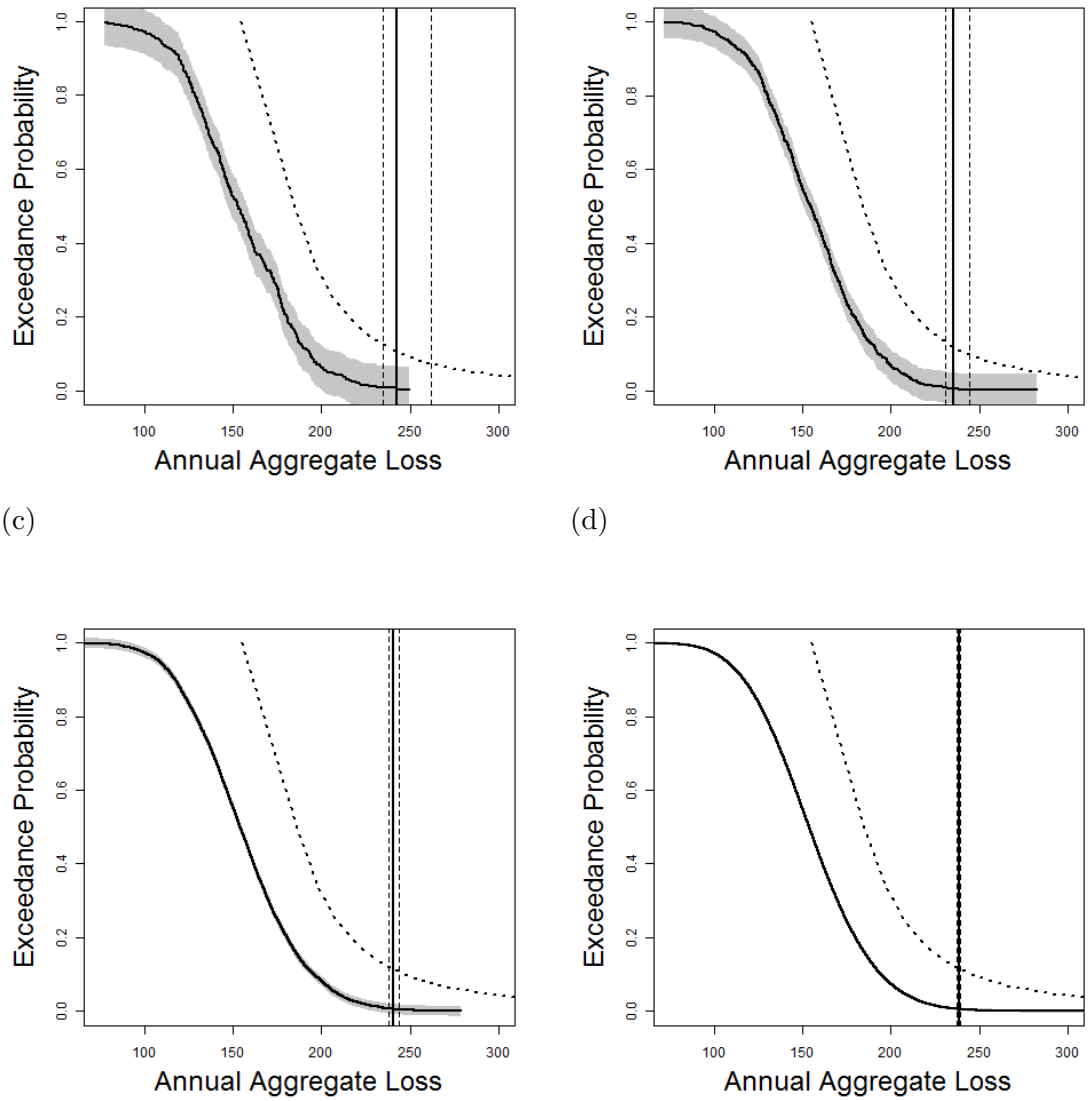

(c) (d)

Figure 4.10: Simulated AEP curves for the aggregate loss distribution for model M_1 (black solid line) with 95% DKW confidence bands (grey shading), Cantelli bounds (dotted line), $VaR_{0.995}$ (vertical solid black line) and 95% bootstrapped confidence intervals for $VaR_{0.995}$ (vertical black dashed lines) for a) $m = 500$ simulations b) $m = 1000$, c) $m = 10,000$ and d) $m = 100,000$.

The mean annual aggregate loss for all simulation run lengths is within 1% of

the sample mean aggregate loss (Table 4.1). The estimates of the risk measures were all reasonably consistent ($\approx 3\%$ difference between the smallest and largest estimates). Considering the bootstrapped confidence intervals for the $VaR_{0.995}$, when $m = 500$, there is a proportional uncertainty of $\approx 12\%$, decreasing to $\approx 0.8\%$ when $m = 100,000$. It is desirable to ensure that any differences between simulated risk measures is due to the different modelling assumptions and not variation inherent in the Monte Carlo simulation process. For this reason the models M_1, M_2, M_3, M_4 are simulated $m = 100,000$ times each. The effect of different modelling assumptions on the risk measures is now considered.

m	$\bar{s}$	$VaR_{0.995}(s)$	$ES_{0.995}(s)$	DKW
500	-0.0%	242 (235,262)	247	0.061
1000	$+0.2\%$	235 (231,244)	250	0.043
10,000	$+0.4\%$	240 (238,244)	252	0.014
100,000	$+0.0\%$	238 (237,239)	250	0.004

Table 4.1: Simulated aggregate losses for M_1 using different numbers of simulations m. The mean annual aggregate loss $\bar{s}$ is reported as the percentage difference from the sample estimate from the Gothenburg observations. Bootstrapped confidence intervals for the $VaR_{0.995}$ are reported in brackets.

In Figure. 4.11 the AEP curves, from 100,000 simulations each, of models M_1, M_2, M_3 and M_4 are shown. Comparing the curves, the inclusion of clustering and dependence can be seen to increase the exceedance levels for all exceedance probabilities less than 0.2. From visual inspection of the plot the following preliminary inferences can be made. Firstly, overdispersion in the counts distribution increases the tail of the aggregate risk distribution. Secondly including frequency-intensity dependence also increases the tail of the aggregate risk distribution, and has a greater effect than overdispersion alone. Thirdly, the inclusion of both frequency-intensity dependence and overdispersion increases the tail of the aggregate risk, and has a greater impact than clustering or frequency-intensity dependence individually.

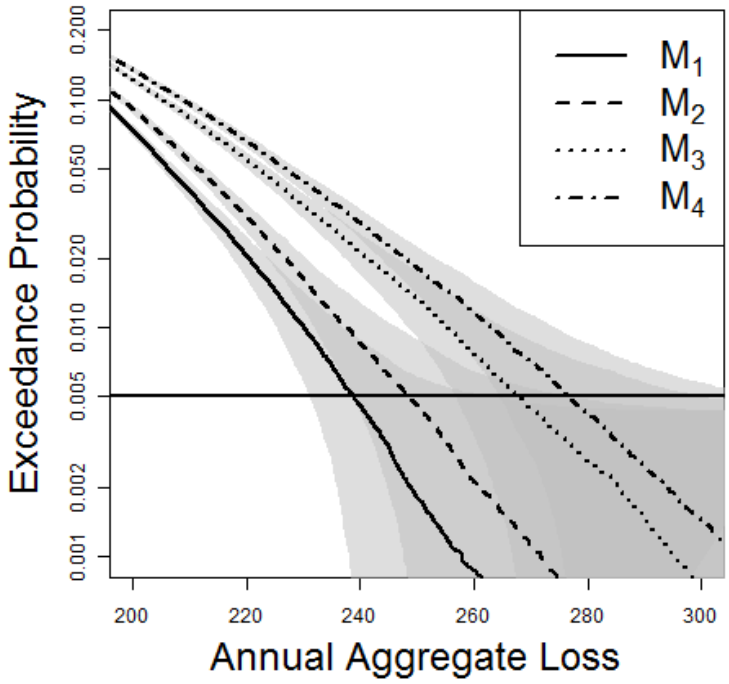

Figure 4.11: Plot of the simulated AEP curves for Gothenburg for the models M_1, M_2, M_3, M_4. The horizontal line marks the $VaR_{0.995}$

The risk measures for the model M_1 are used as the baseline values to quantify the changes in the $VaR_{0.995}$ and $ES_{0.995}$ when clustering and dependence are included. The ratio of the $VaR_{0.995}$ for M_2/M_1 is 1.04; introducing overdispersion into the counts but assuming frequency and intensity independence, has resulted in a 4% increase in the 200 year return level for the aggregate loss. The ratio of the $VaR_{0.995}$ for M_3/M_1 is 1.12; so frequency-intensity dependence has resulted in an increase of 12% in the risk measure, without allowing for clustering. Finally the ratio of the $VaR_{0.995}$ for M_4/M_1 is 1.15; a 15% increase when clustering and frequency intensity dependence are included in the aggregate loss model. The ratios of the expected shortfalls, ES, show approximately the same changes for the inclusion of clustering and dependence.

	$\bar{s}$	s_s^2	$VaR_{0.995}(s)$	$ES_{0.995}(s)$
Gothenburg	154.84	1588.3	-	-
M_1	+0.0%	−42.0%	238 (237,239)	250
M_2	+0.1%	−31.7%	249 (248,250)	262
M_3	+0.2%	−8.2%	268 (266,269)	285
M_4	+0.1%	+4.2%	277 (275,278)	295

Table 4.2: Simulated aggregate losses for Gothenburg. The sample mean $\bar{s}$ and variancess_s^2 for each model are reported as the percentage difference from the sample mean and variance from the Gothenburg observations. For the $VaR_{0.995}$ the bootstrapped confidence intervals are reported in brackets.

To help assess which model most closely reflects the observed behaviour of the aggregate losses, the mean and variance of the aggregate loss as well as the dispersion of extreme events for the models is compared to the sample values for Gothenburg. From the summary statistics in Table 4.2, the simulated mean aggregate annual loss $\bar{s}$ for all models is within 1% of the sample mean aggregate loss for Gothenburg. The variance for the simulated losses is between $30 - 42\%$ lower than the sample variance at Gothenburg for the models without frequency-intensity dependence (M_1, M_2). The variance of the simulated aggregate losses for the model with frequency-intensity dependence but without clustering (M_3) is lower than the variance of the Gothenburg losses (-8%), but provides a better approximation than either M_1 or M_2. The model M_4 with dependence and clustering provides the closest approximation to the observed variance in the aggregate losses $(+4\%)$.

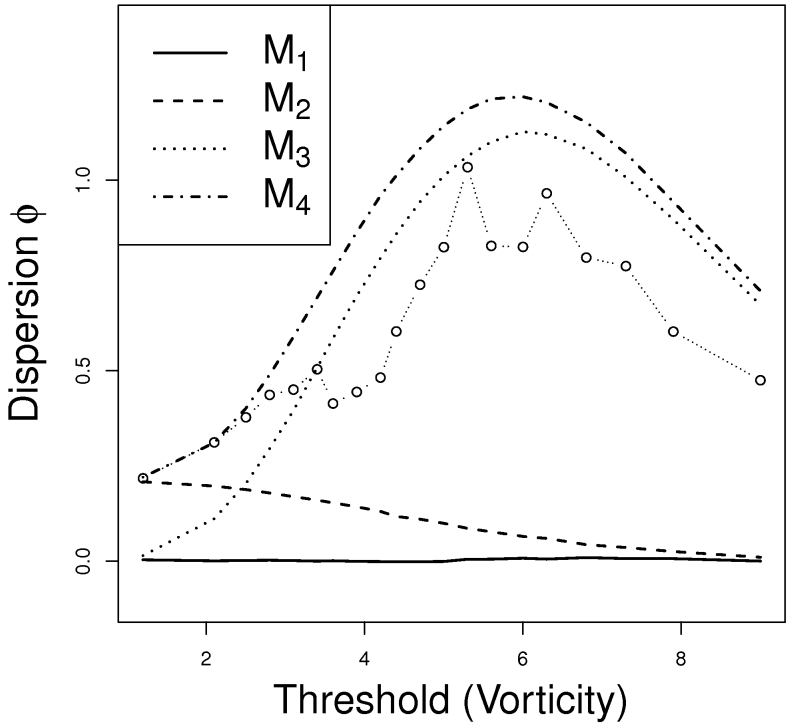

Figure 4.12: Plot of the dispersion in counts for each model M_1, M_2, M_3, M_4 for increasing vorticity thresholds. The circles indicate the sample dispersion for Gothenburg.

The dispersion of counts exceeding an intensity threshold for the 4 models and for the observed Gothenburg counts is shown in Fig. 4.12. The dispersion of the models with dependence, M_3, M_4, can be seen to most closely reflect the dispersion at Gothenburg. The model M_1 with Poisson distributed N, is equidispersed ($\phi(N) = 0$)for all intensity thresholds. The model M_2 with negative binomially distributed N, has dispersion $\phi(N) = 0.2$ for all counts, but this decreases with increasing intensity threshold. Considering the dispersion of counts for M_2 exceeding the $50th$ percentile of the intensity distribution, $\phi(N_u) = 0.11 \approx 0.1$, as expected from Eqn. 4.2 ($q = 0.5$; $\phi = 0.5 * 0.2 = 0.1$). The model M_3 is equidispersed when considering all counts ($\phi(N) = 0$), but increases to around $\phi(N_u) = 0.6$ when considering the subset of events exceeding the $70th$ percentile of the intensity distribution. Therefore when N and X are positively dependent the occurrence of

extremes will cluster regardless of the choice of frequency distribution. For M_4, the dispersion for all counts is $\phi(N) = 0.2$, increasing to $\phi = 1$ for events exceeding the $70th$ percentile, before decreasing to $\phi = 0.7$ for events exceeding the 95th percentile.

The decrease in dispersion for the most intense events for both the observed dispersion and models M_3 and M_4 is somewhat counter-intuitive. This behaviour may partially be due to the scarcity of data; the uncertainty surrounding the behaviour of extremes is high. Bootstrapped confidence intervals were constructed for the 3-monthly counts (see Fig. 2.1) but these provide loose bounds and are not particularly informative. Also, the relation between the mean intensity and counts is not necessarily linear (hence the use of copulas) and there may be some physical upper limit to the clustering of extreme cyclones.

The $VaR_{0.995}$ estimates from the GPD model for Gothenburg are outside of the bootstrapped confidence intervals of M_2, M_3, M_4. Only the M_1 $VaR_{0.995}$ contains the GPD model values within its limits, and this model was shown to underestimate the sample variance of the aggregate risk. This would further indicate that the GPD model is unsuitable for modelling the aggregate loss of extra tropical cyclones.

Alternative simulation models were also considered briefly for Barcelona (not shown). As Barcelona cyclones had low correlation between the frequency and intensity, and counts were not over-dispersed ($\phi(N) \approx 0.0$), there was little different between the models $M_1 - M_4$.

4.5 Summary

Methods for exploring the behaviour of extremes of the aggregate loss distribution have been discussed. The effect of frequency-intensity dependence on extremes of the aggregate loss distribution have been investigated, as well as the sensitivity of the aggregate loss to clustering with and without frequency intensity dependence.

Non-parametric Cantelli bounds and bootstrap confidence intervals were used to investigate the effect of frequency-intensity dependence on the empirical exceedance levels for extra tropical cyclones passing near Gothenburg and Barcelona. Positive (negative) dependence was shown to result in a increase (decrease) in the exceedance levels. Due to the length of the data set (53 years), empirical models were found to be inadequate for estimating the value-at-risk VaR and expected shortfall ES for the 1 in 200 year return period.

Generalised Pareto distributions were used to investigate if the aggregate loss distributions could be modelled directly, avoiding considerations of the distribution of the frequency and intensity of individual losses and the covariance between. These models showed an adequate fit for the observed return levels, but it was concluded that the models could be underestimating extremes of the aggregate distribution.

A Monte Carlo simulation approach was then used to investigate the effect of frequency-intensity dependence and clustering on the extremes. Dependence resulted in clustering of extremes, whether or not the frequency distribution included overdispersion. Conversely without frequency-intensity dependence extremes did not cluster even when the frequency distribution was overdispersed.

Dependence between the frequency and intensity of events increased the risk measures for the aggregate risk distribution; $VaR_{0.995}$ and $ES_{0.995}$, by around 12% without allowing for clustering in the model formulation. Clustering was found to result in a 4% rise in the risk measures without frequency-intensity dependence. The inclusion of both dependence and clustering in the model resulted in an increase of 15% compared to the model with neither.

Chapter 5

Incorporation of dependency into the loss component of Catastrophe Models

5.1 Aim

Catastrophe models are widely used in the insurance/reinsurance industry to quantify the financial risk posed by natural hazards (Grossi and Kunreuther, 2005). The output of these models is an *event loss table* which is used to approximate the distribution of financial losses which could result from a particular type of hazard. This chapter briefly outlines the structure of a catastrophe model. Models for the annual aggregate losses which are compatible with the event loss table are then introduced. The purpose of these models is to investigate how best to incorporate the findings of the previous two chapters regarding frequency-intensity dependence and clustering into the catastrophe model framework. The performance of these models is then illustrated using the event loss table of a hypothetical insurer.

5.2 Catastrophe models

Natural hazards have a low frequency and a high severity in comparison to other forms of insured risk (Clark, 2002). A consequence of this is that traditional actuarial techniques which rely on a high frequency/low severity of claims are inadequate for managing the risk from natural hazards (Banks, 2005). Alternative approaches which use statistical and deterministic methodologies to model the physical risk of a hazard and translate it into financial loss have been developed, usually referred to as catastrophe models (Woo (2002); Grossi and Kunreuther (2005)).

Although the need for a more sophisticated approach to managing risk has been advocated in the literature since the 1970s (see Friedman (1972)), catastrophe models were not widely adopted by the insurance community until the unprecedented natural catastrophe losses of the early 1990s. These losses included the series of windstorms which affected Europe in 1990, hurricane Andrew in 1992 and the Northridge earthquake of 1994 (Grossi and Kunreuther, 2005). Hurricane Andrew alone resulted in 9 insurers becoming insolvent when it caused around $15.5 billion in insured losses. In the years since Andrew, catastrophe models have become increasingly sophisticated as well as receiving greater recognition from the insurance community (Clark, 2002). The construction of a catastrophe model varies between modellers but the same basic approach is used. A natural hazard is defined in terms of its physical parameters, then the hazard is applied to an inusrance portfolio and the resulting financial loss is calculated through a vulnerability function (Grossi and Kunreuther, 2005). The formulation of a catastrophe model is described in the next section.

5.2.1 Mathematical formulation of a catastrophe model

The objective of a catastrophe model is to quantify the financial risk from a particular type of natural hazard. The input for a catastrophe model is the physical parameters of the hazard and the insurer's portfolio, and the output is a table of losses and their frequency of occurrence. Catastrophe models consist of four main

components; the exposure database, the hazard module, the vulnerability module and the financial loss module (see Figure 5.1).

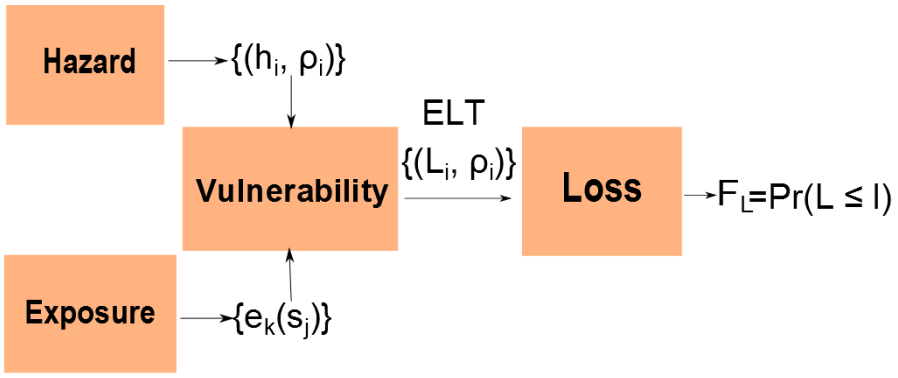

Figure 5.1: Component modules in a catastrophe model.

Exposure database - a database of insured properties, this is the insurer's exposure for a given region. For loss estimation the most important information is the location and construction type of the property. The location is necessary to be able to apply the local intensity of the hazard, and the damage caused by a given hazard intensity is largely a function of hazard intensity and construction type (Grossi and Kunreuther (2005)). For each construction type $k = 1, 2, \ldots, K$ at location $j = 1, 2, \ldots, J$ there are variables $e_k(s_j)$, where s_j is the location, and $e_k(s_j)$ is the exposure (total insured value). The exposure $e_k(s_j)$ is an aggregation of properties of type k within a specified region, usually defined by post codes.

Hazard module - a catalogue of historical and simulated hazard events, each of which is characterized by an annual rate of occurrence and spatial maps of the hazard's intensity (e.g. maximum wind speed). For most types of hazard, only the variables for a small number of historic events will be available. Most of the events in the catalogue will be perturbations of historic events or synthetic events which have been simulated from a parametric or numerical weather prediction (NWP) model. Each event in the catalogue is of the form $(i, \rho_i, h_i(s))$, where $i = 1, 2, ..., I$ is the event id, ρ_i is the annual rate of occurrence and $h_i(s)$ is the hazard intensity

at location s.

Vulnerability module - the vulnerability of a building of a construction type k is a function of the hazard h. This vulnerability function is usually estimated from historical data using engineering expertise (Grossi and Kunreuther, 2005). A typical form is

$$V_k(h_i, s_j) = \Phi_k V(h_i(s_j), s_j),$$

where Φ_k is a multiplicative factor to model the effect of construction type. The insured loss of buildings of type k at location s_j due to hazards h_i is then given by

$$l_{i,j,k} = e_k(s_j)\Phi_k V(h_i(s_j), s_j).$$

The vulnerability $V_{j,k}$ is a damage ratio in the interval $[0, 1]$; the loss corresponding to a given hazard h and exposure e is a fraction of the total insured value exposed. The total loss due to event i, L_i is the sum of the losses for each construction type at each location,

$$L_i = \sum_{j=1}^{J}\sum_{k=1}^{K} l_{i,j,k} = \sum_{j=1}^{J}\sum_{k=1}^{K} e_k(s_j)\Phi_k V(h_i(s_j)).$$

An upper bound for the loss L_i is given by $E_i = \sum_{j=1}^{J}\sum_{k=1}^{K} e_k(s_j)$, which is the total exposure of all construction types at all locations. This assumes the vulnerability function is deterministic. However, the loss can also be defined where the vulnerability is a stochastic function of the hazard h_i. This results in secondary uncertainty for the loss of event i, the primary uncertainty being related to the occurrence of the event. This secondary uncertainty is due to variation within the damage of exposures of the same construction type experiencing the same hazard intensity. The secondary uncertainty is not considered here, but for a discussion of the effect of secondary uncertainty in the event losses on the resulting aggregate loss see Diers (2008).

Financial loss module - once the monetary losses due to a hazard have been modelled via the vulnerability function the insured losses can then be calculated.

This is done by taking into consideration policy cover limits and deductibles, loss triggers, attachment points etc (Grossi and Kunreuther, 2005). The final output of the catastrophe model is called an *event loss table* (ELT), and is of the form $(i, \rho_i, E[L_i], Var[L_i], E_i)$. The parameters i and ρ_i are the same as in the hazard module. Here, $E[L_i] = \mu_i$ is the expected loss, $Var[L_i] = \sigma^2_{L_i}$ the secondary uncertainty, and E_i the total exposure (maximum loss) for the ith row.

The ELT can then be to approximate the annual losses for the user's portfolio (see Section 5.3). These losses are often represented using exceedance probability (EP) curves. As well as the aggregate exceedance probability (AEP) which was considered in Chapter 4, the conditional exceedance probability (CEP) and occurrence exceedance probability (OEP) are of interest to insurers. The conditional exceedance probability is the probability that the loss of a single event exceeds a threshold x,

$$CEP(x) = Pr(X > x) = 1 - F_X$$

where F_X is the cumulative distribution function of X. The OEP is the probability that the maximum loss in a year $X_{max} = max(X_1, ...X_N)$ exceeds a threshold x;

$$OEP(x) = Pr(X_{max} > x).$$

5.3 Methods

In this section probability models for annual losses are introduced which are compatible with event loss tables. The parameters of the ELT are used to specify the distributions of the frequency N and intensity X of losses, which in turn determine the distribution of the annual aggregate loss $S = X_1 + ... + X_N$ and the annual maximum loss X_{max}. For the rest of the chapter it is assumed that there is no secondary uncertainty for the individual rows of the ELT; for event i the loss is $X_i = \mu_i$.

5.3.1 Current Practice

Typically the individual rates are assumed to be stationary in time and the rows in an ELT are independent of one another. Each row of the ELT is then modelled as a compound Poisson or Negative Binomial process, and the aggregate loss is the the sum of the losses over all the rows:

$$S = \sum_{i=1}^{I} S_i = \sum_{i=1}^{I} N_i X_i,$$

where $N \sim Pois(\rho_i)$, and X_i is the expected loss for row i. The mean and variance of S is

$$E[S] = \sum_{i=1}^{I} E[N_i X_i] = \sum_{i=1}^{I} \rho_i \mu_i$$

$$Var[S] = \sum_{i=1}^{I} Var[N_i X_i] = \rho_i \mu_i^2$$

as $E[N_i] = Var[N_i] = \rho_i$, $E[X_i] = \mu_i$, $Var[X_i] = 0$ and $Cov(N_i Y_i, N_j X_j) = 0$ if $i \neq j$. The cumulative distribution function of S is denoted $F_S(x) = P(S \leq x)$. As in Chapter 4, F_S can be approximated using Monte Carlo simulation methods. If each row is simulated individually then estimating F_S requires the simulation of thousands of compound processes thousands of times each. However the following property of Poisson compounds greatly simplifies the simulation process.

Theorem For some natural number I, let $S = S_1 + ... + S_I$ be the sum of independent Poisson compounds $S_1, \ldots, S_I$, where $S_i \sim CPois(\rho_i, F_{X_i})$, $i = 1, \ldots, I$. Then S has a compound Poisson distribution,

$$S \sim CPois(\rho, F_X),$$

where

$$\rho = \sum_{i=1}^{I} \rho_i, \;\; F_X = \sum_{i=1}^{I} \frac{\rho_i}{\rho} F_{X_i}.$$

(for a proof see Rolski et al. (2009) Section 4.2.2). The annual losses can then be simulated as follows; first the number of losses are simulated from $N \sim Pois(\rho)$ then N individual losses are selected by sampling from F_X (e.g. by bootstrap resampling

of the L_i). The CEP for the event loss table with no secondary uncertainty ($X_i = \mu_i$) is

$$CEP(x) = 1 - Pr(X \leq x) = \frac{\sum_{\mu_i > x} \rho_i}{\sum_{i=1}^{I} \rho_i}, \tag{5.1}$$

where $\sum_{\mu_i > x} \rho_i$ is the sum of all rates whose expected loss μ_i exceeds x. The assumption of stationarity for the rates is not appropriate for many types of natural hazard. Studies have shown that extra tropical cyclones, Atlantic hurricanes and U.S. floods exhibit overdispersion which is caused by rate-variation due to changes in the background atmospheric conditions with time (Mailier et al. (2006); Vitolo et al. (2009); Villarini et al. (2013)). In Chapter 3, it was also shown that background atmospheric conditions result in covariance between the frequency and intensity of extra tropical cyclones. Models which allow for this time variation in the rates and frequency-intensity dependence are now introduced.

5.3.2 Mixture model approach

The mixture model approach outlined in this section is already widely used in credit risk modelling (Crouhy et al. (2000); Frey and McNeil (2003)). Credit risk portfolios take a similar form to event loss tables; a portfolio will consist of a bank's loans each of which is characterized by a probability of defaulting and a corresponding loss. Although loans are assumed to default independently of each other they can be affected by the same set of background factors such as the rate of inflation, interest rates etc. To include this in the credit risk models the loans are regressed on a common set of random variables which represent these factors. In this section, similar techniques have been adapted for catastrophe modelling (Fig. 5.2).

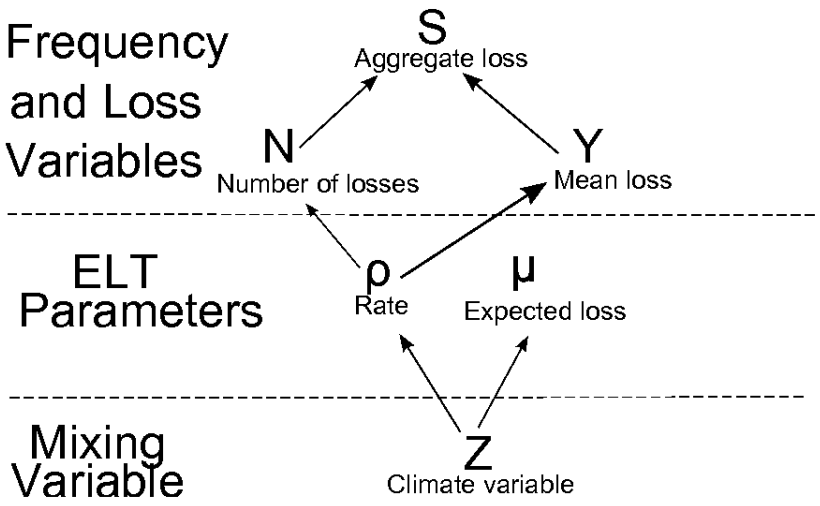

Figure 5.2: Schematic of the relationship between the observed variables S, N, Y, the event loss table parameters and any additional unobserved model variables.

The rate of hydro-meteorological hazards are assumed to depend upon the background atmospheric conditions. The effect of changes in the atmospheric conditions can be included in the annual losses by the introduction of a random variable Z. Here Z is some measure of the state of the climate during the relevant time period. For example, if the aggregate loss is due to winter extra tropical cyclones over Europe, then Z might represent the winter mean of the NAO index. The stochastic rates are denoted λ_i and are related to Z deterministically through some link function g;

$$g(\lambda_i) = \beta_{0,i} + \beta_{1,i} Z,$$

where the parameters $\beta_{0,i}$,$\beta_{1,i}$ are selected such that $E[\lambda_i] = \rho_i$ so that the mean number of times each row is sampled remains unchanged. A Poisson process with a stochastic rate λ_i is called a Poisson mixture distribution. A consequence of mixing the rates is that the counts are now more variable; $Var[N] > E[N]$ (see Chapter 2). Although the rows are now related to a common factor, they are conditionally independent of each other given Z, and the aggregate loss can still be modelled as a single compound process for each realization of Z (McNeil et al., 2005). Specific

forms for the link function g and climate variable Z are now investigated.

Bernoulli model. Here the state of the climate is modelled for simplicity with a binary random variable $Z \sim Ber(\theta)$. The rates are related to Z by a linear link function,

$$\lambda_i = \beta_{0,i} + \beta_{1,i} Z. \tag{5.2}$$

The intercept parameter is non-negative, $\beta_{0,i} \geq 0$, otherwise if $Z = 0$, then $\lambda_i < 0$. The expectation of λ_i is $E[\lambda_i] = \rho_i$ and

$$E[\lambda_i] = \beta_{0,i} + \beta_{1,i}\theta = \rho_i,$$

then rearranging for $\beta_{0,i}$

$$\beta_{0,i} = \rho_i - \theta\beta_{1,i}$$

and as $\beta_{0,i} \geq 0$,

$$\beta_{1,i} \leq \frac{\lambda_i}{\theta} \tag{5.3}$$

Log normal mixture. Here the mixing variable follows a standardized normal distribution $Z \sim N(0, 1)$, and is related to the rates with a log-link function

$$log(\lambda_i) = \beta_{0,i} + \beta_{1,i} Z. \tag{5.4}$$

This approach has the advantage that as Z is now continuous it can reflect the full range of variability in the climate. The log-link function is the usual form for Poisson regression studies of count data (e.g. Mailier et al. (2006); Katz (2002)). The log transformation also ensures that λ_i is non-negative, allowing greater flexibility in the parameterization of $\beta_{0,i}, \beta_{1,i}$.

5.3.3 Parameter estimation: constant dispersion

The mean number of losses from each row annually is specified by the rate parameter $E[N_i] = \rho_i$, but not the variance of the counts, $Var[N_i]$. Here it is assumed that although the variance in the total annual number of losses, $Var[N]$, is not defined by the ELT it is known to the modeller, and so $\phi(N) = Var[N]/E[N] - 1$ is also known to the modeller. Then if the mean and variance of N are known the

beta parameters can be estimated using the Method of Moments. In this section the dispersion for each row is assumed to have the following form,

$$Var[N_i]/E[N_i] = \phi\rho_i + 1 \tag{5.5}$$

similar to that of the negative binomial distribution. The overdispersion parameter ϕ is specified by the modeller and does not depend on i (hence constant dispersion). Note that from Eqn. 5.5 the variance of the ith row $Var[N_i]$ is a function of the rate parameter ρ_i but not the intensity μ_i.

If $Var[N]$ and $E[N]$ are known then the dispersion parameter ϕ can be estimated. First note that the variance of N is

$$Var[N] = E[\lambda] + Var[\lambda], \tag{5.6}$$

see Section 2.2.3. The expectation of λ is, $E[\lambda] = E[\lambda_1 + ...\lambda_I] = \rho$. The variance of λ, where λ_i is related to the mixing variable Z via a log or link function as specified in the previous section, can be shown to be,

$$Var[\lambda] = \phi \left(\sum_{i=1}^{I} \rho_i \right)^2$$

see Appendix C. Then rearranging Eqn. 5.6 for ϕ

$$\phi = \frac{Var[N] - \sum_{i=1}^{I} \rho_i}{\left(\sum_{i=1}^{I} \rho_i \right)^2} = \left(\frac{Var[N]}{E[N]} - 1 \right) \frac{1}{\sum_{i=1}^{I} \rho_i}. \tag{5.7}$$

As $Var[N]$, $E[N]$ and $\sum_{i=1}^{I} \rho_i$ are all known ϕ can thus be calculated for the models with linear or log link.

Bernoulli model. A Bernoulli model for the aggregate loss, with rate as specified in Eqn. 5.2 has mean

$$E[\lambda_i] = \beta_{0,i} + \beta_{1,i}\theta$$

and variance

$$Var[\lambda_i] = \beta_{1,i}^2 \theta(1-\theta). \tag{5.8}$$

As these moments are known then $\beta_{0,i}$ and $\beta_{1,i}$ can be determined. Equation 5.8 can be rearranged for $\beta_{1,i}$;

$$\begin{aligned} \beta_{1,i}^2\theta(1-\theta) &= \phi\rho_i^2 \\ \beta_{1,i} &= \pm\rho_i\sqrt{\frac{\phi}{\theta(1-\theta)}} \end{aligned} \tag{5.9}$$

and $\beta_{0,i}$ is then

$$\beta_{0,i} = \rho_i - \beta_{1,i}\theta. \tag{5.10}$$

For this choice of dispersion the rates for the Bernoulli model scale identically with Z. This can be shown by expressing $\beta_{0,i}, \beta_{1,i}$ in terms of θ, ρ_i, ϕ using Eqns. 5.9, 5.10,

$$\lambda_i = \rho_i\left(1 + \frac{\phi}{\theta(1-\theta)}(Z-1)\right) = \rho_i c_1,$$

where c_1 is a constant and does not depend on i. A consequence of this is that the CEP remains unchanged for different values of Z,

$$\begin{aligned} CEP(x) = 1 - F_X(x) &= \frac{\sum_{\mu_i>x}\lambda_i}{\sum_{i=1}^{I}\lambda_i} \\ &= \frac{\sum_{\mu_i>x}\rho_i c}{\sum_{i=1}^{I}\rho_i c} = \frac{\sum_{\mu_i>x}\rho_i}{\sum_{i=1}^{I}\rho_i} \end{aligned}$$

which is the CEP for the current practice model with stationary rates (Eqn. 5.1). Therefore X is independent of Z.

Log normal model The same approach as in the Bernoulli model can be used to calculate the regression coefficients and dispersion parameter. The log normal model with a stochastic rate as specified in Eqn 5.4 has mean and variance

$$\begin{aligned} E[\lambda_i] &= E[e^{\beta_{0,i}+\beta_{1,i}Z}] = e^{\beta_{0,i}+\beta_1^2/2} \\ Var[\lambda_i] &= e^{2\beta_{0,i}+\beta_{1,i}^2}(e^{\beta_{1,i}^2}-1). \end{aligned}$$

see e.g. Aitkin et al. (2009) Section 8.3. Since $E[\lambda_i] = \rho_i$ and $Var[\lambda_i] = \phi\rho_i^2$,

$$\phi = \rho_i(e^{\beta_1^2}-1),$$

rearranging for β_1,

$$\beta_1 = \sqrt{log(1+\phi)} \tag{5.11}$$

and $\beta_{0,i}$ is then

$$\beta_{0,i} = log(\rho_i) - \frac{1}{2}log(1+\phi). \tag{5.12}$$

As in equation 5.3.3 the ratio of the rates λ_i will scale with Z, with constant c_2 where

$$c_2 = e^{-(1/2)log(1+\phi)+log(1+\phi)^{1/2}Z}.$$

5.3.4 Intensity dependent dispersion

With constant dispersion all the ELT rates scale identically with Z and thus the conditional exceedance probability (and the mean loss per event) is independent of Z. Therefore the frequency N and intensity X remain independent. As discussed in Chapters 3 and 4 independence is not a valid assumption for some natural hazards and results in the underestimation of the extremes of the aggregate loss. The parameter $\beta_{1,i}$ is now assumed to depend on μ_i and the dispersion parameter ϕ_i is now modelled as a function of the ith rows intensity,

$$\phi_i = f(\mu_i, \rho_i).$$

To estimate $\beta_{0,i}$,$\beta_{1,i}$ a method of moments approach as in the previous section is used, except the dispersion of counts exceeding an intensity threshold u, $\phi(N_u)$ is now considered. For the linear link function the variance of counts exceeding a threshold u is,

$$\phi(N_u)E[N_u] = \left(\sum_{\mu_i>u} \rho_i\sqrt{\phi_i}\right)^2, \tag{5.13}$$

where $E[N_u]$ is the mean number of events exceeding u; $E[N_u] = \sum_{\mu_i>u}\rho_i$. To calculate ϕ_i, it is first necessary to sort the event loss table by the expected loss μ_i; largest to smallest. The dispersion parameter for the first row (largest expected loss) ϕ_1, can then be calculated by first noting that the dispersion of the 1st row $Var[N_1]/E[N_1] - 1$ is equal to the dispersion of counts exceeding μ_1; $Var[N_u]/E[N_u]-1$, where $u = \mu_1$. The dispersion parameter can then be calculated from

$$\frac{Var[N_1]}{E[N_1]} = \frac{Var[N_u]}{E[N_u]} = \phi_1\rho_1 + 1 \tag{5.14}$$

by rearranging for ϕ_1 as $Var[N_u]/E[N_u]$ is assumed to be known to the modeller. For the rest of the rows $j = 2, \ldots, I$,expressions for ϕ_j can be obtained by rearranging Eqn. 5.13,

$$\phi_j = \frac{\left(\sqrt{\phi(N_{\mu_j}) \sum_{i=1}^{j} \rho_i} - \sum_{i=1}^{j-1} \rho_i \sqrt{\phi_i}\right)^2}{\rho_j^2} \tag{5.15}$$

where $\phi(N_{\mu_j})$ is the dispersion of counts exceeding μ_j. The same approach can be used with the log-link function, of first calculating the variance of the most intense event and then the variance of the rows $j = 2, ..., I$ (see Appendix C).

Bernoulli model The parameters of the Bernoulli model are calculated as in the previous section, except with non-constant dispersion ϕ_i;

$$\begin{aligned} \beta_{1,i} &= \rho_i \sqrt{\frac{\phi_i}{\theta(1-\theta)}} \\ \beta_{0,i} &= \rho_i - \beta_{1,i}\theta, \end{aligned} \tag{5.16}$$

where ϕ_i is calculated from Eqns 5.14, 5.15.

Log normal model Similarly the log normal parameters can be calculated as

$$\begin{aligned} \beta_{1,i} &= \sqrt{log(1+\phi_i)} \\ \beta_{0,i} &= log\rho_i - \frac{1}{2} log(1+\phi_i). \end{aligned} \tag{5.17}$$

The dispersion ϕ_i now depends upon the intensity of the ith row, and the CEP for the mixture models no longer scales with Z. For the Bernoulli model,

$$c_1 = \rho_i \left(1 + \frac{\phi_i}{\theta(1-\theta)}(Z-1)\right)$$

which is no longer constant for all i. Similarly for the log-normal model

$$c_2 = e^{(-(1/2)log(1+\phi_i) + log(1+\phi_i)^{1/2} Z)},$$

which also depends on i.

5.4 Model implementation

In this section the performance of the different loss models introduced in this chapter is investigated using a synthetic event loss table. This table was developed with input and feedback from the reinsurance industry and is structurally similar to those derived from European windstorm catastrophe models. Although the ELT used here it is not identical to any individual insurer's event loss table it has the same typical characteristics of those currently in use. In particular it contains thousands of unique events characterised by their annual frequency and expected loss, each with very low individual probability of occurrence.

The event loss table used here contains $55,000$ events (see Fig. 5.3), with total rate $E[N] = 8$ loss events per year, expected annual aggregate loss $E[S] = 6,400,000$ and mean loss per event $E[Y] = 800,000$. Here 5 models including a model representing current practice were considered. The models differ in their parameterization of the rates λ_i.

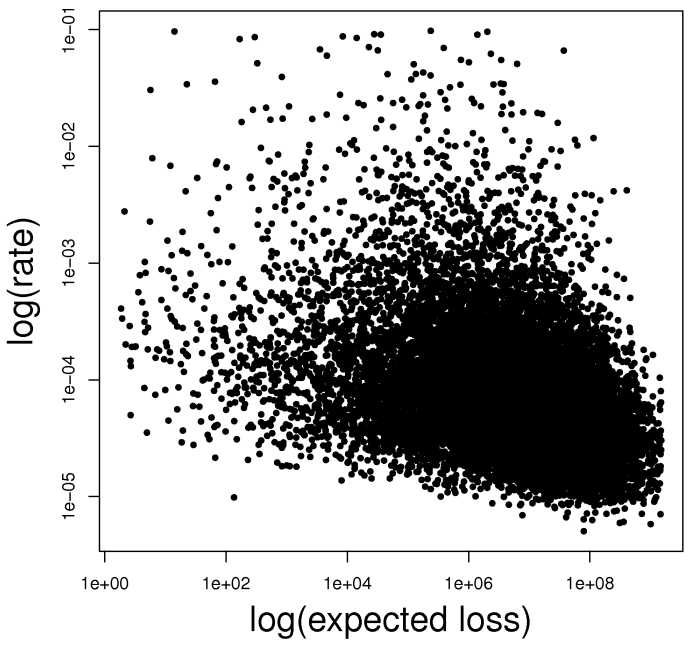

Figure 5.3: Plot of log of the expected loss μ_i against the log of the rate ρ_i for an ELT.

Model $\mathbf{M_1}$ Stationary Poisson process with constant rates, no overdispersion.

$$\lambda_i = \rho_i$$

Model M_1 is representative of current practice, and the frequency and loss distributions are stationary. This model is used as the baseline against which the mixture models are compared.

Model $\mathbf{M_2}$ the rates are related to a Bernoulli mixing variable through the identity (linear) link function, and with constant dispersion parameter ϕ,

$$\begin{aligned}
&\theta = 0.5, \\
&Z_1 \sim Ber(\theta), \\
&\phi(N) = 0.3, \\
&\lambda_i = \beta_{0,i} + \beta_{1,i} Z_1.
\end{aligned}$$

The $\beta_{0,i}, \beta_{1,i}$ parameters can be calculated with $\phi(N)$ and θ from Eqns 5.9,5.10. The model M_2 has clustering but not frequency-intensity dependence.

Model $\mathbf{M_3}$ the rates are related to a Normal mixing variable through the log link function, and with constant dispersion parameter ϕ,

$$\begin{aligned}
&Z_2 \sim N(0,1), \\
&\phi(N) = 0.3, \\
&log(\lambda_i) = \beta_{0,i} + \beta_{1,i} Z_1.
\end{aligned}$$

The dispersion parameter ϕ can be calculated with $\phi(N)$ in Eqn. 5.7 and the $\beta_{0,i}, \beta_{1,i}$ parameters can then be calculated with ϕ from Eqns. 5.11,5.12. The model M_3 has clustering but not frequency-intensity dependence.

Model $\mathbf{M_4}$ the rates are related to a Bernoulli mixing variable through the identity

(linear) link function, and with intensity dependent dispersion parameter ϕ_i,

$$\theta = 0.5,$$
$$Z_1 \sim Ber(\theta),$$
$$\phi(N_u) = 0.3, \text{ for all u such that; } 1 \geq CEP(u) > 0.05$$
$$\lambda_i = \beta_{0,i} + \beta_{1,i} Z_1.$$

The intensity dependent ϕ_i can be calculated from Eqns. 5.14,5.15 and then the $\beta_{1,i}, \beta_{0,i}$ parameters from Eqn. 5.16. However an upper limit for $\beta_{1,i}$ is given by Eqn. 5.3, so for any i which violate this constraint the beta parameter is set as $\beta_i = \rho_i/\theta$. The model M_4 has clustering and frequency-intensity dependence.

Model $\mathbf{M_5}$ Log-link function, mixing distribution $Z_2 \sim N(0,1)$, non constant dispersion parameter ϕ_i;

$$Z_2 \sim N(0,1),$$
$$\phi(N_u) = 0.3, \text{ for all u such that; } 1 \geq CEP(u) > 0.05$$
$$log(\lambda_i) = \beta_{0,i} + \beta_{1,i} Z_1.$$

The intensity dependent ϕ_i can be calculated as in appendix C.2 and then the $\beta_{1,i}, \beta_{0,i}$ parameters can be calculated from ϕ_i. The model M_5 has clustering and frequency-intensity dependence.

5.5 Results

The annual aggregate losses were simulated for each model as follows.

1. Simulate $m = 100,000$ values of the random variable z_j, where $j = 1, \ldots, m$. Then for each j;
2. Calculate the rates $\lambda_{i,j} = h^{-1}(\beta_{0,i} + \beta_{1,i} z_j)$ for $i = 1, \ldots, I$.
3. Simulate n_j from a Poisson distribution $n_j \sim Pois(\sum_{i=1}^{I} \lambda_{i,j})$
4. Sample with replacement n_j losses from the event loss table with probability of i being selected $\lambda_{i,j}/\lambda_j$

5. Calculate the aggregate loss $s_j = x_{1,j} + ...x_{n_j,j}$

6. Calculate the maximum loss $x_{max,j} = max(x_{1,j}, ..., x_{n,j})$

5.5.1 Aggregate exceedance probability

Figure 5.4 shows the simulated AEP curves for the annual loss models $M_1 - M_5$. From the AEP curves little difference can be seen between the models M_1, M_2 and M_3 for all exceedance probabilities. The models M_4 and M_5 with intensity dependent ϕ_i have diverged from the other models by the 0.05 (1 in 20 year) exceedance probability. The AEP curves for M_4, M_5 remain close until the 0.02 (1 in 50 year) exceedance probability after which the exceedance levels for M_5 increase at a faster rate than those of M_4. As with the Gothenburg aggregate loss models, inclusion of frequency-intensity dependence has resulted in increases of the extremes of the aggregate loss. The extremes also appear to be sensitive to the choice of mixing distribution and link function.

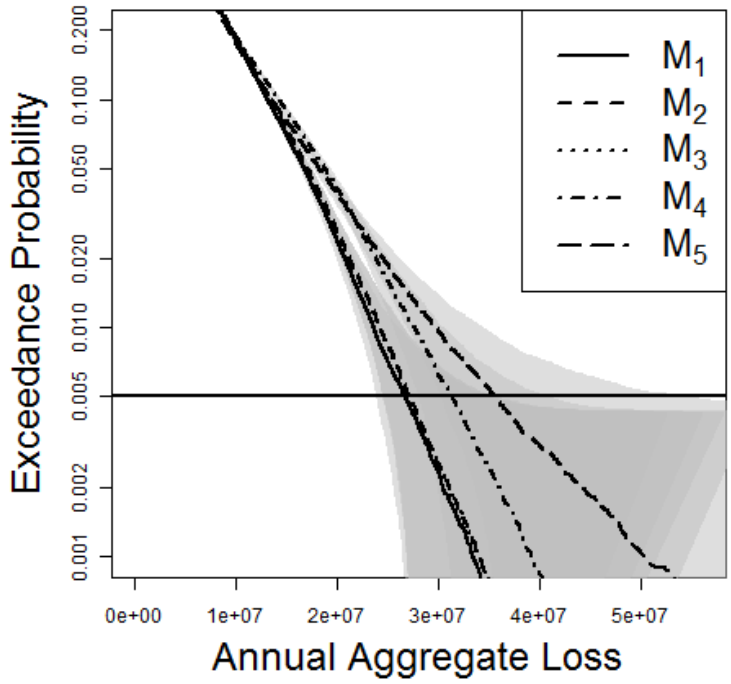

Figure 5.4: Plot of the AEP curves for the loss models. Grey shading indicates the 95 % DKW bands.

Summary statistics for the simulated aggregate losses are reported in Table 5.1. The value-at-risk $VaR_{0.995}$ for the models M_2, M_3 are not significantly different from that of M_1; the bootstrapped confidence intervals for M_2, M_3 contain the $VaR_{0.995}$ for M_1. For M_4, $VaR_{0.995}$ is 18% greater than for the model M_1, and the difference for M_5 is even greater at +32%. The bootstrapped confidence intervals for both of these models do not overlap with either M_1 or each other. The difference between the expected shortfalls $ES_{0.995}$ is even more pronounced, with M_5 50% greater than that of M_1. All models have the same expected annual aggregate loss $E[S] = \sum_{i=1}^{I} \rho_i \mu_i$, as desired.

The findings for the AEP curves from the event loss table are therefore qualitatively similar to those of the previous chapter; positive frequency-intensity dependency increases the extremes of the aggregate risk.

	$\bar{s}$	ϕ_n	$VaR_{0.995}(s)$	$ES_{0.995}(s)$
M_1	6.4	0.00	26.8 (26.4,27.1)	30.5
M_2	+0%	0.30	$+1.4(-0.1,+2.8)\%$	+3%
M_3	+0%	0.32	$+1.3(-0.0,+2.6)\%$	+3%
M_4	+0%	0.27	$+17.1(+15.7,+18.9)\%$	+19%
M_5	+0%	0.29	$+32.9(30.6,35.7)\%$	+50%

Table 5.1: Summary statistics from the simulated annual losses. For the models M_2, M_3, M_4, M_5 the change in the statistics compared to the values for the model M_1 (%) are reported. The bootstrapped confidence intervals for $VaR_{0.995}$ are reported, in brackets, as the percentage change from the M_1 $VaR_{0.995}(S) = 26.8$

Figure 5.5 shows the AEP curves for the loss models $M_2 - M_5$ conditional on the values of the mixing variables Z_1/Z_2. For all mixture models the upper tail of the aggregate loss distribution can be seen to depend upon the mixing variable. The effect of the mixture model on the aggregate loss can be seen to be greatest for the models with intensity dependent dispersion (Fig 5.5 c,d). The AEP curves for M_5 show a greater variation for different values of the continuous mixing variable Z_2 compared to the AEP curves for the model M_4 with binary mixing variable Z_1. This could be a possible reason for the divergence of the AEP curves for M_4 and M_5 in Fig. 5.4.

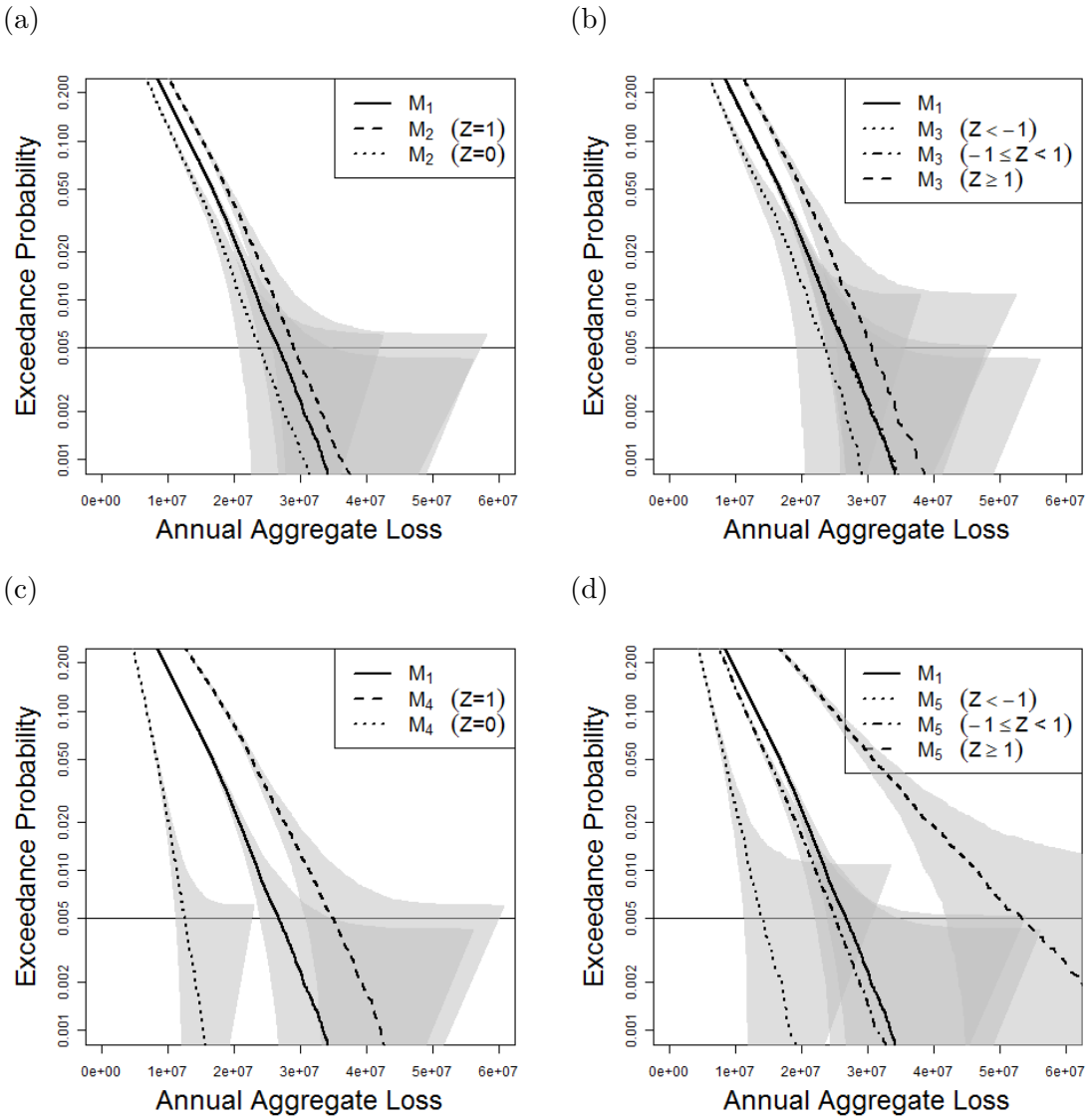

Figure 5.5: Plots of the AEP curves for the mixture models conditional on the mixing variables Z_1, Z_2. Grey shading indicates the 95% DKW bands. a) M_2 b) M_3 c) M_4 d) M_5

5.5.2 Conditional exceedance probability

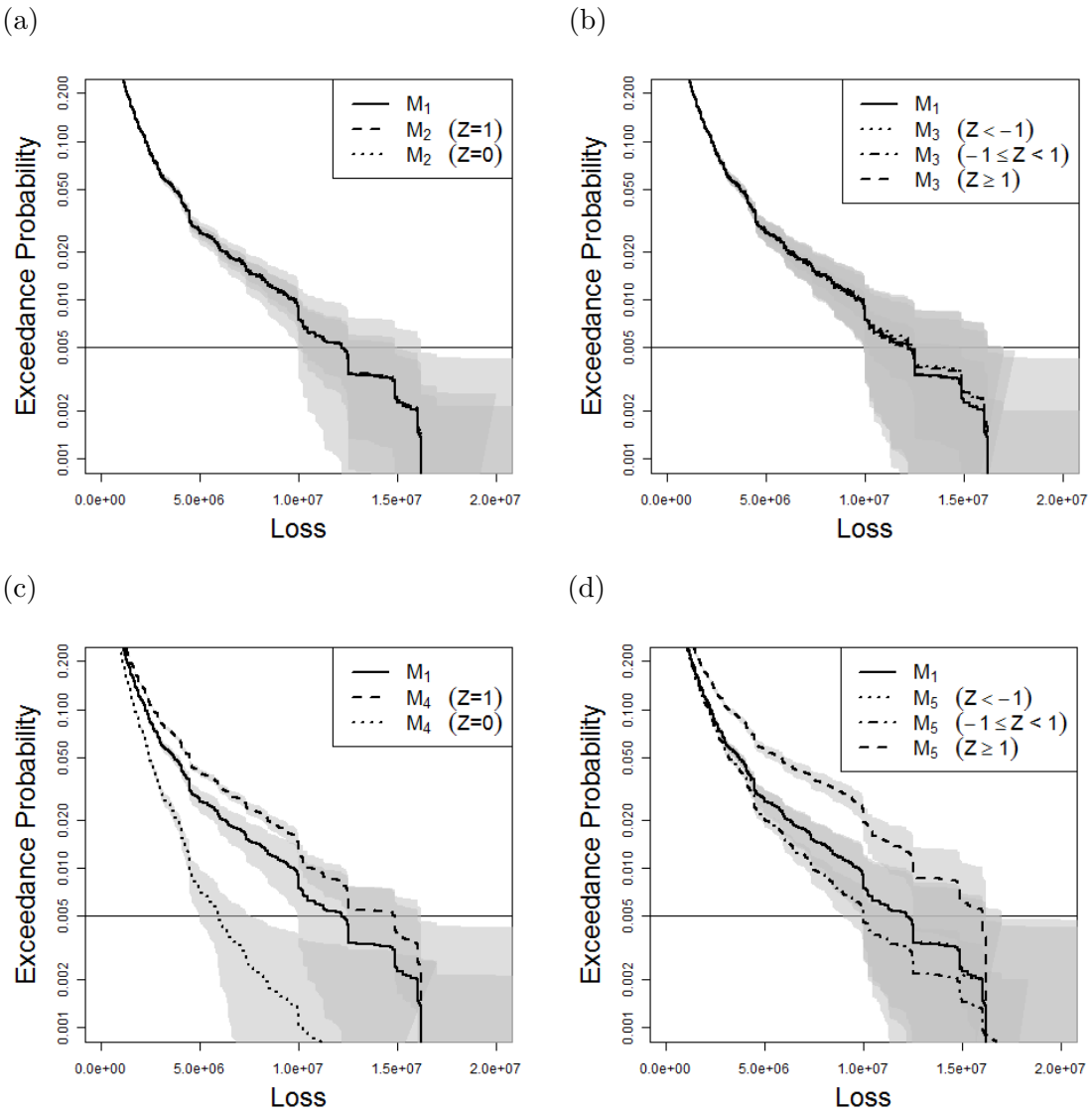

Figure 5.6: Plots of the CEP curves for the simulated losses x conditional on the mixing variable z. The CEP curve for M_1 has been included for in all plots (solid black line). Grey shading indicates the 95% DKW bands, a) M_2 b) M_3, c) M_4 d) M_5.

The effect of the mixing variables on the CEP is now considered. Figure 5.6 shows the CEP curves for the loss models conditional on the mixing variables Z_1, Z_2. As discussed in Section 5.3.4 for the models with constant dispersion parameter ϕ the ratio of the rates scale with Z. Consequently there is no difference between the

CEP curves for M_2, M_3 which are identical to that of M_1 for all values of the mixing variables Z_1, Z_2. The CEP curves for M_4 and M_5 do depend upon the mixing variable Z_1 and Z_2; the CEP(x), $Pr(X > x)$ increases with Z. The mean loss per event Y for M_4, M_5 conditional on Z_1, Z_2 is shown in Fig. 5.7. For the model M_4, the mean loss per event $\bar{y}$ when $Z_1 = 0$; $\bar{y} = 530,000$ and when $Z_1 = 1$; $\bar{y} = 990,000$, therefore the mean expected loss per event ($E[Y]$) is almost doubled for years when $Z_1 = 1$. Similar conclusions can be drawn for the model M_5 with continuous mixing distribution; Y is positively (non-linearly) dependent upon Z_2.

(a) (b)

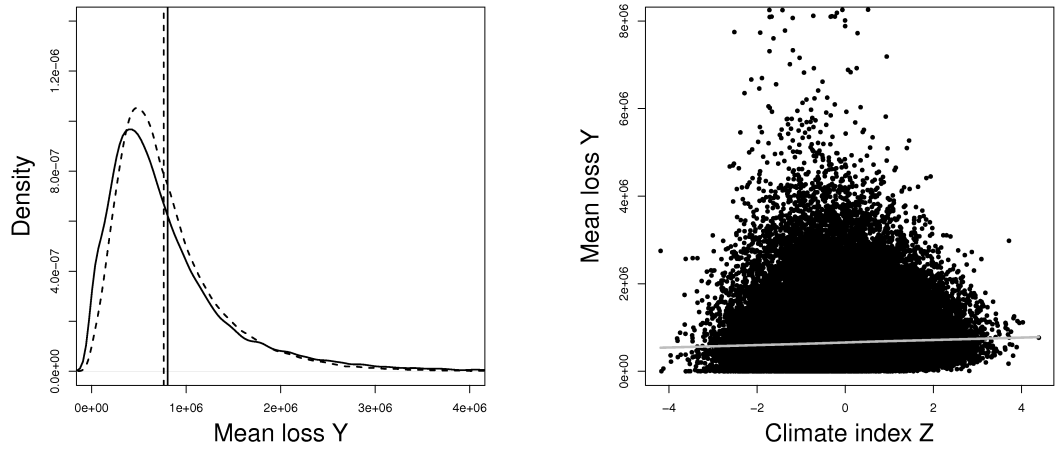

(c) (d)

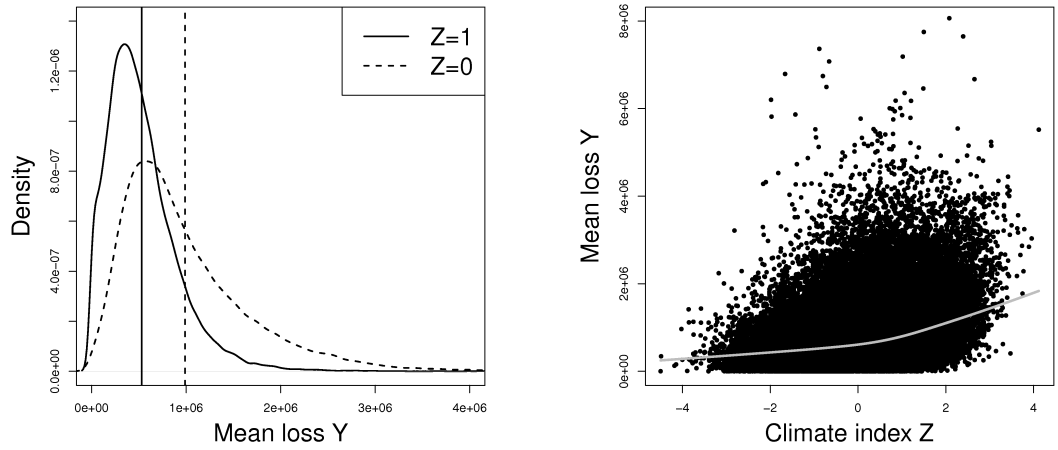

Figure 5.7: Densities of the simulated mean loss per event conditional on the Bernoulli mixing variable; $z_1 = 1$ and $z_1 = 0$ a) M_2 c) M_4. Plots of the mean simulated loss per event y against the normal mixing variable z_2, with a Lowess line b) M_3 d) M_5

5.5.3 Occurence exceedance probability

The OEP curves for the 5 models are shown in Fig. 5.8. There is no visible difference between the 5 models. The distribution of the maximum loss F_{Xmax} is thus insensitive to clustering with or without frequency intensity dependence. Some differences can be seen when considering the OEP curves conditional on the mixing variables Z_1, Z_2. The occurence exceedance levels for the models M_4 and M_5 are much smaller when $Z_1 = 0$ and $Z_2 < -1$ respectively. For larger values of the mixing variable the OEP curves have converged by the 0.005 exceedance probability. This is due to the structure of the ELT; an upper limit is imposed on the distribution of the maximum losses by the largest loss μ_i in the dataset.

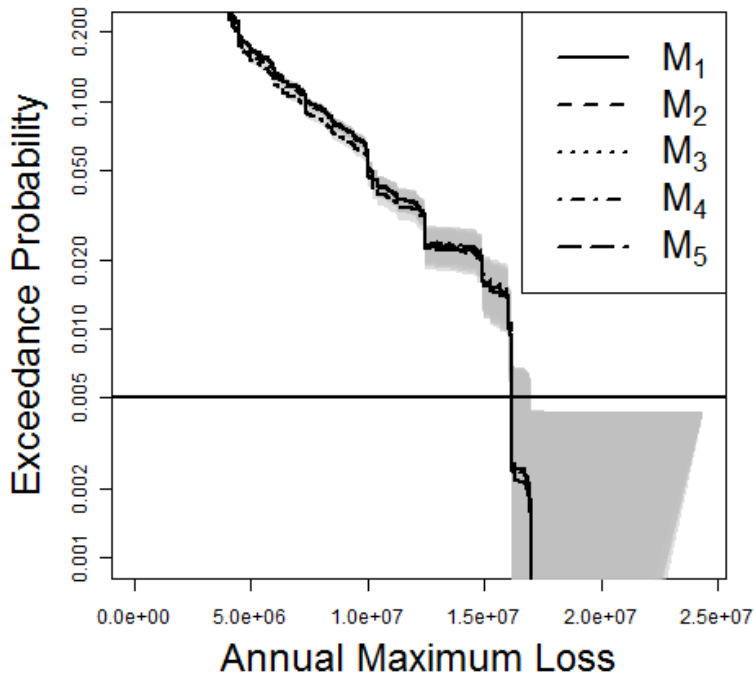

Figure 5.8: Plot of the OEP curves for the loss models. Grey shading indicates the 95% DKW bands

(a)

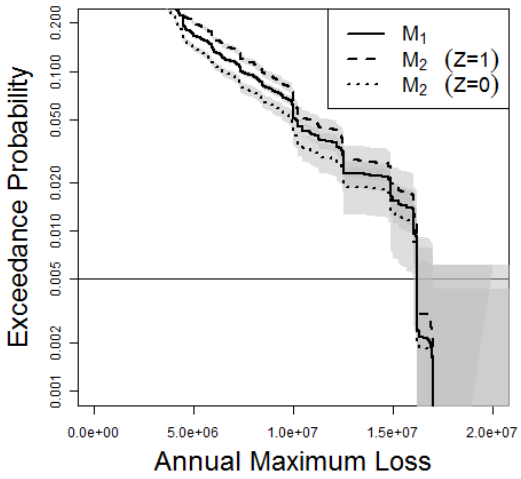

(b)

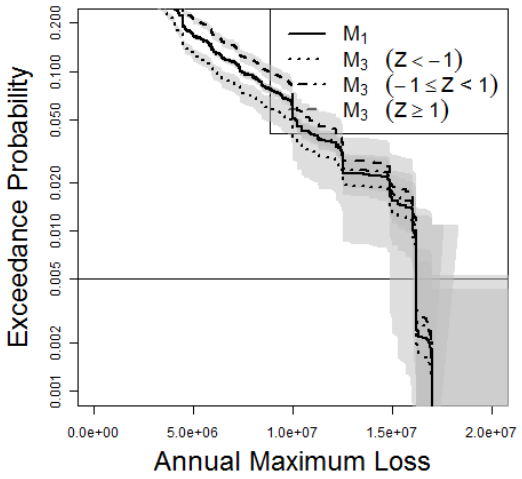

(c)

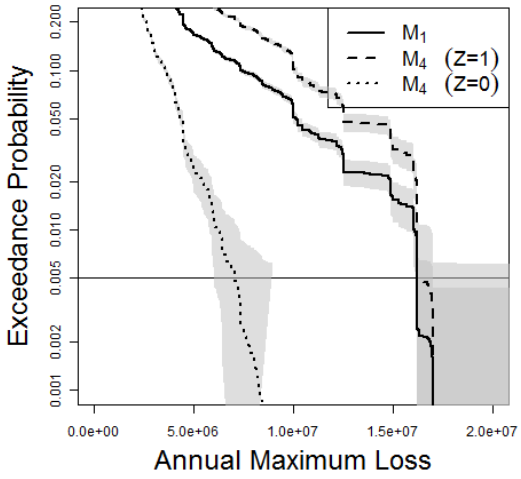

(d)

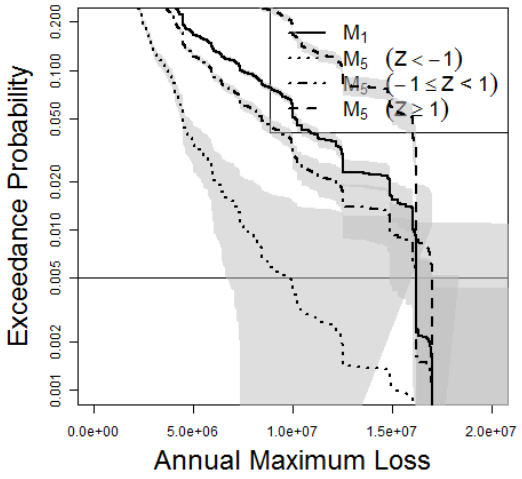

Figure 5.9: Plots of the OEP curves for the mixture models conditional on the mixing variables z_1, z_2. Grey shading indicates the 95% DKW bands. a) M_2 b) M_3 c) M_4 d) M_5

5.5.4 Clustering and frequency-intensity dependence

In Section 5.5.2 the distribution of individual losses, the CEP, was shown to depend upon Z, for the models with intensity dependent dispersion. There is also dependence between N and Z for all models with or without frequency intensity dependence. Correlations between the mean loss and the mixing variables as well as the number of losses are reported in Table 5.2. The sample correlations between the simulated variables are approximately equal for M_2 and M_3 and for M_4 and M_5. The relationship between N,X and Z is therefore determined by the choice of dispersion parameters ϕ_i and not by the link function or mixing variable. Due to the mutual dependence on the mixing variable the frequency of loss events and mean loss are also correlated for M_4 and M_5 (Fig. 5.10).

	$\text{cor}(n, z)$	$\text{cor}(y, z)$	$\text{cor}(s, z)$	$\text{cor}(y,n)$
M_1	0.00	0.00	-	0.00
M_2	0.46	0.00	0.23	0.00
M_3	0.45	0.00	0.23	0.00
M_4	0.46	0.37	0.49	0.18
M_5	0.46	0.33	0.49	0.17

Table 5.2: Sample correlations between the frequency n, mean loss per event $y = s/n$ and mixing variable z

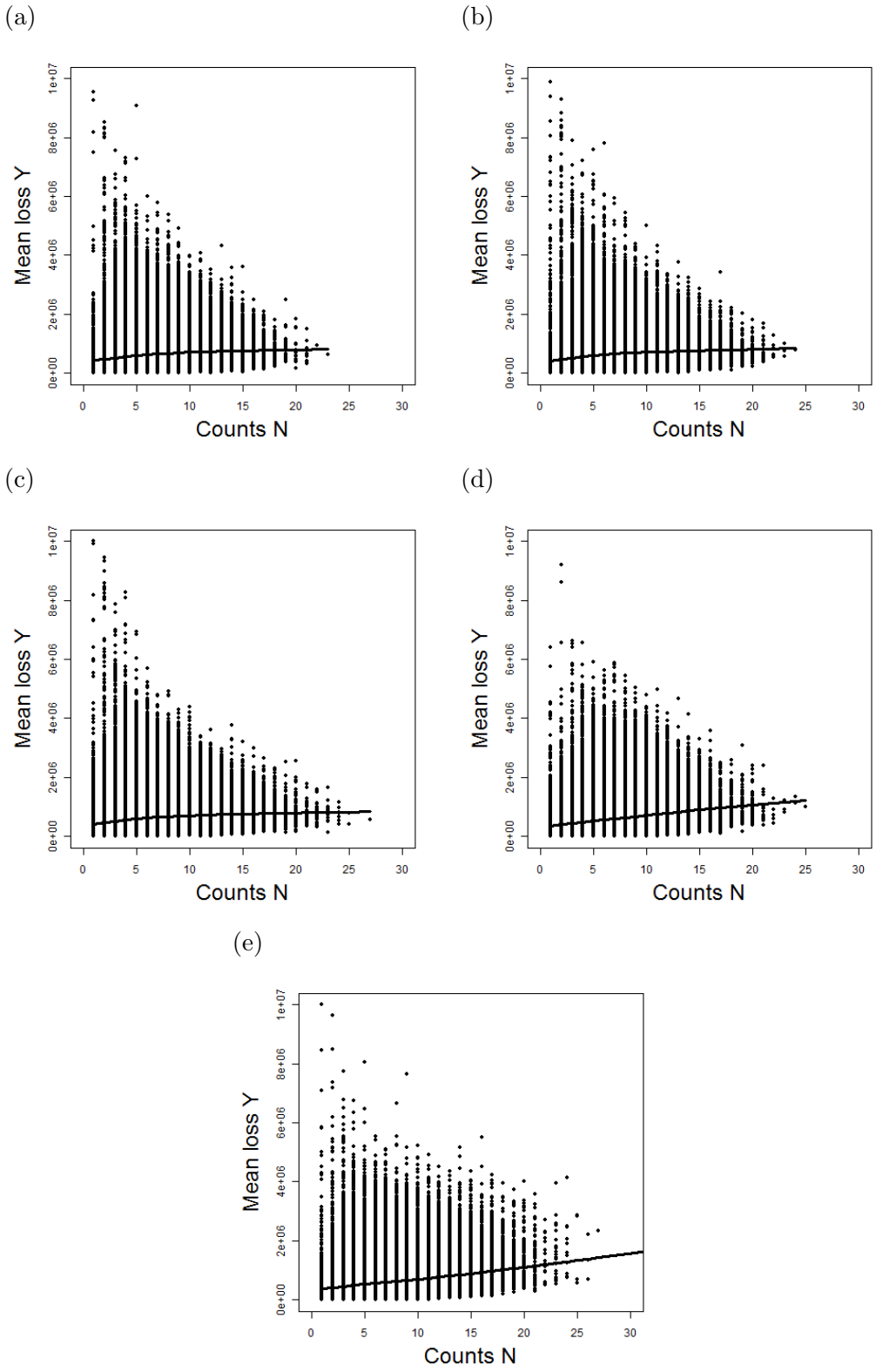

Figure 5.10: Plots of the simulated number of losses n against the simulated mean loss y, with lowess lines. a) M_2 b) M_3 c) M_4 d) M_5

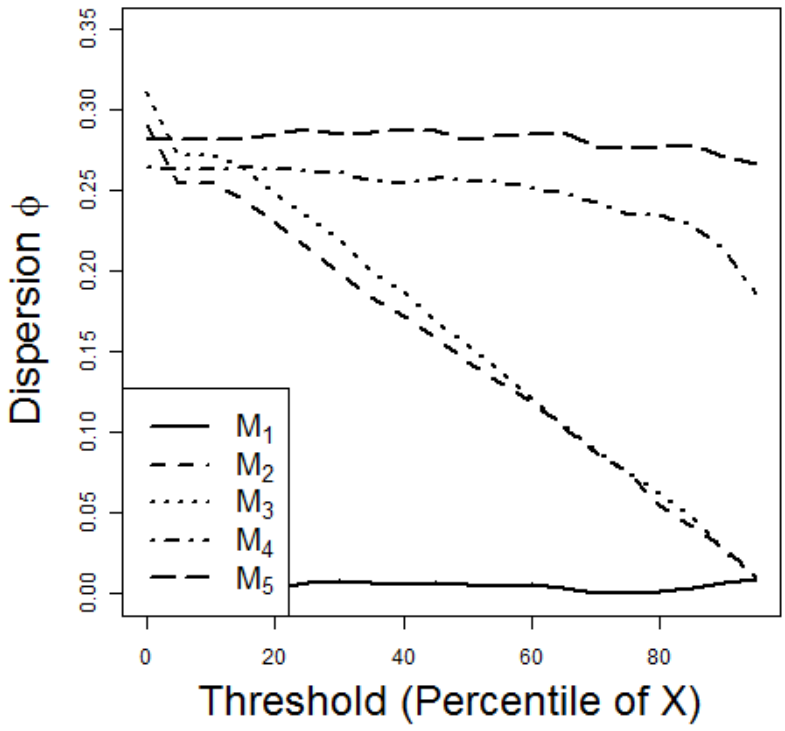

Figure 5.11: Plot of the dispersion of counts N against intensity thresholds for the 5 loss models.

Figure 5.11 shows the dispersion of counts exceeding a loss threshold. The models $M_2 - M_5$ have been parametrised such that $\phi(N) = 0.3$ when considering all counts. The dispersion of M_2 and M_3 decays linearly with increasing intensity threshold, which is consistent with the findings of Chapter 4; when the frequency and intensity (loss) are independent the occurrence of extreme events converges to a Poisson process. The decrease in the dispersion can be calculated from equation 4.11 (Chapter 4); if the dispersion of all counts is ϕ_N the dispersion of events above the 50th percentile of the loss distribution F_X is $0.5\phi_N = 0.5 * 0.3 = 0.15$, (see Fig. 5.11). For the model M_4 dispersion remains reasonably constant at $\phi \approx 0.27$ until the higher percentiles of the loss distribution F_X after which dispersion decays. This is due to the upper limit for the ϕ_i parameters imposed by Eqn 5.3. The dispersion for M_5 stays roughly constant $(0.28 < \phi(N_u) < 0.29)$for all individual loss thresholds up to and including the $95th$ percentile. It thus seems likely that

the differences between the upper tail of the AEP curves for M_4 and M_5 is due to the restrictions on the dispersion parametrisation for M_4 (Eqn 5.3), rather than the differences in the mixing-variable and link function.

From this simulation study using an ELT similar conclusions can be drawn as from the copula simulation approach of Chapter 4. Frequency-intensity dependence is necessary for the clustering of extremes, which in turn increases the risk measures for the AEP. Additionaly the distribution of maximum losses (OEP) has been shown to be insensitive to frequency-intensity dependence and clustering.

5.6 Conclusions

This chapter has explored the modelling of the financial risk from natural hazards using catastrophe loss models. In particular the assumptions used in the financial component for modelling the annual losses has been investigated. The performance of the current practice approach of modelling losses using a stationary Poisson process has been compared with a variety of mixture models. The purpose of the mixture models was to investigate the effect of including over dispersion and frequency-intensity dependency on the loss distributions.

Here two choices of mixing distribution Z (Bernoulli and Normal) with two choices of link function (linear and log) were considered, along with different parametrizations of the dispersion. The aggregate annual losses were found to be sensitive to the inclusion of frequency-intensity dependence through the dispersion parametrization. As was found in the previous chapter, this relation is necessary to capture the clustering of extreme events. The inclusion of clustering and frequency-intensity dependence in the financial loss models resulted in increases in the risk measures $VaR_{0.995}(+33\%)$ and $ES_{0.995}(+50\%)$.

The choice of mixing variable was found to be of less importance than the dispersion parametrization. The main advantage of using the log link/normal mixing

distribution was that it allows greater flexibility in the dispersion parametrization than the linear/Bernoulli mixing combination. The Bernoulli mixing distribution with intensity dependent dispersion could not fully capture the variability in extremes due to constraints in the choice of beta parameters. This in turn resulted in an underestimation of the extremes of the annual aggregate loss. The distribution of maximum losses was found to be insensitive to the mixture models.

For the models with intensity dependent dispersion, the dispersion was assumed constant at $\phi(N_u) = 0.3$ for all intensity thresholds u up to the 95th percentile. It may be that the dispersion of losses for a particular natural hazard increases with the intensity threshold, such as with Gothenburg windstorms, where dispersion increased to $\phi = 1$ for events exceeding the $70th$ percentile of the intensity distribution. If the dispersion for windstorm related losses shows similar behaviour then the difference between the current practice model and the intensity-dependent mixture models will likely be even greater.

Chapter 6

Discussion and Conclusions

6.1 Summary of findings

This thesis has developed and tested a framework for modelling the aggregate risk of natural hazards. Previous studies have focused on estimating individual attributes of natural hazards, such as the frequency or intensity, without allowing for dependency between them. This is the first study to rigorously investigate the effect of climatic factors and physical processes such as clustering on the distribution of aggregate losses.

Collective risk models, which are used in insurance and risk management for modelling total claim amounts, have been extended here to model the aggregate loss distribution for natural hazards. In Chapter 3, this framework was applied to extra tropical cyclones (ETCs) using a gridded database of cyclone tracks for the Northern Hemisphere, covering October-March winters from 1950-2003. Extra tropical cyclones were selected as the case study for this thesis as they are responsible for large cumulative insured losses over Europe. The aggregate losses from such events have also been of concern for the insurance community in recent winters due to prominent clusters of storms, such as those of the recent 2013/14 winter over the UK.

Using the framework, the variance of the aggregate loss distribution for ETCs was shown to be sensitive to covariance between the frequency and mean intensity of events. Substantial positive correlation was found between the frequency and mean intensity over the exit regions of the North Atlantic and North Pacific storm tracks, and negative correlation over the Kuroshio and Gulf Stream. Assuming no positive correlation resulted in large biases in the variance of the aggregate loss. The inclusion or omission of dependence between the intensities of consecutive cyclones was found to not significantly effect the modelled variance. It was hypothesised that the positive correlation over Europe between the frequency and intensity was due to joint modulation by underlying large-scale flow patterns. Regression of the cyclone counts and local mean vorticity onto the SCP, NAO and EAP indices was shown to reproduce most of the observed positive correlation over Northern Europe. The East Pacific Pattern and North Pacific/Atlantic patterns accounted for most of the positive correlation over the North Pacific. Large scale flow patterns however were not able to account for the negative correlation, over the Gulf Stream and Kuroshio.

The correlation between the frequency and local mean vorticity was also considered for the subset of the 50% most intense cyclones at each grid point. The positive correlation was largely unchanged when considering the subset of more intense cyclones. However the negative correlation diminished and so was predominantly due to joint trends in the weaker systems. The negative correlation was not considered further as it was located in regions with no exposure. The results were found to be robust to the choice of reanalysis dataset.

Statistical methods were used in Chapter 4 to explore the extremes of the aggregate loss distribution. Cyclones passing near two locations were considered; Gothenburg and Barcelona. At Gothenburg there was statistically significant positive correlation between the frequency and local mean vorticity (r = 0.47), and at Barcelona there was weak negative correlation (r = -0.1). The non-parametric empirical estimates for the exceedance probabilities were constrained by the length

of the dataset (53 winters). To make non-parametric inferences about the effect of frequency-intensity dependence on the annual aggregate loss distribution beyond this level, Cantelli bounds were used to investigate the effect of frequency-intensity dependence on the upper bounds of the exceedance levels. Inclusion of the positive frequency-intensity dependence at Gothenburg resulted in higher upper bounds for the extremes of the aggregate loss distribution compared to the case without dependence. Conversely, the weak negative dependence at Barcelona resulted in a small decrease in the upper bounds with dependence for the extremes of the annual aggregate loss compared to the bounds without dependence. Generalized Pareto distributions (GPD) were fitted to the aggregate risk distribution at both locations to model extremes of the aggregate risk parametrically. The GPD model performed well for the observed exceedance probabilities but was unsuitable for modelling the 1 in 200 year losses. This was due to an upper bound to the fitted distribution which appeared to be to low; the maximum possible aggregate loss according to the model was not much larger than the observed maximum loss from 53 winters of data.

The sensitivity of extremes of the aggregate loss distribution to the inclusion of clustering, with and without frequency-intensity dependence, was investigated using a Monte Carlo simulation approach. The inclusion of frequency-intensity dependence was shown to be necessary to model the clustering of extreme events. When the underlying rates were overdispersed, but the frequency and intensity of events were independent, the occurrence of extreme events converged to a Poisson process. The inclusion of frequency-intensity dependence increased the loss measures for the 1 in 200 year return level of the aggregate loss by around $11 - 12\%$ without allowing for clustering in the model formulation. Clustering was found to result in a 4% rise in these risk measures when dependence was not included in the model. The inclusion of both dependence and clustering in the model resulted in an increase of 15% in the risk measures at the 200 year return level.

Chapter 5 investigated how to incorporate the findings of the previous two chapters into the financial component of a catastrophe loss model. Clustering was introduced with and without frequency-intensity dependence using a mixture model approach, where the mixing variable represented the state of the climate. The performance of the current practice approach of modelling losses using a stationary Poisson process was compared with the mixture models. Two choices of mixing distribution (Bernoulli and Normal) and two choices of link function (linear and log) were considered. The log-link with Normal mixing distribution was found to be preferable as it allowed for greater flexibility in the parameter estimation. As in Chapter 4, frequency-intensity dependence was necessary to capture the clustering of extreme events in the loss model. Clustering without frequency-intensity dependence resulted in a 2% increase in the 200 year return level loss measures for the financial models aggregate loss distribution, rising to a 32% increase when frequency-intensity dependence was included. It was assumed for simplicity in Chapter 5 that the amount of overdispersion observed in insured losses would be the same as that observed in the physical measure of the hazard (vorticity).

6.2 Thesis questions revisited

- *Is there dependence between the frequency and mean intensity of hazards within a season/year?*

  For extra tropical cyclones over northern Europe and the eastern North Pacific there is substantial positive dependence between the frequency and mean intensity (vorticity) of events within a season. There is also some evidence of negative dependence between the frequency and intensity of these cyclones over the Gulf stream and Kuroshio.

- *How does frequency-intensity dependence affect the distribution of aggregate losses (aggregate risk)?*

The variance and extremes of the aggregate loss distribution are highly sensitive to frequency-intensity dependence. Falsely assuming independence between the frequency and intensity is shown to result in large biases in the variance of the aggregate risk. The inclusion of positive dependence is shown to be necessary to model the clustering of extreme event.

- *How can the dependency be diagnosed and incorporated into the loss component of catastrophe models?*

  The dependency was diagnosed using a variety of statistical methods applied to time series of the frequency and mean intensity of extra tropical cyclones. A mixture model approach was found to be a simple and effective way of including dependency into the loss component of a CAT model. The inclusion of frequency intensity dependence resulted in increases in the 200 year return level of the aggregate loss of around 32%.

6.3 Discussion

During the course of this project several different approaches for introducing clustering and frequency intensity dependence into an insurer's event loss table were considered which were not included in the thesis. For example, one alternative was to divide the event loss table loosely into strong and weak events using Princicpal Component Analysis. The clustering algorithm was then specified so that the probability of an event being sampled from either the strong or weak groups was dependent upon the simulated climate variable. These methods were more straightforward than the approach presented in Chapter 5 but allowed for less control over the tuning of the intensity thresholded dispersion.

It should also be mentioned that event loss tables often contain information regarding the location and physical intensity (e.g. mean sea level pressure or storm severity index) of the loss events. This additional data could be used to assist in

estimating the parameters for the sampling algorithm presented in Chapter 5.

Another important consideration when developing a clustering method was that the methodology would need to be understandable and acceptable to the insurance community. As mentioned in Chapter 5 the mixture model approach is already widely used in credit risk management. The work here has merely extended the models to allow for the different nature of the relationship between the mixing variable and event rates in natural hazard modelling as opposed to credit risk modelling.

The clustering method for extra tropical cyclone ELTs was intended to be sufficiently general to applied to the ELTs for other types of hazard, such as flood or tropical cyclones. However some further considerations would need to be taken into account before applying the method to other hazards. Consider flood events, where as well as clustering of events due to clustering of the meteorological triggers (e.g extra tropical cyclones) there can be a clustering of events at different locations along the same river due to a single meteorological trigger. Therefore some further consideration would be required and changes made to the algorithm before it could be applied to a flood portfolio. One suggestion would be to model the frequency using a self exciting Poisson, or a Poisson clustered process (e.g. Poisson-Poisson), to more closely reflect the nature of the clustering of flood events.

6.4 Possible directions for future work

Extra tropical cyclones have been used here as a test bed for developing models for the aggregate risk of natural hazards. One suggestion for future work is to apply the framework developed here to other hydro-meteorological natural hazards such as tropical cyclones or floods. However it would be necessary to make alterations when applying the algorithm to different natural hazards as discussed above.
As with previous studies which provided the motivation for this investigation, no spatial aspect was considered for the statistical models. A potentially very important extension to this work would be to include a spatial aspect and have freedom

from the grid, as in (Economou et al., 2014).

Another possible extension to this work would be to consider covariance between the aggregate risks of different types of natural hazards. For example the covariance of the aggregate risk of Atlantic tropical cyclones (hurricanes) and extra tropical cyclones could be investigated. This work would be of benefit for the insurance community for use in the diversification[1] of portfolios. If two hazards are uncorrelated or negatively correlated an insurer could reduce their risk from extremes of either type by spreading their exposure between both. Conversely if two types of hazard were positively correlated, an insurer with exposure to both but modelling them as independent would be underestimating their financial risk.

Finally it would be of interest to use climate model projections and this framework to investigate how the aggregate risk of storms may change in the future.

[1]Diversification - a risk control technique that spreads loss exposures over a myriad of areas http://www.irmi.com/online/insurance-glossary/terms/d/diversification.aspx

Appendix A

A.1 Collective risk models

In the collective risk model the aggregate loss, S, is modelled as the sum of a random number N of random intensities X_i,

$$S = X_1 + \ldots X_N = \sum_{i=1}^{N} X_i.$$

The mean of S in terms of the frequency N and individual intensity X_i, from the law of total expectation is

$$E[S] = E_N[\sum_{i=1}^{N} E[X_i|N]]$$

The expectation of S can be expressed in terms of N and mean intensity $Y = (1/N)\sum_{i=1}^{N} X_i$, as,

$$E[S] = E[NY] = E[N]E[Y] + Cov[N, Y],$$

since $Cov[N, Y] = E[NY] - E[N]E[Y]$. If N and X, Y are independent and X_i, X_j independent then the expectation becomes

$$E[S] = E[N]E[X] = E[N]E[Y].$$

The variance of S, from the law of total variance, is in terms of X;

$$Var[S] \quad = \quad E_N[Var[\sum_{i=1}^{N} X_i|N)]] + Var_N[E[\sum_{i=1}^{N} X_i|N]],$$

see e.g. McNeil et al. (2005) Section 10.2. The variance of S in terms of Y;

$$Var[YN] = E[N^2Y^2] - E[NY]^2.$$

Then by noting that;

$$E[N^2Y^2] = Cov[N^2, Y^2] + E[N^2]E[Y^2],$$

the variance of S can be decomposed into seperate contributions from N,Y and the covariance between them;

$$\begin{aligned} Var[NY] &= Cov[N^2, Y^2] + E[N^2]E[Y^2] - (Cov[N, Y] + E[N]E[Y])^2 \\ &= Cov[N^2, Y^2] - (Cov[N, Y])^2 - 2Cov[N, Y]E[N]E[Y] \\ &\quad + Var[N]E[Y]^2 + Var[Y]E[N^2]. \end{aligned}$$

For the case N and X_i, Y are independent, the variance is

$$\begin{aligned} Var[S] &= E[N]Var[X] + Var[N]E[X]^2 \\ &= Var[N]E[Y]^2 + Var[Y]E[N^2] \end{aligned}$$

see Frishman (1971).

A.2 Analysis of modelling assumptions

To investigated the effect of modelling assumptions, such as N and X independent, a collective risk model was proposed where,

$$\mu_X|N = \beta_0 + \beta_1 N$$

$$\sigma_{XX}|N = \begin{cases} \sigma_X^2 & \text{for} \quad i = j \\ \rho\sigma_X^2 & \text{for} \quad i = j \pm 1 \\ 0 & \text{otherwise,} \end{cases}$$

where σ_{XX} is the covariance and ρ the correlation between X_i and X_j. This gives

$$\begin{aligned} \mu_S = & \quad E_N\left[\beta_0 N + \beta_1 N^2\right] = \beta_0\mu_N + \beta_1\left(\sigma_N^2 + \mu_N^2\right) \\ \sigma_S^2 = & \quad E_N[N\sigma^2 + 2N(N-1)\rho\sigma^2] + Var_N\left(\beta_0 N + \beta_1 N^2\right) \\ = & \quad \sigma^2\mu_N + 2\left(\mu_N - 1\right)\rho\sigma^2 \\ + & \quad \beta_0^2\sigma_N^2 + \beta_1^2\sigma_{N^2}^2 + 2\beta_0\beta_1\left(\mu_{N^3} - \mu_N\mu_{N^2}\right) \end{aligned} \tag{A.1}$$

since $Var\left(\beta_0 N + \beta_1 N^2\right) = \beta_0^2 Var[N] + \beta_1^2 Var[N^2]^2 + 2\beta_0\beta_1 Cov[N, N^2]$
and $\text{Cov}[N, N^2] = \mu_{N^3} + \mu_N \mu_{N^2}$

A.3 Sample estimators

Consider a dataset with years $t = 1, 2, ..., T$. Each year there are n_t events, and for each event there is a severity measure $x_{1,t}, x_{2,t}...x_{n_t,t}$. The estimators for the sample mean and variance of variable n are denoted $\bar{n}, s_n^2$,

$$\begin{aligned} \bar{n} &= \frac{1}{T}\sum_{t=1}^{T} n_t \\ s_n^2 &= \frac{1}{T-1}(\sum_{t=1}^{T} n_t - \bar{n})^2. \end{aligned}$$

The mean vorticity y_t in year t is

$$\begin{aligned} y_t &= \frac{1}{n_t}\sum_{i=1}^{n_t} x_{i,t} \\ \bar{y} &= \frac{1}{T}\sum_{t=1}^{T} y_t. \\ s_y^2 &= \frac{1}{T-1}(\sum_{t=1}^{T} y_t - \bar{y})^2 \end{aligned}$$

The sample estimator for the covariance between n and y is

$$cov(n, y) = \frac{1}{T-1}\sum_{t=1}^{T}(n_t - \bar{n})(y_t - \bar{y}).$$

The sample aggregate risk is

$$\begin{aligned} s_t &= \sum_{i=1}^{n_t} x_{i,t} \\ \bar{s} &= \frac{1}{T}\sum_{t=1}^{T} s_t. \\ s_s^2 &= \frac{1}{T-1}(\sum_{t=1}^{T} s_t - \bar{s})^2 \end{aligned}$$

Is the sample correlation biased?

Is the correlation between y and n in Chapter 3 biased since estimates for the mean vorticity at time t, y_t depend on the sample size n_t? That is, will estimates of the mean vorticity y_t increase with sample size n_t, even if there is no physical reason for underlying dependence? Given $y_t = (1/n_t)\sum_{i=1}^{n_t} x_i$, the mean and variance of the sample estimator for the mean vorticity y_t is

$$E[y_t] = \mu_Y, Var[y_t] = \frac{\sigma_X^2}{n_t}.$$

where μ_Y is the population mean vorticity, and σ_X^2 is the population variance of the individual intensities (see Rice (2007) Section 7.3.3). Therefore the expectation of the mean vorticity y_t is not dependent upon the sample size but the variance of the estimator for the mean vorticity[1]. However it is straightforward to show that the sample correlation of n and y requires only $E[y_t]$ and not $Var[y_t]$. The expectation of the sample estimator for the population covariance σ_{NY}^2 is;

$$E[cov(n,y)] = \frac{1}{T-1}\sum_{i=1}^{T} E\Big[n_i y_i - \frac{n_i}{T}\sum_{j=1}^{T} y_j - \frac{y_i}{T}\sum_{j=1}^{T} n_j + \frac{1}{T^2}\sum_{j=1}^{T} n_j \sum_{j=1}^{T} y_j\Big]$$

$$= \frac{1}{T-1}\sum_{i=1}^{T}\Big[E[y_i n_i] - \frac{1}{T}\sum_{j=1}^{T} E[n_i y_j] - \frac{1}{T}\sum_{j=1}^{T} E[n_j y_i] + \frac{1}{T^2}\sum_{j=1}^{T}\sum_{k=1}^{T} E[n_j y_k]\Big]$$

$$= \frac{1}{T-1}\sum_{i=1}^{T}\Big[\sigma_{NY} + \mu_N\mu_Y - \frac{2(\sigma_{NY}+\mu_N\mu_Y)}{T} - \frac{(T-1)\mu_N\mu_Y}{T} + \frac{T(T-1)\mu_N\mu_Y}{T^2}$$

$$+ \frac{(\sigma_{NY}+\mu_N\mu_Y)}{T}\Big] = \frac{(T-1)\sigma_{NY}}{T-1} = \sigma_{NY}$$

as $E[n_i y_i] = \sigma_{NY} + E[n_i]E[y_i]$, and $E[y_i] = \mu_Y$, which does not depend upon the sample size (n_i). The expectation of the estimator for the variance of the mean $E[s_y^2] = \sigma_Y^2$;

$$E[s_y^2] = \frac{1}{T-1}E\Big[\sum_{i=1}^{T}(y_i - \bar{y})^2\Big]...$$

which can be expanded as with the covariance and shown to require only estimates of $E[y_i]$ and not $Var[y_i]$. The correlation estimator of n and y is therefore unbiased;

$$cor(n,y) = \frac{cov(n,y)}{\sqrt{s_n^2 s_y^2}}.$$

[1]Note: The variance of the *estimator* for the mean vorticity $Var[y_t]$ is not the same as the variance of the mean vorticty σ_Y^2

Appendix B

B.1 Axioms of coherence

The main function of risk measures are for determining risk capital, portfolio management and premium pricing (McNeil et al., 2005). It is desirable for a risk measure to be *c*oherent as defined by the axioms of coherence. As in McNeil et al. (2005) we define S_1, S_2 as losses from 2 distinct portfolios and ϱ as the risk measure (e.g. the value-at-risk or the expected shortfall). The risk measure ϱ is coherent if the following hold

- **translation invariance** - for every $w \epsilon \mathbb{R}$ we have $\varrho(S + w) = \varrho(S) + w$
- **positive homogeneity** for every $v > 0$ $\varrho(vS) = v\varrho(S)$
- **sub-additivity** for all S_1, S_2 we have $\varrho(S_1 + S_2) \leq \varrho(S_1) + \varrho(S_2)$
- **monotonicity** If $S_1 \leq S_2$ then $\varrho(S_1) \leq \varrho(S_2)$

see for example Dowd and Blake (2006) for more on the axioms of coherence. Translational invariance is necessary as it states that by adding or subtracting an amount to a loss (or position) alters the users capital requirement by exactly that amount. Positive homogeneity means that the risk from a portfolio is proportional to its size. Monotonicity implies that if the losses from the first portfolio S_1 are greater than losses from the second portfolio S_2 then the risk should be greater. Sub-additivity is the most important for diversification as it states that an aggregate portfolio made up of smaller portfolios is not exposed to greater risk than the

sum of the constituent portfolios.

To show that the VaR is not sub-addative a counter example is used, as in Dowd and Blake (2006). Consider two portfolios which are at risk from independent claims S_1,S_2, which for simplicity are both binary random variables which take the values 0 or 100, and $Pr(S_1 = 100) = Pr(S_2 = 100) = 0.04$. Considering the aggregate portfolio which is exposed to both claims, the probability of the loss being 0 is $0.96^2 = 0.9216$, the probability of the loss being 200 is $0.04^2 = 0.0016$, and a loss of 100 with probability $1 - 0.04^2 - 0.96^2 = 0.0768$. The $VaR_{0.95}(S_1 + S_2) = 100$, but $VaR_{0.95}(S_1) + VaR_{0.95}(S_2) = 0$. Therefore the VaR violates sub-additivity.

Appendix C

C.1 Parameter estimation: Linear link function

Let λ_i be linearly related to the mixing variable Z;

$$\lambda_i = \beta_{0,i} + \beta_{1,i} Z$$

where the mean and variance of λ_i are $E[\lambda_i] = \rho_i$, $Var[\lambda_i] = \phi\rho_i^2 = \beta_{i,i}^2 Var[Z]$. The variance of a Poisson variable N_i, with random intensity λ_i is

$$Var[N_i] = E[\lambda_i] + Var[\lambda_i] = (\phi\rho_i + 1)\rho_i,$$

see Section 2.2.3. For the linear link function the covariance between the rate parameters for two rows of the ELT λ_i and λ_j is

$$\begin{aligned} Cov[\lambda_i, \lambda_j] &= E[\lambda_i\lambda_j] - E[\lambda_i]E[\lambda_j] \\ &= E[(\beta_{0,i} + \beta_{1,i}Z)(\beta_{0,j} + \beta_{1,j}Z)] - E[(\beta_{0,i} + \beta_{1,i}Z)]E[(\beta_{0,j} + \beta_{1,j}Z)] \\ &= \beta_{1,i}\beta_{1,j}Var[Z] = \sqrt{\phi_i\phi_j}\rho_i\rho_j \end{aligned}$$

since $Var[\lambda_i] = \phi\rho_i^2 = \beta_{1,i}^2 Var[Z]$. The variance of $\lambda_i + \lambda_j$ is,

$$\begin{aligned} Var[\lambda_i + \lambda_j] &= Var[\lambda_i] + Var[\lambda_j] + 2Cov[\lambda_i, \lambda_j] \\ &= \rho_i^2\phi_i + \rho_j^2\phi_j + 2\rho_i\rho_j\sqrt{\phi_i}\sqrt{\phi_j} = (\rho_i\sqrt{\phi_i} + \rho_j\sqrt{\phi_j})^2. \end{aligned}$$

Using the same approach the variance of $Var[\lambda_i + \lambda_j + \lambda_k]$ can be derived,

$$Var[\lambda_i + \lambda_j + \lambda_k] = \left(\rho_i\sqrt{\phi_i} + \rho_j\sqrt{\phi_j} + \rho_k\sqrt{\phi_k}\right)^2$$

and for an ELT with $i = 1, \ldots, I$ rows

$$Var[\lambda] = \left(\sum_{i=1}^{I} \rho_i \sqrt{\phi_i} \right)^2$$

where $\lambda = \sum_{i=1}^{I} \lambda_i$. For constant dispersion parameter ϕ which does not depend upon i,

$$Var[\lambda] = \left(\sum_{i=1}^{I} \sqrt{\phi} \rho_i \right)^2 = \phi \left(\sum_{i=1}^{I} \rho_i \right)^2 \tag{C.1}$$

C.2 Parameter estimation: Log link function

Let λ_i be log-linearlly related to the mixing variable Z;

$$log(\lambda_i) = \beta_{0,i} + \beta_{1,i} Z$$

where the mean and variance of λ_i are $E[\lambda_i] = \rho_i$, $Var[\lambda_i] = \phi \rho_i^2 = e^{2\beta_{0,i} + \beta_{1,i}^2} (e^{\beta_{1,i}^2} - 1)$. The variance of a Poisson variable N_i, with random intensity λ_i is

$$Var[N_i] = E[\lambda_i] + Var[\lambda_i] = (\phi \rho_i + 1) \rho_i.$$

The variance of two log-linearly related variables, $\lambda_i + \lambda_j$ is

$$Var[\lambda_i + \lambda_j] = Var[\lambda_i] + Var[\lambda_j] + 2Cov[\lambda_i, \lambda_j],$$

and the covariance is

$$Cov[\lambda_i, \lambda_j] = \rho_i \rho_j (e^{\sqrt{log(1+\phi_i)} \sqrt{log(1+\phi_j)}} - 1)$$

When ϕ_i does not depend on i the covariance becomes

$$Cov[\lambda_i, \lambda_j] = \rho_i \rho_j (e^{log(1+\phi_i)} - 1) = \rho_i \rho_j \phi$$

and thus the expression for $Var[\lambda]$ for the linear function holds (Eqn C.1). When ϕ_i does depend on i (intensity dependent dispersion) then the covariance is

$$Cov[\lambda_i, \lambda_j] = \rho_i \rho_j ((1 + \phi_j)^{\beta_i/2} - 1).$$

The variance of $\lambda_i + \lambda_j$ is then

$$Var[\lambda_i + \lambda_j] = \rho_i^2 \phi_i + \rho_j^2 \phi_j + 2\rho_i \rho_j ((1 + \phi_j)^{\beta_i/2} - 1). \tag{C.2}$$

The same approach can then be used as with the linear link function in Section 5.3.4; the rows of the ELT can be sorted by their expected loss μ_i and the parameters for the most intense event μ_1 can be calculated. Then Eqn. C.2 can be solved using numerical techniques for ϕ_j, as all other terms are known.

Glossary of Acronyms

AAL	Annual Aggregate Loss
AEP	Aggregate Exceedance Probability
CEP	Conditional Exceedance Probability
CMIP5	Coupled Model Inter Comparison Project 5
CPC	Climate Prediction Centre
EAP	East Atlantic Pattern
ELT	Event Loss Table
EP	East Pacific/North Pacific
ETC	Extra Tropical Cyclone
ERA-40	European Centre for Medium-Range Weather Forecasts 40 Year Re-analysis
EWP	East Atlantic/ West Russian
GCM	Global Climate Model
GPD	Generalised Pareto Distribution
MLE	Maximum Likelihood Estimator
NCEP-NCAR	National Centers for Environmental Prediction and the National Center for Atmospheric Research
NAO	North Atlantic Oscillation
NWP	Numerical Weather Prediction
OEP	Occurrence Exceedance Probability
PML	Probable Maximum Loss
PNA	Pacific North American
POL	Polar/Eurasian
Q-Q	Quantile-Quantile
SCP	Scandinavian Pattern
TNH	Tropical Northern Hemisphere
UNISDR	United Nationals International Strategy for Disaster Reduction
WP	West Pacific

Glossary of Notations

$Ber(.)$	Bernoulli probability density function
$Cov[.,.]$	covariance between . and .
$C(.,.)$	copula describing the joint distribution of . and .
$e_k(.)$	the insured exposure of construction type k at location .
E_i	the total insured exposure for all construction types at all locations which are exposed to event i.
$E[.]$	expected value of .
ES_α	expected shortfall of .
$F(.)$	cumulative distribution function $F(.) = Pr(X \leq .)$
$F^{-1}(.)$	quantile function
$Ga(.)$	Gamma probability density function
$g(.)$	link function
$h_i(.)$	hazard intensity for event i at location .
i	parameter index $i = 1,$
j	parameter index $j = 1, \ldots, J$
k	parameter index $k = 1, \ldots, K$
$l_{i,j,k}$	the insured loss from building type k at location j from event i
L_i	the total insured loss from all locations for all property types exposed to hazard i
m	number of observations or simulations
n_t	value of variable n at time t
$N(.)$	Normal probability density function
$NB(.)$	Negative Binomial probability density function
$\bar{n}$	sample mean of the variable n
$Pois(.)$	Poisson probability density function
r	Pearson's correlation
ρ_τ	Kendall's tau

s_j	location j
s_n^2	sample variance of the variable n
t	time index $t = 1, .., T$
u	threshold
$V_k(.,.)$	vulnerability of construction type k
	to hazard intensity . at location .
$Var[.]$	variance of .
VaR_α	value at risk
x_t	value of variable x at time t
y_t	value of variable y at time t
$z_{k,t}$	value of explanatory variable z_k at time t
$(1-\alpha)$	confidence interval width
α_0, β_0	intercept parameters
α_k, β_k	regression coefficients associated with explanatory variable z_k
θ	mean parameter for the Bernoulli distribution
ρ_i	rate parameter for the ith row of the event loss table.
μ_i	expected loss for the ith row of the event loss table.
μ_N	mean parameter for N.
λ	rate parameter of the Poisson distribution
ξ	shape parameter
ϕ_i	dispersion parameter for the ith row of the event loss table
$\phi(.)$	dispersion of .
Φ	standard normal density function
σ	standard deviation or scale parameter
σ^2	variance parameter
Σ	covariance matrix
$\sum_{i=1}^{I} x_i$	summation of the variables x_i, for $i = 1, \ldots, I$

Bibliography

Aitkin, M., B. Francis, J. Hinde, and R. Darnell (2009). *Statistical modelling in R*. Oxford University Press, 576pp.

Baldwin, M. P., X. Cheng, and T. J. Dunkerton (1994). Observed correlations between winter-mean tropospheric and stratospheric circulation anomalies. *Geophysical Research Letters 21*(12), 1141–1144.

Banks, E. (2005). *Catastrophic risk: Analysis and Management*. Wiley, 178pp.

Barnston, A. and R. Livezey (1987). Classification, seasonality and persistence of low-frequency atmospheric circulation patterns. *Monthly Weather Review 115*(6), 1083–1126.

Barredo, J. I. (2010). No upward trend in normalised windstorm losses in Europe. *Nat. Hazards Earth Syst. Sci 10*, 97–104.

Bengtsson, L., S. HHagemann, and K. I. Hodges (2004). Can climate trends be calculated from reanalysis data? *Journal of Geophysical Research: Atmospheres (1984–2012) 109*(D11).

Bjerknes, J. and H. Solberg (1922). *Life cycle of cyclones and the polar front theory of atmospheric circulation*. Grondahl.

Borch, K. (1967). The theory of risk. *Journal of the Royal Statistical Society. Series B (Methodological)*, 432–467.

Bueh, C. and H. Nakamura (2007). Scandinavian pattern and its climatic impact. *Quarterly Journal of the Royal Meteorological Society 133*(629), 2117–2131.

Cameron, A. C. and P. Trivedi (2013). *Regression analysis of count data*, Volume 53. Cambridge University Press,412.

Carlson, T. N. (1991). *Mid-latitude weather systems*. New York, NY (United States); Routledge, Chapman Hall, Inc, pp507.

Clark, K. (2002). The use of computer modeling in estimating and managing future catastrophe losses. *Geneva Papers on Risk and Insurance- Issues and Practice 27*(2), 181–195.

Clark, K. (2013). Opening the black box. *Global Reinsurance March 2013*, 38–40.

Cole, C. R., D. A. Macpherson, and K. A. McCullough (2010). A comparison of hurricane loss models. *Journal of Insurance Issues*, 31–53.

Coles, S. (2001). *An introduction to statistical modeling of extreme values*. Springer, pp209.

Crouhy, M., D. Galai, and R. Mark (2000). A comparative analysis of current credit risk models. *Journal of Banking & Finance 24*(1), 59–117.

Dacre, H. F. and S. L. Gray (2009). The spatial distribution and evolution characteristics of North Atlantic cyclones. *Monthly Weather Review 137*(1), 99–115.

Davison, A. C. (1997). *Bootstrap Methods and their Application*, Volume 1. Cambridge University press, pp582.

Davison, A. C. (2003). *Statistical models*, Volume 11. Cambridge University Press.

Della-Marta, P. M., H. Mathis, C. Frei, M. A. Liniger, J. Kleinn, and C. Appenzeller (2009). The return period of wind storms over Europe. *International Journal of Climatology 29*(3), 437–459.

Diers, D. (2008). Stochastic modelling of catastrophe risks in DFA models. In *Presentado a Astin Colloquium*, pp. 2–19.

Dowd, K. and D. Blake (2006). After var: The theory, estimation, and insurance applications of quantile-based risk measures. *Journal of Risk and Insurance 73*(2), 193–229.

Economou, T., S. D. B., and C. A. T. Ferro (2014). Spatio-temporal modelling of extreme storms. *under review in Annals of Applied Statistics*.

Elsner, J. B. and T. H. Jagger (2006). Prediction models for annual US hurricane counts. *Journal of Climate 19*(12).

Embrechts, P., C. Klüppelberg, and T. Mikosch (1997). *Modelling extremal events: for insurance and finance*, Volume 33. Springer, pp648.

Frey, R. and A. J. McNeil (2003). Dependent defaults in models of portfolio credit risk. *Journal of Risk 6*, 59–92.

Friedman, D. G. (1972). Insurance and the natural hazards. *The ASTIN Bulletin: International Journal for Actuarial Studies in Non-Life Insurance and Risk Theory 7*(1), 4–58.

Frishman, F. (1971). *Statistical Distributions in Scientific Work*. Dordrecht, New York: Reidel, pp401–406.

Graham, N. E. and H. F. Diaz (2001). Evidence for intensification of North Pacific winter cyclones since 1948. *Bulletin of the American Meteorological Society 82*(9), 1869–1893.

Grossi, P. and H. Kunreuther (2005). *Catastrophe modeling: A new approach to managing risk*, Volume 25. Springer, pp245.

Hanley, J. and R. Caballero (2012). The role of large-scale atmospheric flow and Rossby wave breaking in the evolution of extreme windstorms over Europe. *Geophysical Research Letters 39*(21).

Harmantzis, F. C., L. Miao, and Y. Chien (2006). Empirical study of value-at-risk and expected shortfall models with heavy tails. *Journal of Risk Finance, The 7*(2), 117–135.

Hodges, K. I. (1994). A general method for tracking analysis and its application to meteorological data. *Monthly Weather Review 122*(11), 2573–2586.

Hodges, K. I. (1999). Adaptive constraints for feature tracking. *Monthly Weather Review 127*(6), 1362–1373.

Hodges, K. I. et al. (1995). Feature tracking on the unit-sphere. *Monthly Weather Review 123*(12), 3458–3465.

Hoskins, B. J. and K. I. Hodges (2002). New perspectives on the Northern Hemisphere winter storm tracks. *Journal of the Atmospheric Sciences 59*(6), 1041–1061.

Hoskins, B. J. and P. J. Valdes (1990). On the existence of storm-tracks. *Journal of the atmospheric sciences 47*(15), 1854–1864.

Houston, D. B. (1960). Risk theory. *The Journal of Insurance 27*(1), 77–82.

Jagger, T. H. and J. B. Elsner (2006). Climatology models for extreme hurricane winds near the United States. *Journal of Climate 19*(13).

Jagger, T. H., J. B. Elsner, and M. A. Saunders (2008). Forecasting US insured hurricane losses. *Climate extremes and society*, 189–208.

Joe, H. (1997). Multivariate models and dependence concepts: Monographs on statistics and applied probability, 73. *Chapmann & Hall, London, pp399*.

Kalnay, E., M. Kanamitsu, R. Kistler, W. Collins, D. Deaven, L. Gandin, M. Iredell, S. Saha, G. White, J. Woollen, et al. (1996). The NCEP–NCAR 40-year reanalysis project. *Bulletin of the American meteorological Society 77*(3), 437–471.

Katz, R. (2002). Stochastic modeling of hurricane damage. *Journal of Applied Meteorology 41*(7), 754–762.

Katz, R. W. and M. B. Parlange (1998). Overdispersion phenomenon in stochastic modeling of precipitation. *Journal of Climate 11*(4), 591–601.

Katz, R. W., M. B. Parlange, and P. Naveau (2002). Statistics of extremes in hydrology. *Advances in water resources 25*(8), 1287–1304.

Kircher, C. A., R. V. Whitman, and W. T. Holmes (2006). Hazus earthquake loss estimation methods. *Natural Hazards Review 7*(2), 45–59.

Kistler, R., W. Collins, S. Saha, G. White, J. Woollen, E. Kalnay, M. Chelliah, W. Ebisuzaki, M. Kanamitsu, V. Kousky, Y. Zhu, A. Leetmaa, R. Reynolds, M. Chelliah, W. Ebisuzaki, W. Higgings, J. Janowick, K. Mo, C. Ropelewski, J. Wang, R. Jenne, and D. Joseph (2001). The NCEP-NCAR 50-year reanalysis: Monthly means cd-rom and documentation. *Bulletin of the American Meteorological society 82*(2), 247–267.

Klawa, M., U. Ulbrich, et al. (2003). A model for the estimation of storm losses and the identification of severe winter storms in Germany. *Natural Hazards and Earth System Science 3*(6), 725–732.

Kukush, A., Y. Chernikov, and D. Pfeifer (2004). Maximum likelihood estimators in a statistical model of natural catastrophe claims with trend. *Extremes 7*(4), 309–336.

Kunreuther, H., E. Michel-Kerjan, and N. Ranger (2013). Insuring future climate catastrophes. *Climatic change 118*(2), 339–354.

Kunz, M., S. Mohr, M. Rauthe, R. Lux, and C. Kottmeier (2010). Assessment of extreme wind speeds from regional climate models–part 1: Estimation of return values and their evaluation. *Natural Hazards and Earth System Science 10*(4), 907–922.

Kvamstø, N. G., Y. Song, I. A. Seierstad, A. Sorteberg, D. Stephenson, et al. (2008). Clustering of cyclones in the ARPEGE general circulation model. *Tellus A 60*(3), 547–556.

Leckebusch, G. C., D. Renggli, and U. Ulbrich (2008). Development and application of an objective storm severity measure for the northeast atlantic region. *Meteorologische Zeitschrift 17*(5), 575–587.

Leckebusch, G. C. and U. Ulbrich (2004). On the relationship between cyclones and extreme windstorm events over Europe under climate change. *Global and planetary change 44*(1), 181–193.

Leckebusch, G. C., U. Ulbrich, L. Fröhlich, and J. G. Pinto (2007). Property loss potentials for European midlatitude storms in a changing climate. *Geophysical Research Letters 34*(5).

Mailier, P., D. Stephenson, C. Ferro, and K. Hodges (2006). Serial clustering of extratropical cyclones. *Monthly weather review 134*(8), 2224–2240.

Massart, P. (1990). The tight constant in the Dvoretzky-Kiefer-Wolfowitz inequality. *The Annals of Probability*, 1269–1283.

McNeil, A. J. and R. Frey (2000). Estimation of tail-related risk measures for heteroscedastic financial time series: an extreme value approach. *Journal of empirical finance 7*(3), 271–300.

McNeil, A. J., R. Frey, and P. Embrechts (2005). *Quantitative risk management*. Princeton Series in Finance, Princeton, pp538.

McNeil, A. J., R. Frey, and P. Embrechts (2010). *Quantitative risk management: concepts, techniques, and tools*. Princeton university press.

Mumby, P. J., R. Vitolo, and D. B. Stephenson (2011). Temporal clustering of tropical cyclones and its ecosystem impacts. *Proceedings of the National Academy of Sciences 108*(43), 17626–17630.

Neu, U., R. Caballero, and J. Hanley (2012). IMILAST–a community effort to intercompare extratropical cyclone detection and tracking algorithms: assessing method-related uncertainties. *Bulletin of The American Meteorological Society-(BAMS)*.

Pielke Jr, R. and C. Landsea (1998). Normalized hurricane damages in the United States: 1925-95. *Weather and Forecasting 13*(3), 621–631.

Pielke Jr, R. A., J. Gratz, C. W. Landsea, D. Collins, M. A. Saunders, and R. Musulin (2008). Normalized hurricane damage in the United States: 1900–2005. *Natural Hazards Review 9*(1), 29–42.

Pinto, J., E. Fröhlich, G. Leckebusch, and U. Ulbrich (2007). Changing European storm loss potentials under modified climate conditions according to ensemble simulations of the ECHAM5/MPI-OM1 GCM. *Natural Hazards and Earth System Science 7*(1), 165–175.

Pinto, J. G., N. Bellenbaum, M. K. Karremann, and P. M. Della-Marta (2013). Serial clustering of extratropical cyclones over the North Atlantic and Europe under recent and future climate conditions. *Journal of Geophysical Research: Atmospheres*.

Pinto, J. G., S. Zacharias, A. H. Fink, G. C. Leckebusch, and U. Ulbrich (2009). Factors contributing to the development of extreme North Atlantic cyclones and their relationship with the NAO. *Climate dynamics 32*(5), 711–737.

Prabhu, N. U. (1961). On the ruin problem of collective risk theory. *The Annals of Mathematical Statistics 32*(3), 757–764.

Raible, C. C. (2007). On the relation between extremes of midlatitude cyclones and the atmospheric circulation using ERA40. *Geophysical research letters 34*(7).

Raible, C. C., P. M. Della-Marta, C. Schwierz, H. Wernli, and R. Blender (2008). Northern Hemisphere extratropical cyclones: A comparison of detection and tracking methods and different reanalyses. *Monthly Weather Review 136*(3), 880–897.

Rice, J. A. (2007). *Mathematical statistics and data analysis, International student edition*. Duxburry Press, pp 603.

Rogers, J. C. (1997). North Atlantic storm track variability and its association to the North Atlantic Oscillation and climate variability of northern Europe. *Journal of Climate 10*(7), 1635–1647.

Rolski, T., H. Schmidli, V. Schmidt, and J. Teugels (2009). *Stochastic processes for insurance and finance*, Volume 505. John Wiley & Sons, pp 654.

Rootzén, H. and N. Tajvidi (1997). Extreme value statistics and wind storm losses: a case study. *Scandinavian Actuarial Journal 1997*(1), 70–94.

Rossi, F., M. Fiorentino, and P. Versace (1984). Two-component extreme value distribution for flood frequency analysis. *Water Resources Research 20*(7), 847–856.

Rougier, J., R. S. J. Sparks, and L. J. Hill (2013). *Risk and Uncertainty Assessment for Natural Hazards*. Cambridge University Press, 574.

Royden, H. L. (1953). Bounds on a distribution function when its first n moments are given. *The Annals of Mathematical Statistics*, 361–376.

Salvadori, G. (2007). *Extremes in nature: an approach using copulas*, Volume 56. Springer.

Sansom, P. G., D. Stephenson, C. Ferro, G. Zappa, and L. Shaffrey (2013). Simple uncertainty frameworks for selecting weighting schemes and interpreting multimodel ensemble climate change experiments. *Journal of Climate 26*(12).

Schwierz, C., P. Köllner-Heck, E. Z. Mutter, D. N. Bresch, P. Vidale, M. Wild, and C. Schär (2010). Modelling European winter wind storm losses in current and future climate. *Climatic change 101*(3-4), 485–514.

Seierstad, I. A., D. B. Stephenson, and N. G. Kvamstø (2007). How useful are teleconnection patterns for explaining variability in extratropical storminess? *Tellus A 59*(2), 170–181.

Sienz, F., A. Schneidereit, R. Blender, K. Fraedrich, and F. Lunkeit (2010). Extreme value statistics for North Atlantic cyclones. *Tellus A 62*(4), 347–360.

Sinclair-Knight, L. (2002). *Collins Paperback Dictionary and Thesaurus*. HarperCollins.

Sklar, A. (1973). Random variables, joint distribution functions, and copulas. *Kybernetika 9*(6), 449–460.

Smolka, A. (2006). Natural disasters and the challenge of extreme events: risk management from an insurance perspective. *Philosophical Transactions of the Royal Society A: Mathematical, Physical and Engineering Sciences 364*(1845), 2147–2165.

Stephenson, D. B. (2008). *Definition, diagnosis, and origin of extreme weather and climate events*, Volume 348. Cambridge University Press: New York.

Stephenson, D. B., V. Pavan, M. Collins, M. M. Junge, and R. Quadrelli (2006). North Atlantic Oscillation response to transient greenhouse gas forcing and the impact on European winter climate: a CMIP2 multi-model assessment. *Climate Dynamics 27*(4), 401–420.

Trigo, I. F. (2006). Climatology and interannual variability of storm-tracks in the Euro-Atlantic sector: a comparison between ERA-40 and NCEP–NCAR reanalyses. *Climate Dynamics 26*(2-3), 127–143.

Ulbrich, U., G. C. Leckebusch, and J. G. Pinto (2009). Extra-tropical cyclones in the present and future climate: a review. *Theoretical and Applied Climatology 96*(1-2), 117–131.

Uppala, S. M., P. Kållberg, A. Simmons, U. Andrae, V. Bechtold, M. Fiorino, J. Gibson, J. Haseler, A. Hernandez, G. Kelly, et al. (2005). The ERA-40 reanalysis. *Quarterly Journal of the Royal Meteorological Society 131*(612), 2961–3012.

Vere-Jones, D. (1995). Forecasting earthquakes and earthquake risk. *International Journal of Forecasting 11*(4), 503–538.

Vickery, P. J., J. Lin, P. F. Skerlj, L. A. Twisdale Jr, and K. Huang (2006). HAZUS-MH hurricane model methodology. i: hurricane hazard, terrain, and wind load modeling. *Natural Hazards Review 7*(2), 82–93.

Villarini, G., J. A. Smith, R. Vitolo, and D. B. Stephenson (2013). On the temporal clustering of US floods and its relationship to climate teleconnection patterns. *International Journal of Climatology 33*(3), 629–640.

Vitolo, R., D. Stephenson, I. Cook, and K. Mitchell-Wallace (2009). Serial clustering of intense European storms. *Meteorologische Zeitschrift 18*(4), 411–424.

Wallace, J. M. and P. V. Hobbs (2006). *Atmospheric science: an introductory survey*, Volume 92. Academic press.

Wang, X., V. Swail, and F. Zwiers (2006). Climatology and changes of extratropical cyclone activity: Comparison of ERA-40 with NCEP-NCAR reanalysis for 1958-2001. *Journal of Climate 19*(13), 3145–3166.

Whitaker, J. S. and P. D. Sardeshmukh (1998). A linear theory of extratropical synoptic eddy statistics. *Journal of the atmospheric sciences 55*(2), 237–258.

Woo, G. (1999). *The mathematics of natural catastrophes*. Imperial College Press, pp292.

Woo, G. (2002). Natural catastrophe probable maximum loss. *British Actuarial Journal 8*(5), 943–959.

Woollings, T., A. Hannachi, and B. Hoskins (2010). Variability of the North Atlantic eddy-driven jet stream. *Quarterly Journal of the Royal Meteorological Society 136*(649), 856–868.

Zappa, G., L. C. Shaffrey, K. I. Hodges, P. G. Sansom, and D. B. Stephenson (2013). A Multimodel Assessment of Future Projections of North Atlantic and European Extratropical Cyclones in the CMIP5 Climate Models*. *Journal of Climate 26*(16).

Zhang, X., J. E. Walsh, J. Zhang, U. S. Bhatt, and M. Ikeda (2004). Climatology and interannual variability of Arctic cyclone activity: 1948-2002. *Journal of Climate 17*(12), 2300–2317.